GRADUATE THESIS/DISSERTATION APPROVAL FORM AND SIGNATURE PAGE

Instructions: This form must be completed by all master's and doctoral students with a thesis or dissertation requirement. Please type or print clearly as this form MUST be included as page 1 of your thesis or dissertation via electronic submission to ProQuest. All theses and dissertations must be formatted according to the University and department/program requirements. **Reminder:** It is the responsibility of the student to submit any/all edits requested by the Examining Committee to the Faculty Mentor or Supervising Professor for final approval and signature via the Graduate Program Completion Form.

Type: ☐ Master's Thesis ☑ PhD/Doctoral Thesis or Dissertation

Thesis or Dissertation Title: Evaluating the Local Release, Systemic Transport, and Biological Significance of Cobalt Chromium Debris in Total Knee Replacement

Author's Name: Christina M. Arnholt

Month and Year: September 2020

The signatures below certify that this thesis / dissertation (circle one) is complete and approved by the Examining Committee.

Committee Chairperson's Name: Paul Brandt-Rauf

Title: Dean

Department: BMES

Institution (*if other than Drexel University*): Drexel

Signature: Paul Brandt-Rauf

Committee Member's Name: Steven Kurtz

Title: Research Professor

Department: BIOMED

Institution (*if other than Drexel University*):

Signature: Steven Kurtz Digitally signed by Steven Kurtz Date: 2020.09.03 11:34:53 -04'00'

Committee Member's Name: Li-Hsin Han

Title: Assistant Professor

Department: MEM

Institution (*if other than Drexel University*):

Signature: Li-Hsin Han 2020.09.03 11:43:14 -04'00'

Committee Member's Name: JosephSarver

Title: Teaching Professor

Department: BMES

Institution (*if other than Drexel University*):

Signature:

Committee Member's Name: Adam Briscoe

Title: Orthopaedics Technology Manager

Department: Research and Development

Institution (*if other than Drexel University*): Invibio Ltd.

Signature: Briscoe

Committee Member's Name: Sriram Balasubramanian, PhD

Title: Associate Professor

Department: BMES

Institution (*if other than Drexel University*): Drexel

Signature:

Evaluating the Local Release, Systemic Transport, and Biological Significance of Cobalt Chromium Debris in Total Knee Replacement

A Thesis

Submitted to the Faculty

of

Drexel University

by

Christina M. Arnholt

in partial fulfillment of the

requirements for the degree

of

Doctor of Philosophy

September 2020

Dedication

To my support system: my mom, Cindy Arnholt,

and my husband, Chris Ousey.

I love you.

Acknowledgements

I have to start by thanking my mom, Cindy Arnholt. She has always told me I could be anything I wanted to be, made any problematic situation more comfortable, and always made me feel supported. I love you so much, mom, and I couldn't have done this without you. I want to thank my husband, Chris Ousey, for helping me relax in times of high stress and allowing me to bounce ideas off of him. Thanks love. I would also like to thank my sister, Nicole Detweiler, and my dad, James Arnholt. Thank you for always being proud and supportive.

To my mentor, Dr. Steven Kurtz, thank you for giving me such a fantastic opportunity. You have urged me to be myself and to stand tall. You taught me how to communicate my ideas clearly and succinctly while standing in a room full of hundreds of other scientists and surgeons. You showed me how to network and to create lasting professional relationships. You have always challenged me to be better while always communicating that I was phenomenal. Thank you for giving me a chance. I promise I will live up your legacy.

To my family at the Implant Research Core (IRC), both past and present, thank you for always being loving and supportive. To Hannah Spece, thank you for being someone that I could lean on, someone that I could bounce ideas off of, and for always thinking outside of the box. Also, special thank you for reviewing each of my dissertation chapters along the way. To Dan MacDonald, thank you for reading all of my papers and for giving good advice. To Genymphas Higgs, thank you for being a big brother, for inspiring me to be as good as you were. To Jackie Schachtner, thank

you for being like a little sister, for letting me mentor you, and for always making me so proud.

To my family at Exponent Inc., both past and present, thank you for providing guidance and experience, while always being approachable. To Josh White, thank you for having such a positive attitude, for sharing your laboratory experience, and for always being excited for the next challenge. To Judd Day, thank you for helping me begin my first project all those years ago, and for still having an answer to all of my questions. To Richard Underwood, thank you for pushing, for teaching me so much about tribology, and for helping me become a better scientist. To Rebecca Kitchmire and Mia Obradovic, thank you gals for helping me store all of my materials, and for being such fabulous co-ops.

To my colleagues from the University of Tennessee, thank you for being such excellent collaborators. To Dr. William Mihalko, thank you for teaching me about surgery, for allowing me to work with cadavers, for providing advice and experience throughout different projects. To Julie Lowell, Meredith Perkins, and Griffin Heise, thank you for being so lovely and helpful through our collaboration. To my colleagues in Cleveland Clinic, specifically Dr. Michael Mont, Anton Khlopas, and Hiba Anis, thank you for your help in collecting different experimental materials.

To my colleagues from England, thank you for being such excellent teachers and collaborators. To Adam Briscoe and his colleagues at Invibio, thank you for being inquisitive, for sharing good ideas, and for always asking the difficult questions. To Dr. Joanne Tipper, thank you for teaching me about particle isolation

and for being so welcoming and supportive. To Jayna Patel and Saurabh Lal, thank you for teaching me about your methods and for being so welcoming and kind. To Kathryn Chamberlain Hughes, thank you for being the best friend a girl ever had, and for pushing me to be better.

To my committee members, Drs. Paul Brandt-Rauf, Sriram Balasubramanian, Joseph Sarver, Li-Hsin Han, and Adam Briscoe, thank you for providing support and guidance. Thank you for asking the difficult questions and for encouraging me to "Think the deep thoughts."

“Most people think that it is intellect which makes a great scientist.

They are wrong: it is character.”

- **Albert Einstein**

Table of Contents

Table of Contents

List of Tables

List of Figures

Figure 2.4.2: Examples of severe third-body damage and scratching on the bearing surface. (A) Vertical plowing with erratic scratching throughout the left bearing surface. (B) Aggressive plowing with erratic scratching toward the left of the bearing surface.

Figure 2.4.3: (A) High magnification digital photograph of the region circled in red in (B) revealing the circular damage scars that are associated with ICIC [3]. (B) Digital photography of a femoral condyle that illustrates the macro appearance of the ICIC affected area (circled in red and blue), which have a frosted appearance. (C) Three-dimensional stacked image created using digital photograph of ICIC damage in circled blue region. (D) The ICIC damage area varied among the femoral components. The median area that was affected by ICIC was 0.07 mm^2 (interquartile range: 0.12 mm^2).

Figure 2.4.4: (A) Macro photograph of corrosion between the cement mantle and backside of a femoral component. (B) Digital micrograph of the damaged region, showing discoloration.

Figure 3.3.1: Pictorial description of tissue metal scoring system used to visually evaluate the degree of metallosis in periprosthetic tissue.

List of Abbreviations

TKA	Total Knee Arthroplasty
Ti	Titanium Alloy
CoCr	Cobalt Chromium Alloy
MOM	Metal-on-metal
Ni	Nickel
ICP-MS	Inductively Coupled Plasma Mass Spectroscopy
AAS	Atomic Absorption Spectroscopy
ICP-OES	Inductively Coupled Plasma with Emission Spectrometry
SEM	Scanning Electron Microscope
ECD	Equivalent Circular Diameter
AR	Aspect Ratio
ICIC	Inflammatory Cell Induced Corrosion
THA	Total Hip Arthroplasty
MACC	Mechanically Assisted Crevice Corrosion
UHMWPE	Ultra-High Molecular Weight Polyethylene
ALTR	Adverse Local Tissue Reactions

PPB	Parts Per Billion
PEEK	Polyetheretherketone

Abstract

Evaluating the Local Release, Systemic Transport, and Biological Significance of Cobalt Chromium Debris in Total Knee Replacement

Christina M. Arnholt

Total knee arthroplasty (TKA) is one of the most commonly performed orthopedic surgeries during which a tibial tray, either titanium (Ti) or cobalt-chromium (CoCr) alloys, a polyethylene insert, and a cobalt-chromium alloy femoral component are implanted. Sensitivity to metal debris re-emerged as a concern in arthroplasty, with relatively little research focused on metal release in TKA. The overall focus of this work was to describe the potential biological burden of metallic debris from TKA. This dissertation investigated TKA devices, and tissues collected from routine revision and post-mortem TKA retrievals.

The causes of damage to the metal components which lead to metallic release were evaluated, specifically looking at third-body damage using a semiquantitative method. This method was used to determine the severity and coverage of third-body damage on the bearing surface of femoral components. Using the semiquantitative third-body damage score, total knee arthroplasty components could be observed at multiple retrieval centers and compared.

Secondly, metal debris and its characteristics (tissue metal concentration, particle size, and particle shape) were studied to determine if they were uniform throughout the knee joint capsule. The relationship between metal debris and

observed damage to the femoral component or observed biological reactions were also analyzed. The analysis of different regions within the joint capsule provided evidence that the chosen tissues for model analysis represent the entire joint capsule. Additionally, observations of metallic debris observed from the joint capsule could describe the characteristic shapes and sizes expected from total knee arthroplasty.

Finally, we used a biokinetic model to discuss the mobility of cobalt metal ions through the body. This approach involved the study of peripheral blood metal concentration and peri-prosthetic tissue metal concentration. The local movement of cobalt from the joint capsule into the bloodstream was modeled as debris movement directly from the synovial fluid to the bloodstream as a corrosion byproduct. Additionally, this model included a second transport of bearing surface debris movement from the synovial fluid to the joint capsule and then to the bloodstream. The remaining portions of the model originated from a biokinetic model of inorganic cobalt circulation with the exposure point of ingestion linked through an ailment track model. This model was altered so that the exposure point was the joint capsule, and the model was then calibrated to the periprosthetic tissue and blood of 7 retrieved TKA devices. The use of blood and peri-prosthetic tissues for metallic concentration measurements allowed the created model to be calibrated to total knee arthroplasty patients. With this calibrated model, the cobalt movement could describe an average TKA patient. With this model, the burden of metallic debris released from TKA could begin to be described.

The execution of these aims provided an assessment of total knee arthroplasty components, an assessment of debris regarding dose, shape, size, material, and an assessment of the mobility of cobalt from the joint capsule.

Chapter 1: Background and Significance

1.1 Introduction / Significance:

Total knee arthroplasty (TKA) is one of the most commonly performed orthopedic surgeries, with over 700,000 primary and revision TKA procedures occurring annually in the United States [6]. TKA failure, often requiring a revision procedure, is a multifactorial issue which may be influenced by surgeon technique, implant characteristics, and patient factors [7]. In TKA, revisions attributed to metal reactions include hypersensitivity to ionic metals, foreign body reactions to wear debris particles, and responses to metal corrosion products [8], which can exhibit as hypersensitivity or dermatitis [9]. Retrieval studies suggest that in vivo metallic debris release mechanisms for TKA may include bearing surface wear (including third-body wear), mechanically-assisted corrosion at the cement-implant interface, and mechanically-assisted taper corrosion in modular junctions [10]. Postmortem analysis has allowed for extensive analysis into these topics of interest within arthroplasty [11, 12], helping to elucidate the characteristics of polyethylene wear rates, debris accumulation sites and osteolysis [13-16], bone cement interlock [17-19], and metal sensitivity [20-22], as shown in Table 1.1. These methods are still needed, as patient satisfaction after receiving TKA remains in the mid to high 80th percentile [23-27], with postoperative pain being one of the main revision reasons. Additionally, new concerns regarding patient adverse reactions to cobalt resulting from THA have arisen. Some of these reactions have been shown to be associated with severe material loss from THA devices. A systematic review of THA identified

25 cases of THA with adverse reactions to elevated cobalt levels [28]. The study reported that blood cobalt levels were associated with thyroid symptoms [28]. A specific case study analyzed the biological samples for cobalt ions and the medical device for signs of wear. The maximum liner wear depth of the metal THA liner was measured at 400 μm, and laboratory findings of elevated biological cobalt levels were reported (serum cobalt levels of 83mg/L, cerebrospinal fluid cobalt levels of 2.2 mg/L, and joint fluid cobalt levels of 3200 mg/L) [29]. These findings were thought to be associated with symptoms such as anxiety, headaches, irritability, fatigue, tinnitus, and hearing loss [29]. One year after revision THA surgery, the symptoms abated, and serum cobalt levels lowered to 23mg/L [29]. Acknowledging that both TKA and THA devices use the same medical cobalt-chromium molybdenum, the current concerns and investigations into the adverse reactions to metal in THA create a need to understand the potential for similar reactions within TKA. A large portion of this work will focus on the movement of cobalt due to the current knowledge of cobalt transport throughout the body and the knowledge of symptoms associated with high biological concentrations of cobalt.

1.2 Metal Sensitivity and Biological Reactions

Cobalt, a metal element with chemical properties consistent with iron and nickel, is generally observed in two valence states cobaltous Co(II) and cobaltic Co(III) [30]. The form of cobalt derived from metal prosthesis is Co(II), which is also the form observed from cobalt-containing dietary supplements [31]. Cobalt is a trace element essential for the human body [30, 31]. It is involved with the

prevention of nutritional deficiencies, the function of the immune system, and the regulation of gene expression [30]. Cobalt (III) is also a component of cyanocobalamin (vitamin B12) [32], which is required for the production of red blood cells [30, 31]. Historically, cobalt has been used to treat anemia through the form of $CoCl_2$ [30]. However, some patients experience adverse side effects with this therapeutic use, specifically thyroid impairment in children and reversible vision and hearing impairment in adults [30]. Also, within the subpopulation of patients with sickle cell anemia, renal failure was observed in lower and theoretically less symptomatic doses of cobalt [30]. Due to the extensive occurrence of cobalt in nature, humans are frequently exposed to cobalt daily through ambient air, food, and drinking water [31]. It is thought that the primary exposure to cobalt is through the diet for the general population. The highest cobalt concentrations are found in items such as chocolate, butter, coffee, fish, nuts, and green leafy vegetables [30]. However, total diet studies have shown that the mean dietary Co intake ranges from 0.13 to 0.48 μg/kg BW/day, which is within the range for the tolerable daily Co intake (1.6-8 μg/kg BW/day of Co) [30]. At one time, cobalt was a compound used as a beer foam stabilizing agent. From this use, it was observed that in response to a dose of 0.09 mg Co/kg-d, well-nourished beer drinkers did not experience adverse effects. In contrast, malnourished beer drinkers suffered severe cardiomyopathy [30].

Occupational exposures to cobalt are also a risk factor for adverse effects. Hard metal industries represent 15% of cobalt worldwide and are believed to be the main source of occupational cobalt exposure [31]. This exposure generally occurs

through inhalation but can also occur through dermal uptake. The uptake of this is determined by the airborne dose of cobalt, the duration of time exposed to cobalt, the breathing volume per minute, and the percent retention of dust in the airways [31]. Because of this knowledge, the levels of airborne cobalt have been decreased over the years with reports maintaining the recommended occupational exposure limit (American Conference of Governmental Industrial Hygienists 0.02 mg/m^3, Austrian Occupational Safety and Health Administration 0.1 mg/m^3, National Institute for Occupational Safety and Health 0.05 mg/m^3, Swedish Work Environment Authority 0.02 mg/m^3).

Finally, cobalt also has medical exposure points. The biological reactions to implant debris and corrosion products have previously been investigated to understand their cytotoxic effects [33-35]. Cobalt chromium alloys corrode and produce a phosphate hydrate-rich material called orthophosphate, which can range from submicron to 500 μm in size [33, 34]. This material has the potential to activate macrophage monocytes and stimulate bone reabsorption in a dose-dependent manner [34]. Cobalt chromium debris found in tissues has been surrounded by fibrosis and necrosis with foreign body giant cells. Titanium alloys are generally more stable and retain the composition of the base alloy in particles with a thick oxide layer on the surface [33]. However, while Ti alloy debris has been associated with macrophages and fibrocyte activity, foreign body giant cells were generally absent [34]. The continuous production of debris is associated with cells that act as storage vessels, such as histiocytes, or giant cells which phagocytose the particles and have the

potential to later form granulomas with necrotic regions [35]. Locally, osteolysis, inflammation, and hypersensitivity can occur due to this debris [33]. The innate immune system uses macrophages to phagocytose debris, produce danger inflammatory signals, and present debris to T-cells for an adaptive immune response [33]. In tissue with local metallosis, inflammatory cytokines (TNFa, IL-6, and Il-1b) in peri-prosthetic tissues have been observed [33]. Metallosis is defined as the infiltration of metallic debris into the periprosthetic tissue structures [36] and is generally characterized as a visual tissue discoloration.

Adverse reactions to metal have been studied considerably in THA, but less extensively in TKA. Periprosthetic metal concentrations measured in metal-on-metal (MOM) THA ranges from 1.4 to 4604.0 μg/g metal content for Co, Cr and, nickel (Ni) [37]. Higher concentrations of metal (222 μg/g mean metal concentration) have been associated with a lymphocytic response. In comparison, smaller concentrations of metal (3 μg/g mean metal concentration) have been associated with macrophage responses [37]. Cobalt and chromium ions have also been found in systemic bodily fluids such as urine, synovial fluid, and blood. However, the concentrations have generally been much lower than the tissue surrounding the joint replacement (e.g. <1 μg/L) [38]. It should also be noted that local periprosthetic tissues have been shown to have larger metal concentrations (22 to 6,000 mg/L) compared to systemic samples such as blood (0.006 mg/L), urine (0.024 mg/L), and organs (liver 3 mg/L, brain 1 mg/L, and kidney 1 mg/L) in THA [39]. These findings were supported in a separate study that found urinary cobalt concentrations that ranged from 20 to 40 μg/L across

four patients and organ metal concentrations that range from 1 mg/L to 27 mg/L [40]. Despite this knowledge of metal concentrations in periprosthetic THA tissues, the current understanding of metal concentrations in TKA is limited.

1.3 Tissue Digestion and ICP-MS Analysis

Detection of metallic debris within biological matrixes such as peri-prosthetic tissue, blood, synovial fluid, or peripheral organs can be performed using different methods such as atomic absorption spectroscopy (AAS), inductively coupled plasma mass spectroscopy (ICP-MS) [41], and inductively coupled plasma with emission spectrometry (ICP-OES) [42]. However, ICP-MS is the preferred method due to increased sensitivity and specificity of the technique achieved through multi-element and multi-isotopic capabilities, as well as low detection limits [41, 42].

1.4 Particle Isolation and Characterization

An increased inflammatory response has been associated with specific implant debris characteristics, including particle load, aspect ratio, and chemical reactivity. Particle load refers to the size and volume of the particles [43]. A greater particle volume with smaller particles (0.4 μm) exhibits a greater inflammatory reaction due to smaller particles being more easily phagocytosed [33]. Additionally, the general shape of the particles is important, where elongated fiber-like particles elicit a stronger inflammatory response [43]. The potential for implant debris to have a chemical reaction is also important due to potential hypersensitivity, cytotoxicity, and DNA damage [33].

The hypothesized size range for particle phagocytosis is between 150 nm-10 μm, for a range of peri-implant cell types such as osteoblasts, fibroblasts, and endothelial cells [43]. Additionally, submicron particles (less than 150 nm) can be ingested by endocytosis or pinocytosis [43]. It was suggested that the size of metal particles may not be as critical as the particle's reactive surface area [44]. However, it is also noted that micron-sized particles persist within the joint capsule [44], while nanoparticles are hypothesized to be uptaken by macrophages and transported with intracellular phagosomes [45].

To isolate and then characterize metallic debris particles from peri-prosthetic tissues, protein, and contaminant removal is necessary through the solubilizing of the tissue [46, 47]. Since the material being analyzed is a metal, chemical treatments for decomposition such as strong bases and acids cannot be used as they could damage or alter the particles [46, 48]. Thus, a proteinase K and papain digestion are ideal with ultracentrifugation to create a hard pellet of the metal particles being analyzed [46].

Debris characterization requires scanning electron microscope (SEM) analysis. ASTM F1877 provides guidance on the magnification settings in relation to the debris size of interest [49]. Standard particles can have a variety of morphologies, such as spherical or globular fibrillar [49], which related directly to the bioreactivity [43]. Beyond this, there is also guidance on particle dimensional measurements, which can be used to classify and compare particles between studies. These include equivalent circle diameter (ECD) and aspect ratio (AR) [49]. The ECD is a diameter that belongs to a circle whose area is equivalent to the area of the particle being

analyzed, calculated as $ECD = (\frac{4*A}{\pi})^{\frac{1}{2}}$ with units of length [49]. AR refers to a ratio of the major diameter and minor diameter. The major diameter is the longest straight line that can be drawn across the outline, and the minor diameter is the longest straight line drawn perpendicular to the major diameter, calculated as $AR = \frac{d_{max}}{d_{min}}$ [49]. The aspect ratio was used to estimate particle shape, where $1 \leq AR < 1.5$ is round, $1.5 \leq AR < 2.5$ is oval, and $AR \geq 2.5$ is needle-shaped [50]. Within the literature, cobalt-chromium alloy particle debris was observed in tissues as small black spheres ranging from 1 to 4 μm [51].

While analyzing particles captured after filtration, it is important to distinguish between agglomerates and large particles. This can be done by properly dispersing particles with agitation before filtration using sonication, vortexing, and aspiration techniques. Additionally during image analysis particles can be differentiated within an agglomerate and counted properly.

1.5 Modeling of Cobalt transport in vivo

Research interest has grown around metallosis within the joint capsule, creating an emerging conversation about systemic biological complications such as mental, neurological, cardiovascular, and endocrine effects [52]. However, there currently is not a large-scale case-controlled study linking these events with cobalt or other metal ion concentrations [52]. Additionally, cobalt is a naturally occurring metal that has various exposure methods to the general population [30].

Biokinetic modeling describes the physiological processes happening within the body through numerical descriptions that could explain hypothetical situations [53]. These models have historically been used to describe doses from exposure to radionuclides through time-dependent distribution, retention, and excretion [54]. They are generally coupled with a dosimetric model that describes radiation transport from the biokinetic model [54]. Biokinetic models from the 1950s were composed of simple mathematical formulae derived from curve fits of data to describe the movement of element tracers in human subjects and laboratory animals [54]. In the 1980s, models began to only pertain to a reference adult with specific age and gender. Age-specific models were created due to the lack of data about children's radiobiological behavior [54]. Gender-specific models allow for hermaphrodite reference adults, meaning the model pertained to both male and female adults [54]. Two general categories exist for biokinetic models describing physiology, models that describe basic physiological systems like blood circulation, and element-specific models that describe the characteristic behavior of elements in the body [54]. The cobalt model used in this research would be an example of the second category. The model is composed of different compartments representing areas of element retention or collection and transport coefficients describing how the element moves between compartments in a time-dependent manner. Different studies control one specific cobalt exposure type while detailing the relationship between cobalt intake routes, the toxicity mechanisms, and clinical consequences [30]. A different approach involves

controlling the biological effects and studying the relationship to different cobalt exposure types [30].

The International Commission of Radiological Protection (ICRP) created a systemic biokinetic model of cobalt movement to react to worker exposure to radionuclides from the nuclear industry [2]. The model framework was patterned after a model describing alkaline earth elements for the ICRP [4]. Physiologically cobalt was not related to alkaline earth elements [4]. However, the structure was thought to be useful for radiation protection purposes and described cobalt movement from donor to receptor compartments as a function of time [4]. The compartments are blood and four systemic tissues: liver, kidney, skeleton, and other organs [2]. The model outlined recycling data and phases of loss, such as urinary and fecal excretion [2].

The systemic biokinetic model of cobalt movement was created using studies of human subjects or laboratory animals exposed to radioactive or stable cobalt under controlled conditions [4]. The modeled prediction of total body retention and blood parameter values were derived from human subjects injected with $^{60}CoCl_2$ and $^{58}CoCl_2$ [4]. The model has an initial exposure point of oral ingestion using the ailment track model outlined by ICRP [1]. The ailment track model describes the movement of cobalt from oral intake, to the mouth, to the esophagus, to the stomach, and the small intestine, as seen in Figure 1.5.1 [1]. The small intestine was the model integration point with the bloodstream [55]. Within this model, each tissue or location, for example, the mouth, is represented by a compartment. The movement of

cobalt from compartment to compartment is described by an arrow which is mathematically represented by a transfer coefficient. For this dissertation, the model's exposure point was altered from oral ingestion beginning at the mouth to the joint capsule beginning at the synovial fluid reservoir. However, the remainder of the systemic model was maintained, Figure 1.5.2. Within this model, 6% of cobalt in the bloodstream moved from a bound compartment to the circulating blood supply [2]. The circulating blood moved 94% of the cobalt to a reservoir, which fed into the organs. This reservoir fed 35% of the cobalt into the liver, which returned 40% of the cobalt to the circulating blood supply [2]. Twenty percent of the cobalt within the liver moved to the intestines, and 5% of cobalt ions remained in the liver [2]. The cobalt in the intestines moved all material into the fecal excretion and out of the body [2]. From the organ reservoir, 16% of the cobalt was transported to other tissues, 30% of cobalt moved to the urinary bladder, 4.5% of cobalt moved to the kidney, and 6% of the cobalt moved to the skeleton [2]. The urinary bladder cobalt ions fed into the urinary excretion, while 0.5% of cobalt ions remained within the kidneys, eventually moving into urinary excretion [2]. The skeleton cobalt ions moved to the trabecular bone surface and cortical bone surface. These ions finally move to bone volume [2]. 15% of cobalt ions remained in the skeleton [2].

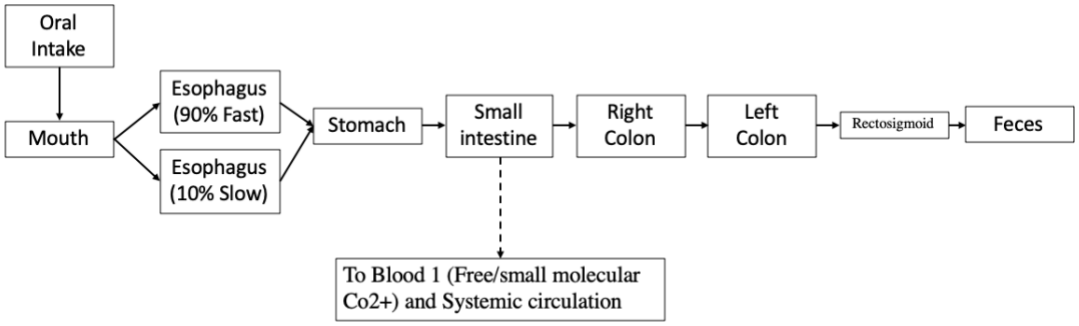

Figure 1.5.1: Pictorial description of ailment track model created by ICRP [1]. The dotted line describes a connection point between small intestines and blood used for systemic cobalt movement with an exposure point related to oral consumption of cobalt.

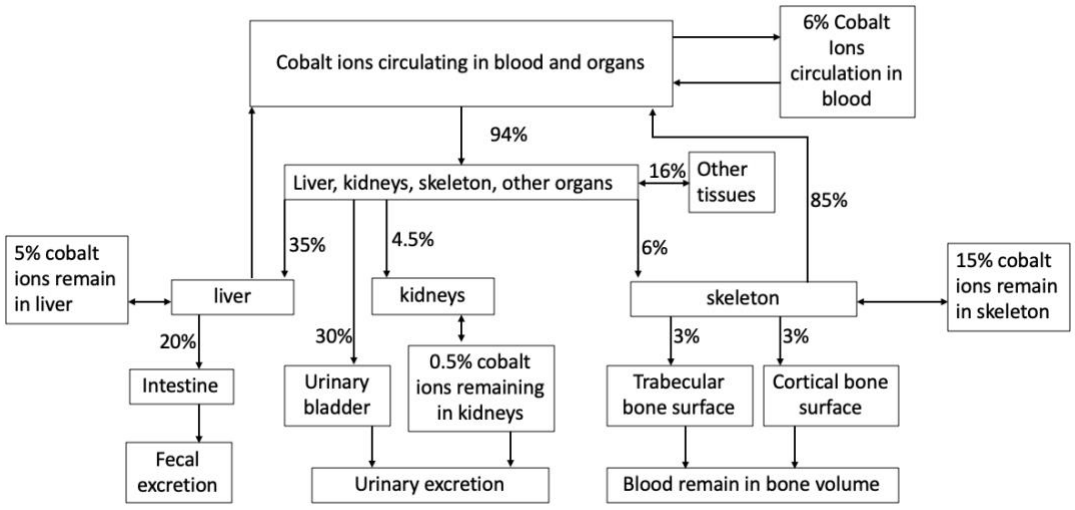

Figure 1.5.2: Pictorial description of the systemic model of cobalt movement throughout the body [2].

A more recent model by Unice et al. involved ten patients (five males and five females) who ingested about 1 mg of cobalt a day for three months [55]. The model describes the movement of cobalt from oral absorption to the blood, extravascular albumin bound cobalt, red blood cells, fecal excretion, and urinary excretion [55]. It has also been proposed that a similar first order kinetic model could be used to describe the movement of cobalt resulting from a total hip arthroplasty [56]. Within this model, a potential direct connection to the blood plasma and an indirect pathway through the periprosthetic tissue was proposed [56]. However, there were no assigned transfer coefficients within this model. These observations were useful in determining the final compartment layout and movement of cobalt in a TKA patient.

1.6 Overview of Specific Aims

1.6.1 Central Hypothesis

It was hypothesized that similar to THA, the in vivo use of TKA components would result in metal debris accumulating either locally or systematically in the body. It is also hypothesized that the biokinetics of the cobalt metal ions moving throughout the body from the joint capsule could be modeled using a pre-existing biokinetic model of inorganic cobalt.

1.6.2 Specific Aim 1: Determine and quantify the impact of in vivo use and patient factors on metal release in total knee arthroplasty (TKA) devices.

Analysis of total hip arthroplasty observed the degree of metal removed from implant surfaces and correlated it with biological concentrations of cobalt and

chromium [29]. Within this aim, it was assumed that this trend would be consistent for TKA. The causes for damage of metal components leading to metallic release were evaluated, specifically by looking at third-body damage using a semi-quantitative method. This method determined the severity and coverage of third-body damage on the bearing surface of the femoral components. It was hypothesized that metal release would be visible on retrieved cobalt-chrome femoral components.

1.6.3 Specific Aim 2: Identify if metal debris and its characteristics (tissue metal concentration, particle size, and particle shape) are uniform throughout the knee joint capsule.

Particle load, shape, and bioreactivity are critical features in describing metallic debris. The amount of metallic debris would be identified as a metal concentration within a specific tissue weight (mg/L or μg/L). This tissue would be digested within an acid cocktail and analyzed using inductively coupled plasma mass spectroscopy (ICP-MS). Specific regions around the synovial capsule were sampled to determine potential release zones around the artificial joint: the medial gutter, lateral gutter, supra patella, infra patella, and tibia. Cytokines were measured to describe the bioreactivity concerning particle load. Additionally, ASTM: F1877 was adhered to, to describe the particle shape through the aspect ratio, and size through the reported diameters. It was hypothesized that there would be a preferred location within the joint capsule for debris to collect. We hypothesized that this would be the medial and lateral gutters due to the proximity to the articulating surface.

1.6.4 Specific Aim 3: Determine if an existing biokinetic model describing cobalt transport can be updated using literature studies to alter the exposure point and discuss the mobility of cobalt metal ions through the body of a TKA patient.

The model was calibrated using peripheral blood metal concentration and peri-prosthetic tissue metal concentration. There was a relationship between peri-prosthetic tissues and blood cobalt concentrations that connected to an existing model discussing the systemic movement of cobalt. The blood value needed to connect to the remainder of the system to account for the blood value's dynamic concentration. The amount of debris was greater within the joint capsule compared to the blood cobalt concentration and the peripheral organ cobalt concentration. This was described as a greater local burden instead of a systemic burden. However, altering the dosing of the model to simulate a fall or other exaggerated wear scenario showed values consistent with the elevated levels in MOM hip patients with adverse reactions.

Table 1.1: Chronological summary of literature related to postmortem retrieval analysis of total hip and knee arthroplasty.

AUTHOR (YEAR)	STUDY TITLE	PUBLICATION	STUDY GOALS	RESULTS
Jones et al. 1975 [40]	Cobalt Toxicity after McKee Hip Arthroplasty	The Journal of Bone and Joint Surgery	This study explored 7 patients with unsatisfactory McKee hip	• Patch testing revealed that 6 patients were cobalt-positive but nickel- and chrome-negative.

			arthroplasty devices and the significance of cobalt as a cause of symptoms.	• Macroscopic and histological analysis revealed bone necrosis, muscle necrosis and joint capsule necrosis in five patients.
				• Increased cobalt concentrations (determined by atomic absorption spectrophotometry) were observed.
				  o Cases 1,3, 4, and 5 had urinary cobalt measured in μg/L: 20, 26, 40 and 33 respectively.
				  o Case 1 had a joint capsule concentration of 19.5 mg/L.
				  o Cases 3 and 4 had bone concentration of 2.5 and 2.25 mg/L respectively.
				  o Case 1 also had Liver, Brain, Iliac crest, and kidney cobalt concentrations of 3 mg/L, 1 mg/L, 27mg/L, and 1 mg/L respectively.

Dobbs et al. 1980 [39]	Metal Ion Release After Total Hip Replacement	Biomaterials	Metal concentrations (cobalt, chromium, molybdenum, nickel, iron and zinc) were measured using neutron activation analysis in tissue taken from an 81-year-old female at necropsy who had bilateral cobalt	• Measurements indicated that the concentrations of Co and Cr in the organs was high compared to a standard individual. o Lung (Co: 0.24 mg/L, Cr: 0.18 mg/L), kidney (Co: 0.31 mg/L, Cr: 0.39 mg/L), liver (Co: 0.47

			chromium molybdenum (Co-Cr-Mo) total hip replacements. • A M-o-M arthroplasty (14 years in vivo) • A M-o-P arthroplasty (5.5 years in vivo)	mg/L, Cr: 0.61 mg/L), and spleen (Co: 0.23 mg/L, Cr: 0.56 mg/L). • Tissue near the M-o-M joint had heavy amounts of metal debris, compared to the M-o-P joint which appeared uncontaminated. • The concentration changed with distance from the implant.
Heekin et al. 1995 [57]	Morselized Allograft in Acetabular Reconstruction A Postmortem Retrieval Analysis	Clinical Orthopedics and Related Research	Study postmortem specimens treated with morselized allograft to better understand how it behaves in revision THA.	• Morselized allograft bone is useful in THA by restoring bone deficiency in acetabular defects. • The graft incorporates however the extent it incorporates can't be predicted accurately by postoperative radiographs.
Hosip-Flor et al. 1997 [11]	Human Postmortem Retrieval of Total Hip Arthroplasty	The Journal of Arthroplasty	Describe the retrieval procedure, including details on informed consent, and benefits of specimen analysis.	• The use of retrieval programs, in conjunction with establishing early family and patient cooperation, is useful for advancement in orthopedic science.
Lester et al. 1997 [58]	Cross-section Radiographic Analysis of 10 Retrieved Titanium Alloy Press-fit Femoral Endoprostheses	The Journal of Arthroplasty	Analyze retrieved titanium alloy femoral stems using cross-sectional radiographic analysis.	• Radiographic and clinical findings demonstrated the ability of the titanium alloy material and the design of the pressfit implant to achieve satisfactory primary and secondary stability in elderly patients.
Jacobs et al. 1998 [12]	Postmortem Retrieval of Total Joint Replacement Components	Journal of biomaterials research	Improve the understanding of clinical outcomes of orthopedic implants through the development of a procedure to	• It is possible to produce and utilize such a program to collect postmortem retrievals. • The continued collection of these devices has allowed key

			recruit successful implants still in place at the patient's death.	understanding for a variety of different study questions.
Urban et al. 2000 [59]	Dissemination of wear particles to liver, spleen, and abdominal lymph nodes of patients with hip and knee replacement	Journal of Bone and Joint Surgery	Study the distribution of debris particles for patients who had either total hip and knee replacement to see the prevalence and histopathological response in the liver, spleen, and abdominal paraaortic lymph nodes.	• This study showed a systemic distribution of metallic and polyethylene particles for patients with a previously failed implant and in those with a primary surgery. • The greater prevalence of particles for the liver or spleen was seen after reconstructions with mechanical failure. • The majority of patients had low particle concentrations and no apparent pathological importance. • One exception occurred with a patient that had heavy accumulation of wear debris from THA with mechanical failure.

Harman et al. 2001 [60]	Polyethylene Damage and Knee Kinematics After Total Knee Arthroplasty	Clinical Orthopedics and Related Research	Characterizes the relationship between in vivo knee kinematics and polyethylene damage.	• There was a noted correlation between damage location from retrievals and the contact location measured.
				  ○ The femoral contact and insert damage occurred mainly in the posterior half of the tibial insert.
				  ○ The largest damage patterns occurred where the femoral contact is the largest.
				• This study showed in vivo fluoroscopic analysis could help

				predict the damage location on polyethylene inserts.
Tonino et al. 2001 [61]	Hydroxyapatite- Coated Acetabular Components Histological and Histomorphometric Analysis of Six Cups Retrieved at Autopsy between three and seven years after successful implantation	The Journal of Bone and Joint Surgery	Study hydroxyapatite-coated acetabular components to determine implant fixation and biological reactivity to hydroxyapatite-particles.	• Cell-mediated hydroxyapatite resorption was thought to be the main cause of coating loss. • The coating showed a slow rate of resorption, without adverse tissue reactions.
Campbell et al. 2003 [21]	Autopsy Analysis Thirty Years after Metal-on-Metal Total Hip Replacement A Case Report	The Journal of Bone and Joint Surgery	Analyze the particle distribution and histological reactions cause by wear debris generated from McKee-Farrar Metal-on-Metal THA replacement.	• This study provided caution against newer generations of metal on metal implants and recommended increased surveillance of patients with these implants in 1st and 2nd generation.
Hirakawa et al. 2004 [13]	Mechanisms of Failure of Total Hip Replacements Lessons Learned from Retrieval Studies	Clinical Orthopedics and Related Research	Analyze retrieved components, in combination with histologic, radiographic, and clinical data to determine the mechanisms of biomaterial failure	• Local reactions to wear debris can initiate the formation of granulomatous tissue that ultimately resulting in aseptic loosening. • Small features such as cement mantle defects, noncircumferential porous coatings, and screw holes can act as pathways for granulomatous leading to implant loosening and osteolysis.
Urban et al. 2004 [62]	Accumulation in Liver and Spleen of Metal Particles Generated at Nonbearing Surfaces in	The Journal of Arthroplasty	Analyze 30 postmortem total hip arthroplasty patients to determine systemic migration of metal particles	• Wear particles from nonbearing surfaces can make up a large source of debris that disseminates to and accumulates in remote organs.

	Hip Arthroplasty		generated at nonbearing surfaces rather than the intended primary bearing surfaces.	○ These particles are in addition to particles from the primary bearing surfaces. • Serum and urine metal concentrations could help identify these patients with increased metal debris volume.
Mann et al. 2013 [63]	Peri-Implant Bone Strains and Micro-Motion Following In Vivo Service: A Postmortem Retrieval Study of 22 Tibial Components from Total Knee Replacements	Journal of Orthopedic Research	Measure the proximal tibial bone strain and implant-bone micro-motion	• Increased bone strain with long term in vivo service could contribute to loosening of TKRs by failure of the tibial peri-implant bone.
Zywiel et al. 2013 [22]	Fatal cardiomyopathy after revision total hip replacement for fracture of a ceramic liner	The Bone and Joint Journal	Case report of patient who died of cobalt-induced cardiomyopathy.	• The whole blood cobalt levels peaked at 6521 µg/l. • Implant retrieval analysis confirmed a loss of 28.3 g mass of the CoCr femoral head.

Chapter 2

2.1 Abstract:

Metal debris and ion release have raised concerns in joint arthroplasty. This study's purpose was to characterize the sources of metallic ions and particulate debris released from long-term (in vivo >15 years) total knee arthroplasty femoral components. A total of 52 CoCr femoral condyles were identified as having been implanted for more than 15 years. The femoral components were examined for the incidence of 5 types of damage (metal-on-metal wear due to historical polyethylene insert failure, mechanically assisted crevice corrosion at taper interfaces, cement interface corrosion, third-body abrasive wear, and inflammatory cell-induced corrosion [ICIC] or electrocautery damage). Third-body abrasive wear was evaluated using the Hood method for polyethylene components, and a similar method quantifying surface damage of the femoral condyle was used. The total area damaged by ICIC was quantified using digital photogrammetry. Surface damage associated with corrosion and/or CoCr debris release was identified in 51 (98%) CoCr femoral components. Five types of damage were identified: 98% of femoral components exhibited third-body abrasive wear (mostly observed as scratching, n = 51/52), 29% of femoral components exhibited ICIC damage (n = 15/52), 41% exhibited cement interface damage (n = 11/27), 17% exhibited metal-on-metal wear after wear-through of the polyethylene insert (n = 9/52), and 50% of the modular femoral components exhibited mechanically assisted crevice corrosion taper damage (n = 2/4). The total ICIC-damaged area was an average of 0.11 ± 0.12 mm2 (range: 0.01-0.46 mm2).

Although implant damage in total knee arthroplasty is typically reported concerning the polyethylene insert, the results of this study demonstrate that abrasive and corrosive damage occurs on the CoCr femoral condyle in vivo.

2.2 Introduction

The release of metal debris from modular and bearing surfaces in total hip arthroplasty (THA) has become a concern due to the potential for adverse biological reactions in the surrounding tissue [34]. The mechanisms of metal release in THA are primarily due to wear, electrochemical dissolution, or a combination of the 2 processes [34]. The CoCr alloys used in orthopedic devices rely on the formation of a passive film to prevent degradation of the alloy [64, 65]. The passive film is one of the key kinetic barriers preventing implant corrosion [34]. These films form and reform spontaneously on the metal surface; however, they are only effective if they can withstand fracture or abrasion caused by fretting, micromotion, applied stress, or if the films are exposed to conditions in which they can rapidly reform [34]. Although there is little literature describing the prevalence of metal release mechanisms in total knee arthroplasty (TKA), the metallic alloys used in TKA are largely the same as those used in THA [66].

Similar to THA, the CoCr femoral component in TKA can undergo material loss due to wear and/or corrosion, with the release of metal debris and metal ions. The theorized mechanisms of metal debris generation in TKA include: mechanically assisted crevice corrosion (MACC) of modular tapers [67], inflammatory cell-induced corrosion (ICIC) or electrocautery damage [68], degradation at the backside interface

with the bone cement layer [34, 64], scratching due to third-body debris (e.g., bone cement particles or metallic debris) [69-73], or complete wear through of the polyethylene tibial insert and subsequent metal-on-metal wear between the femoral condyle and tibial baseplate. Although many of these mechanisms have been studied in depth in THA, ICIC is a newly appreciated phenomenon. ICIC has recently been investigated in both THA and TKA by Gilbert et al. [68] and is described as a corrosive attack by inflammatory cells. However, the resulting scars could be caused by a surgical tool, an electrocautery device, which is frequently used during revision surgery [74]. Continued research regarding ICIC damage has commented on the differences between surgically derived ICIC scars and those thought to be produced from inflammatory cells [75].

At the time of the completion of this work, there was a lack of information on the prevalence, and clinical relevance of metal release in TKA prompted us to search our multi-institutional orthopedic implant retrieval program for femoral components from TKA that were implanted for more than 15 years. We elected to investigate long-term TKA femoral components because we hypothesized that these femoral components would be the most likely to have evidence of degradation.

In this study, we investigated the mechanisms of metal release from CoCr femoral components in TKA by analyzing a series of retrieved long-term retrievals. We asked: (1) what are the sources of metallic ions and particulate debris released from long-term (in vivo > 15 years) TKA femoral components; (2) what is the

prevalence and extent of affected surface area by ICIC; and (3) what is the extent of corrosion damage at the implant cement interface?

2.3 Experimental Design

2.3.1 Clinical Demographics and Implant Characterization

Between 2000 and 2014, more than 2700 TKA systems (consisting of all or some components, depending on availability, including femoral, tibial, and patellar components) were retrieved during revision surgeries as part of an institutional review board approved, multi-institutional orthopedic implant retrieval program. A total of 72 systems were identified as being implanted for greater than 15 years. Of these 72 systems, 20 of the femoral components were retained in the patient during revision surgery and therefore removed from this study. Thus, 52 CoCr femoral components were examined for damage mechanisms that could lead to release of metal debris or particles (Table 2.2.1). The femoral components were implanted for 18 ± 3 years (range: 15-33 years). The patient age at the time of implantation was 57 ± 11 years (range: 21-78 years). Twenty-eight of 52 patients (54%) were female. Seventy-seven percent of the femoral components were from a primary surgery (n =40/52). The systems were predominantly revised for loosening (n = 19/52: 37%), polyethylene wear (n = 15/52: 29%), instability (n =5/52: 10%), and pain (n = 4/52: 8%). Medical records were examined for evidence of metal release and adverse reactions to metal debris. Six patients (12%) had evidence of metallosis or reported metal-on-metal articulation resulting from wear-through of the polyethylene tibial insert.

Table 2.2.1: Clinical Information Corresponding to 52 Retrieved Long-Term (in vivo >15 years) CoCr Femoral Condyles

Clinical Information	
Patients	
Male	24
Female	28
Mean Age at Implantation	57 ± 11 (21-78) years
Mean Time ***in situ***	18 ± 3 (15-33) years
Primary Surgery	40
Reason For Revision	
Loosening	19
Polyethylene Wear	15
Instability	5
Pain	4
Other	9
Metallosis	5

Data are presented as mean ± standard deviation (range) or as a count (n).

The femoral condyles were all CoCr alloy and were from 5 manufacturers (in alphabetical order): Biomet (Warsaw, IN; n = 4/ 52), Depuy Synthes (Warsaw, IN; n = 13/52), Smith and Nephew (Memphis, TN; n =4/52), Stryker (Mahwah, NJ; n =13/52), and Zimmer (Warsaw, IN; n = 18/52). Eight of the fifty-two femoral condyles were fabricated with a porous coating (fiber mesh, n = 3and beads, n = 5) and were not cemented (Table 2.2.2). In 22 cases, porous coatings were used in conjunction with cement fixation including, beads (n = 14/52), plasma spray (n = 3/52), and fiber metal mesh (n = 5/52). The tibial trays were fabricated from historical

gamma air-sterilized ultra-high molecular weight polyethylene (UHMWPE) (n = 38), conventional gamma inert sterilized UHMWPE (n = 10), carbon fiber reinforced UHMWPE (Poly II, Zimmer, Warsaw, IN, [n = 3]), and 1 high-pressure crystallized (Hylamer-M, Depuy Synthesis, Warsaw, IN). None of the polyethylene components in this study were fabricated from highly cross-linked polyethylene.

Table 2.2.2: Device Information Corresponding to 52 Retrieved Long-Term (in vivo >15y) CoCr Femoral Condyles

Device Information	
Number of CoCr Femoral Components	52
Number of porous coatings	22
Porous coatings	
Beads	14
Plasma Spray	3
Fiber Mesh	5
Polyethylene Inserts	
Historical	38
Gamma inert sterilized	10
Carbon-fiber reinforced	3
Hylamer-M	1
Manufacturers	
Biomet (Warsaw, IN)	4
Depuy Synthes (Warsaw, IN)	13
Smith and Nephew (Memphis, TN)	4
Stryker (Mahwah, NJ)	13
Zimmer (Warsaw, IN)	18

Data are presented as counts.

2.3.2 Identification of Damage Mechanisms

Before examination, the femoral components were first cleaned and disinfected in 2 consecutive soaks (20 minutes) with 1:10 ratio of detergent (Discide; AliMed, Dedham, MA) to water solution. The femoral components were then placed in a sonicator for 20 minutes in water to remove any loose debris. Visual inspection (with the naked eye and/or up to 10 magnification with a stereomicroscope) of the femoral components revealed 5 predominant damage mechanisms that could result in the production of metal debris or the release of metal ions. Abrasive wear mechanisms included scratching (due to third-body wear debris particles) and complete wear-through of the polyethylene component resulting in metal-on-metal articulation between the femoral condyle and the tibial baseplate. Corrosive damage mechanisms that were noted included ICIC, MACC in modular tapers, and discoloration of the backside of the femoral component at the interface with the cement layer.

Third-body abrasive wear was semi-quantitatively assessed by inspecting the articulating surfaces (the polyethylene insert and the CoCr femoral condyle) using a modified Hood method only inspecting for third-body wear [76]. For the polyethylene insert, 3 independent observers inspected 8 zones (4 quadrants on each condyle) of the bearing surface for 7 damage modes: burnishing, pitting, delamination, abrasion, embedded debris, scratching, and surface deformation [76]. Any discrepancies between observers were resolved in a meeting among the investigators. For each zone and each type of damage, a score ranging from 0 to 3 was assigned, depending on the

severity of damage of each damage mode. A score of 0 indicated no damage, a score of 1 indicated damage that covered less than 10% of available area, a score of 2 was given when a damage mode covered between 10% and 50% of the surface, and a score of 3 was given when a damage mode covered more than 50% of the surface [76]. Polyethylene failure was defined as full wear through of the polyethylene insert allowing for metal-on-metal articulation. Similarly, the bearing surface of the CoCr femoral component was divided into quadrants and scored for damage by the same 3 investigators (Figure 2.2.1). We assessed each quadrant of the bearing surface femoral components for 3 damage modes: scratching, indentations or lacerations, and pitting. A score of 1 described damage that covered less than 10% of the surface, a score of 2 described damage that was present over 10%-30% of the surface, a score of 3 described damage that covered 30%-50% of the surface, and a score of 4 described damage that covered more than half of the surface.

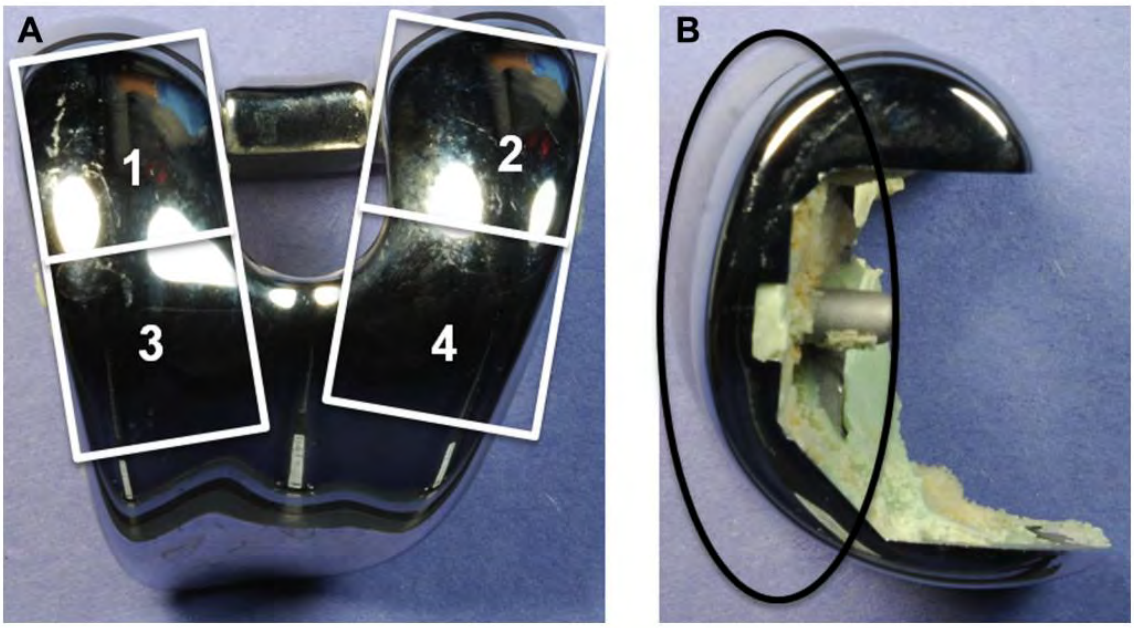

Figure 2.2.1: Each CoCr femoral component was evaluated using a semi-quantitative scoring method for scratching and pitting. (A) The bearing surface was split into posterior (numbers 1 and 2) and anterior (numbers 3 and 4) regions. The medial and lateral regions of the condyles were scored separately resulting in a total of 4 quadrants to describe the condition of the bearing surface. (B) A side view of the primary bearing regions (enclosed within the black oval) that were evaluated.

To identify regions of ICIC damage, components were initially screened via visual inspection at low magnification by two investigators. Regions of interest were identified as having a frosted or discolored appearance. ICIC in these regions was subsequently confirmed using optical microscopy and scanning electron microscopy (SEM, Environmental Scanning Electron Microscope, XL30; FEI, Hillsboro, OR) by looking for characteristic features of ICIC. The affected area includes features that are

interconnected and give the impression of a cell moving on the surface. These features can include a combination of circular crater-like morphologies and irregular crater-like morphologies. These features were 10-100 microns in length, which is consistent with the size of a cell [68]. The extent of ICIC damage was estimated using digital photogrammetry [77]. The area affected by ICIC was confirmed using optical microscopy and outlined using a permanent marker. Images were taken using a digital single-lens reflex camera with a calibrated ruler in the same focal plane as the affected surface. Using commercial computer software (Adobe Photoshop; Adobe Systems Inc, San Jose, CA and GIMP 2.8.14), the affected area was digitally isolated. Using the known pixel dimensions, the affected area was calculated in mm^2. If there were more than 1 region with ICIC on the implant, the regions were summed to obtain a cumulative affected area.

Adhered cement on nonporous devices was removed to evaluate the damage between the cement mantle and backside of the femoral components. To remove the cement, the femoral components were boiled in toluene for 2-3 hours depending on the cement thickness and quantity. After boiling in toluene, the femoral components were sonicated for 10 minutes to remove any residual cement. To ensure that this process did not cause damage to the present study's implants, retrieved components without cement that were unrelated to this study, were subjected to the toluene boiling procedure. The implants were examined before and after boiling. There was no evidence of damage caused by the boiling procedure on these components. After

boiling and sonication, the components were visually inspected for signs of corrosion, staining, and discoloration [34, 64].

A fretting corrosion evaluation was conducted on CoCr femoral condyles that had a modular junction (n = 4). The junctions were visually inspected for evidence of fretting corrosion damage that was characterized using a modified semi-quantitative score adapted from the Higgs-Goldberg method [65, 78]. Within this scoring system, a score of 1 was assigned when the damage was considered minimal, which indicated fretting on less than 10% of the surface. A score of 2 was used to describe mild damage indicating fretting that occurred on more than 10% of the surface. The score of 3 was used to describe moderate damage. A score of 3 was given when fretting occurred on more than 30% of the implant surface with an aggressive local corrosion attack. Finally, a score of 4 was used to describe severe fretting on more than 50% of the surface and a severe corrosion attack with abundant corrosion debris. The femoral components were independently evaluated by 3 experienced investigators. Any differences among these investigator's damage scores were resolved in a conference, resulting in a final damage score for each component.

2.3.3 Statistical Analysis

Depending on the analysis, the data in this study both continuous and ordinal. For continuous variables, we determined that the data were not normal using Shapiro-Wilk test. Therefore, we used nonparametric descriptive statistics for both ordinal and nonmoral data. As such, we report the median and interquartile range throughout this study.

2.4 Results

Surface damage indicative of corrosion and/or wear of the CoCr femoral condyles was identified in 51 of the 52 (98%) femoral components. The 3 most prevalent damage modes were third-body wear, ICIC damage, and discoloration at the cement interface. Fifty-one of the 52 femoral components (98%; Figure 2.4.1) exhibited some third-body wear, 15 femoral components (29%; Figure 2.4.1) had ICIC damage, and 9 of the femoral components (17%; Figure 2.4.1) exhibited wear-through of the polyethylene component resulting in metal-on-metal articulation. Eleven of the 27 (40%; Figure 2.4.1) nonporous-coated femoral condyles had evidence of cement interface degradation in the form of inferred corrosion through noted discoloration, and 2 of the 4 (50%, Figure 2.4.1) modular femoral components had moderate-to-severe MACC taper damage (score 3). Third-body wear (primarily in the form of scratching on the CoCr femoral components) was the most prevalent damage mechanism (Figure 2.4.2). Mild damage was observed in 20 of the 52 (38%) femoral components (score of 1), moderate damage was observed in 19 of the 52 (37%) femoral components (score of 2), and severe damage was observed in 12 of the 52 (22%) femoral components (score of 3). The corresponding polyethylene damage scores for each quadrant of the bearing surface were predominantly a score of 3 of a maximum score of 3 (n = 34/38; 89%), indicating severe damage.

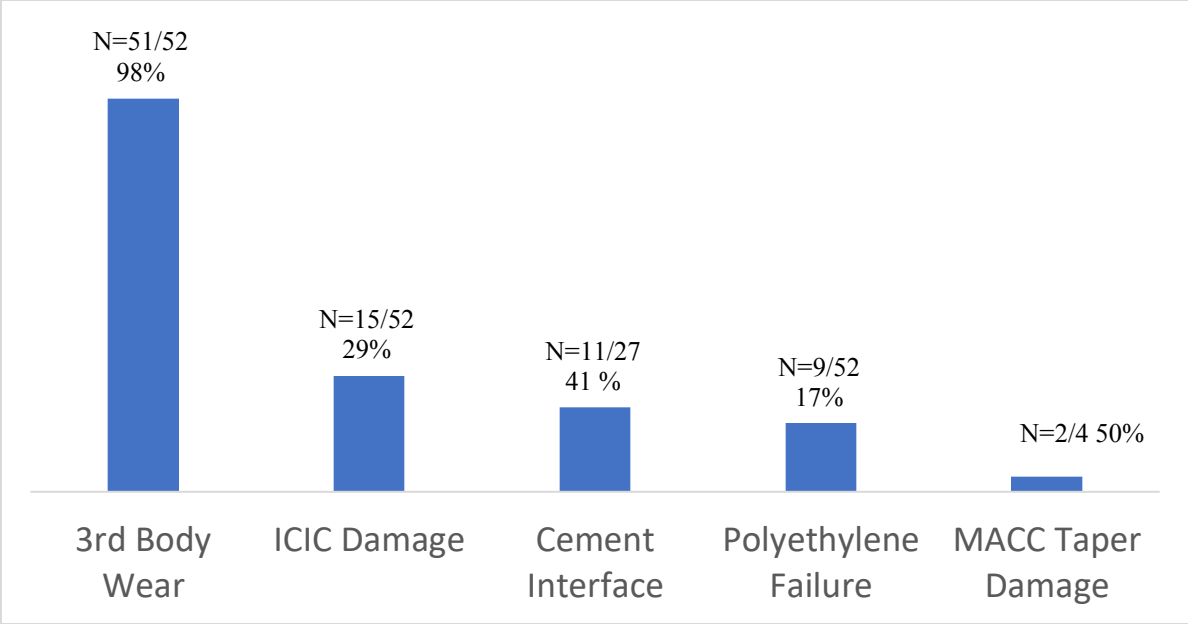

Figure 2.4.1. Third-body wear (typically in the form of scratching, n = 51/52), inflammatory cell induced corrosion (ICIC) damage (n = 15/52) and damage at the cement mantle implant interface (n = 11/27) were the most prevalent of the damage modes. Polyethylene wear-through (n = 9/52) and mechanically assisted crevice corrosion (MACC) taper damage (n = 2/4) were also observed.

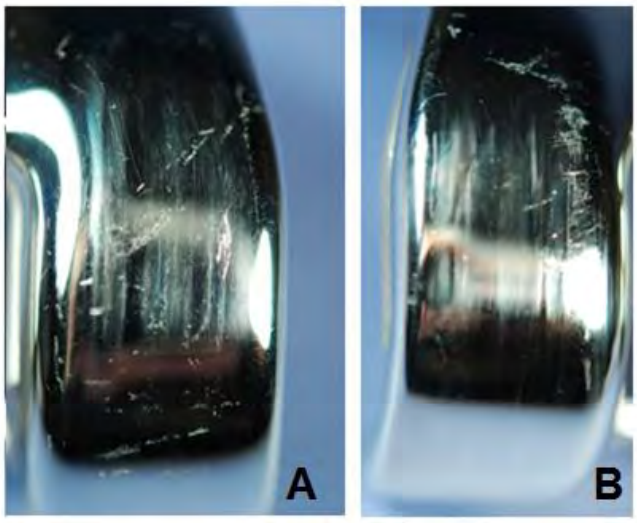

Figure 2.4.2: Examples of severe third-body damage and scratching on the bearing surface. (A) Vertical plowing with erratic scratching throughout the left bearing surface. (B) Aggressive plowing with erratic scratching toward the left of the bearing surface.

ICIC was identified on the bearing surface of 29% (n = 15/52, Figure 2.4.3) of the CoCr femoral components. Suspected affected areas (Figure 2.4.3 B) were observed up to 4000 magnification using digital optical microscopy (Figure 2.4.3 A). The confirmed ICIC damage consisted of circular pits and indentations that were interconnected with a spiraling or trailing morphology consistent with cell movement on the surface (Figure 2.4.3 C). The median cumulative area with ICIC damage was 0.07 mm2 (interquartile range: 0.12 mm^2, Figure 2.4.3 D).

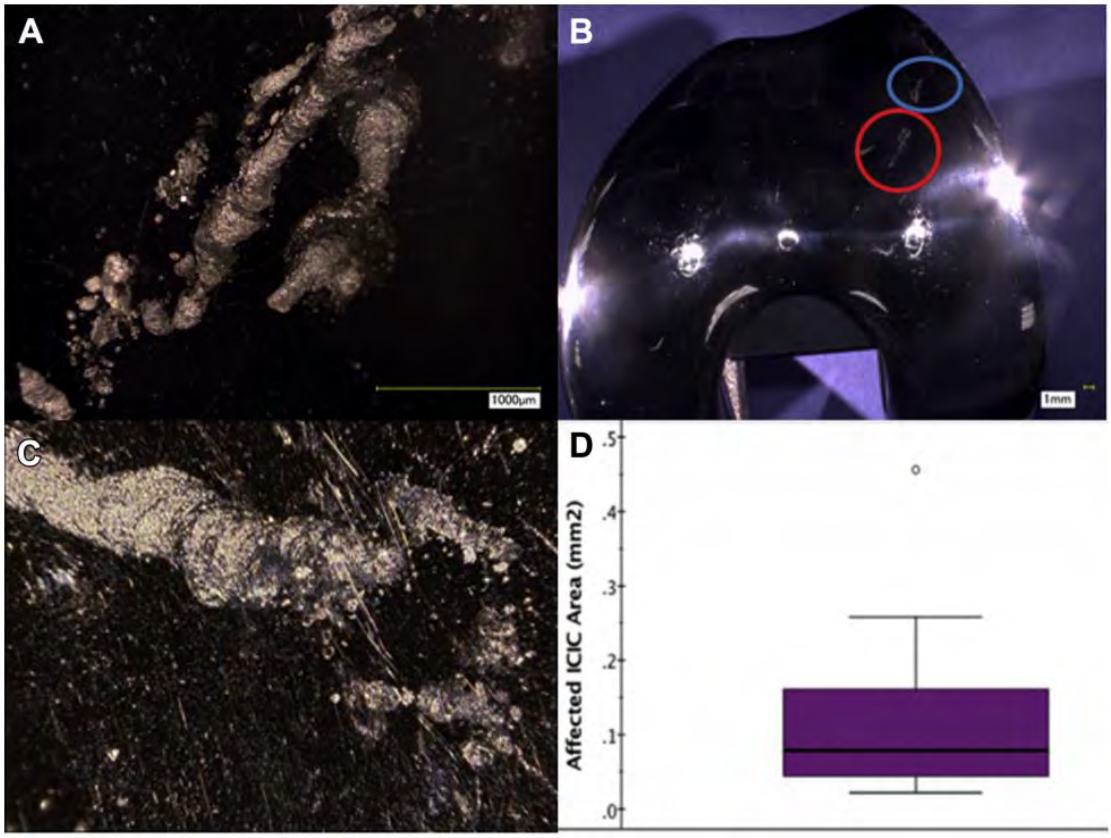

Figure 2.4.3: (A) High magnification digital photograph of the region circled in red in (B) revealing the circular damage scars that are associated with ICIC [3]. (B) Digital photography of a femoral condyle that illustrates the macro appearance of the ICIC affected area (circled in red and blue), which have a frosted appearance. (C) Three-dimensional stacked image created using digital photograph of ICIC damage in circled blue region. (D) The ICIC damage area varied among the femoral components. The median area that was affected by ICIC was 0.07 mm^2 (interquartile range: 0.12 mm^2).

Twenty-seven of the femoral components did not have a porous backside, which allowed for optical observations of corrosion at the interface. Discoloration, staining, fretting scars, or blackened debris were observed in 11 of 27 femoral components (41%, Figure 2.4.4 A and B)

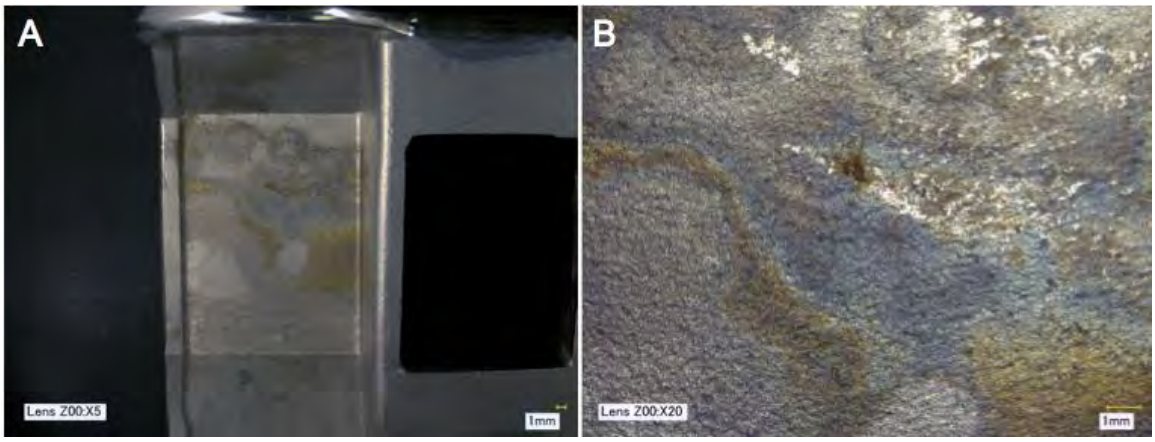

Figure 2.4.4: (A) Macro photograph of corrosion between the cement mantle and backside of a femoral component. (B) Digital micrograph of the damaged region, showing discoloration.

2.5 Discussion:

The release of metal ions and debris has been identified in THA as a concern due to its association with adverse local tissue reactions (ALTRs) in a subset of patients [34]. Although less prevalent, ALTRs have also been seen within TKA. Although TKAs are fabricated from the same materials as THA, symptoms of metal

sensitivity present predominantly in two ways, dermatitis and or synovitis of the knee [79, 80]. Similar to THA[29], the symptoms of metal sensitivity can be resolved by removal of the metallic implant [81]. Additionally, there is evidence of blood metal levels increasing post TKA procedure [5, 82, 83]. The purpose of this retrieval study was to investigate the prevalence of metal release in long-term implanted (>15 years in vivo) TKAs. We found evidence of metal release or corrosive damage in 51 of the 52 (98%) femoral components in this study. The results of this study indicate that the most prevalent forms of ion or metallic debris release were of third-body wear (present in 98% of the components, n = 51/52), ICIC damage (present in 29% of the components, n = 15/52), and damage at the cement mantle interface in nonporous implants (present in 41% of the components, n = 11/27). In addition, polyethylene wear-through was observed (present in 17% of the components, n = 9/52) and MACC taper damage in 50% of the modular implants (n = 2/4).

There were limitations in this study. Only CoCr femoral components that were implanted for greater than 15 years were included in this study, and therefore, the incidence of these damage mechanisms in short-term components remains unclear. We chose implants that were in vivo for an extended period of time because we reasoned that these implants would be most likely to have evidence of damage and/or corrosion. However, due to the long-term duration of these TKA systems, all but 14 of the tibial inserts were fabricated from historical gamma air-sterilized polyethylene (with the remaining 3 components being fabricated from carbon fiber reinforced polyethylene, 10 components being fabricated from gamma inert sterilized

polyethylene, and 1 being fabricated from Hylamer-M polyethylene). Given the improved wear and oxidative properties of newer polyethylene formulations, polyethylene wear through is less likely to appear with contemporary gamma inert sterilized and highly cross-linked polyethylenes. In addition, the damage scoring methods used in this study were semi-quantitative in nature. Although these methods do not help elucidate the volume of material lost, they can be effective in describing the extent of the damage and can be useful for qualitative comparisons to previous studies that used similar techniques. Finally, all these femoral components were retrieved components, restricting the cohort to only represent a population of implants that were revised or removed. However, in the absence of availability of implants recovered at autopsy, analysis of retrieved components remains the primary method by which to gain insight into the in vivo performance joint arthroplasties.

In this study, the most prevalent damage mechanism was scratching on articulating surface possibly caused by third-body debris (i.e., bone chips, bone cement, metallic debris, or carbides) [71]. Previous in vitro studies, have observed increased roughening of the femoral surface, specifically in the form of scratches with the addition of third-body wear debris, bone and poly(methyl methacrylate) particles [73]. These observations were supported by in vivo analysis showing that roughness values for medial and lateral sides of the device were significantly rougher when compared to control components [72]. Retrieval studies have also compared femoral components composed of either oxidized zirconium or cobalt chromium alloy. These studies have shown increased in vivo damage of the cobalt chromium component

[84]. Within this study they observed scratching, striations, pitting, and delamination on the surfaces of femoral components. Simulator studies suggested that scratching induces a rougher surface that leads to faster wear of the polyethylene components [72, 85]. Kretzer et al [86] performed a simulator study in the absence of third-body debris using all polymer bearings within the simulator allowing the resultant metallic wear to be solely from the CoCr implants. The study reported polyethylene (7.28 ± 0.27 mg/106 cycles) and metallic (1.63 ± 0.28 mg for cobalt, 0.47 ± 0.06 mg for chromium, 0.42 ± 0.06 mg for molybdenum, and 1.28 ± 0.14 mg for titanium) wear, reporting 12% of the wear weight as metallic debris [86]. The absence of third-body debris made the authors speculate that this wear could be due to carbides removed from the bulk alloy [86].

Retrieval studies have shown that a relationship exists between third-body particles, increased polyethylene wear, and increased roughness of the CoCr femoral condyle [69, 70]. In the present study, we observed 9 cases of complete wear-through of the polyethylene insert. However, the polyethylenes used in these explants were either gamma air sterilized unfilled polyethylene or carbon fiber reinforced polyethylene. Both these materials are susceptible to oxidative degradation [87-89], which can accelerate the wear processes of polyethylene. Thus, it is unclear whether the polyethylene failures were due to oxidative degradation, third-body wear of the condyles, or a combination of the 2 processes. Future research investigating the effect of articulating CoCr femoral component roughness against wear and oxidative resistant materials (e.g., gamma inert sterilized UHMWPE or highly cross-linked

polyethylene) should elucidate the impact of scratching on the wear performance of polyethylene tibial inserts.

In this study, we observed evidence of ICIC on 29% (n = 15/52) of the long-term TKA femoral components. In a study of metal-on-polyethylene THAs, metal-on-metal hips, and knee components, Gilbert et al [68] observed ICIC on 74% (n =51/69) of the components studied. The theory behind ICIC was that inflammatory cells release acid and reactive oxygen species scar the implant surface [68]. However, a separate study identified that similar scars can be created with the use of an electrocautery device [74], a tool frequently used during revision surgery. Additionally, the presence of iron nodules within the scarred region were cited as evidence of a Fenton reaction [68]. These iron collections could also be due to the electrocautery device which contains iron. A separate study showed that in vivo identified ICIC damage was rougher when compared with in vitro induced electrocautery device damage [75]. Although evidence of ICIC or electrocautery damage was observed in nearly a third of the long-term knees in our collection, the damage did not cover a large area. We estimated that ICIC damage covered 0.11 ± 0.12 mm2 (range: 0.01-0.46 mm^2) of surface area. This is a small percentage of the surface area of a femoral condyle that is typically on the order of thousands of square millimeters. At this time, it is unknown how ICIC or electrocautery damage affects clinical outcomes or whether devices with these scars fare poorer. In addition to ICIC, we observed MACC in 2 of the 4 (50%) CoCr femoral components in this

series. Owing to the limited sample size of components with modular stems in the study, it is difficult to draw conclusions from this finding.

One other source of degradation identified in this study was damage at the backside interface of the femoral component and the cement layer. This was observed in 11 of the 27 (41%) retrievals in this study. The subset of 27 of the 52 total components represent femoral components that did not have a porous backside. Although there is little in the literature on this damage in TKA, several studies have looked at damage at the cement mantle interface in THA. Recently Bryant et al [64] conducted a study on retrieved THA stems to characterize failure mechanisms, one being damage between the cement mantle and femoral stem. Initial spot energy dispersive spectroscopy (EDS) analysis revealed debris collected on the cement particles with a Cr2O3 composition. EDS mapping also identified areas rich in Cr, O, and N, compared with clean bulk material [64]. The observations of Cr-rich oxides are products of fretting corrosion and are indicative of fretting corrosion of CoCr alloys. In a study of 25 cobalt alloy femoral THA femoral components, Jacobs et al [34] reported migrated foreign-body particles with the composition of CrPO4. The particles elicited a foreign-body tissue response through fibrosis, necrosis, and giant cells [34]. Owing to the nondestructive nature of the present study, EDS measurements were not available as the femoral components were too large to fit into the experimental chamber of our institution's SEM. However, we did observe discoloration that is indicative of corrosion (Figure 2.4.3 B). More research is required to understand the composition of these oxide films. However, the clinical

consequences of this damage are not clear, as it is unknown whether the corrosion products from the cement implant interface will be liberated and cause a foreign-body tissue reaction in TKA.

In summary, this study tracked the prevalence of five major damage mechanisms in long-term (in vivo >15 years) TKA femoral components that may lead to release of metal ions or debris. We observed the presence of both abrasive (scratching and third-body wear) and/or corrosive degradation processes (fretting corrosion indicated by discoloration, ICIC, and MACC) in 98% of the explants in this retrieval cohort, n = 51/52. The clinical implications of these findings are as yet unclear as the devices were not revised for ALTRs or biological reactions to CoCr. However, 6 of the 52 patients had reported observations of metallosis that was characterized as dark staining of the tissue surrounding the implant. In addition, some cases of loosening or pain may have been due to debris but was not recognized as such. Therefore, surgeons should be aware of these damage mechanisms that may affect the performance of TKA systems.

Chapter 3

3.1 Abstract:

Historically, implant wear debris has been described in terms of particle load, elongation of particles, and chemical reactivity of the material. To investigate these characteristics in terms of total knee arthroplasty and relevant materials, two cohorts were created. The initial cohort of twenty patients was analyzed to evaluate relationships between metal concentrations, inflammatory cytokines, component wear, tissue collection site, and tissue metallosis. The second cohort of three patients was analyzed to evaluate isolated metal particle size and morphology in relation to visible metallosis, sampling location, and alloy composition. Within the first cohort, the median metal concentrations were 16 μg/L for cobalt (range: 1.3 to 146.4 μg/L), 46 μg/L for chromium (range: 5 to 301.6 μg/L), and 9.8 μg/L for titanium (range: 0.6 to 98.7 μg/L). Increased cobalt concentration was associated with decreased TNFα (ρ= -0.56, p= 0.01) and IL-1β (ρ= -0.48, p= 0.03). Increased chromium concentration was associated with decreased TNFα (ρ= -0.47, p= 0.03), IL-6 (ρ= -0.43, p= 0.04), and MIP-3α (ρ= -0.47, p= 0.03). These findings did not support the hypothesis that tissue metal concentration would correlate with inflammatory cytokines, perhaps due to limitations associated with postmortem synovial fluid or increased cytotoxicity associated with large volumes of metal debris. Within the second cohort, the median particle diameter measured by nanoparticle tracking analysis was 162.5 nm (range: 62.5 - 999.5 nm). The median particle diameter was not significantly different across the five tested locations, and three different material pairings. The median micron-

sized particle equivalent circular diameter and weight of debris from 1um filter for all components was 1.3μm (range: 0.4-32.6 μm) and 0.5mg (range: 0.1 - 1.9 mg), respectively. The equivalent circular diameter was significantly different across the five tested locations ($p<0.001$) and three different material pairings ($p<0.001$). From the 1 μm filters, the particle shape was not significantly different between the three material pairings, and location. The weight of debris captured on the 1 μm filters correlated with the metallosis score ($\rho = 0.82$, $p = 0.002$). These findings support the hypothesis that there was no difference in microparticle morphology or nanoparticle diameter across sample regions and materials, though differences were observed for microparticle diameter. The particles isolated in this study were within the size range for phagocytosis (<10μm). In addition, particles from CoCr alloy components may elicit TNF-α and osteolytic inflammatory cytokines from macrophages.

3.2 Introduction

Metallic debris released from cobalt chromium (CoCr) alloy components has been a concern for total joint arthroplasty since the early 2000's, with increased visibility after the worldwide recall of ASR XL total hip arthroplasty (THA) metal-on-metal (MOM) devices in 2010 [90]. Evidence of metal debris became clear during revision procedures in which clinicians macroscopically observed gray or black discolored periprosthetic tissues, termed metallosis. Metallosis has been described as the infiltration of metallic debris into the periprosthetic tissue structures [36], with aseptic fibrosis or local necrosis associated with metallic corrosion and wear debris released into the synovium [91].

Quantitative characterization of periprosthetic metal debris has been performed for THA, based on particle load (i.e. dose), particle aspect ratio (i.e. shape), and chemical reactivity of the alloy [43, 92]. Particle load has been described using blood metal concentrations, periprosthetic tissue concentrations, and synovial fluid [37, 93], resulting in a recommended threshold of 7 parts per billion (ppb or μg/L) for cobalt and chromium in the UK [94, 95]. Periprosthetic metal concentrations measured in metal-on-metal THA range from 1.4 to 4604.0 μg/g metal content for Co, Cr and, nickel (Ni). Higher concentrations of metal (222 μg/g mean metal concentration) have been associated with a lymphocytic responses, while smaller concentrations of metal (3 μg/g mean metal concentration) have been associated with macrophage responses [37]. Cobalt and chromium ions have also been found in systemic bodily fluids such as urine, synovial fluid, and blood, although the concentrations have generally been much lower than the tissue surrounding the joint replacement (e.g. <1 μg/L) [38]. Cobalt and chromium particle size has been discussed with regards to particle phagocytosis specifically by macrophages, resulting in living macrophages with particles within, and fragmented dead macrophages surrounding [96, 97], with observations of needle-shaped particles ranging from 10-70 nm within the lymph nodes [97]. However, particles generated from metal-on-metal THA hard-on-hard bearings are generally round in shape [45, 92, 98], (Table 3.2.1). Chemically, CoCr alloy is a known sensitizing material [43] with the potential for in vivo tribocorrosion and release of metal, which may be associated with cytotoxic effects for fibroblasts, mononuclear phagocytes, and

lymphocytes [99], inhibition of osteoblasts and osteoclast cells [43, 99], or immune system activation through the formation of metal protein complexes [43].

Table 3.2.1: Brief literature review of metal particle characterizations in total hip arthroplasty and total knee arthroplasty

PUBLICATION AUTHOR (YEAR) JOINT	STUDY TITLE	MATERIALS AND METHODS	PROINFLAMMATORY	DEBRIS SIZE AND SHAPE	METALLOSIS
The Journal of Bone and Joint Surgery Lee et al. 1992 THA [100]	Size of Metallic and Polyethylene Debris Particles in Failed Cemented Total Hip Replacements	• An isolation method, in which metallic debris was extracted from the tissues, and a non-isolation method of routine preparation for light and electron microscopy was used to look at debris • All specimens were obtained at revision surgery from the periarticular tissues of failed, non-infected, cemented • 30 cases with femoral component titanium alloy (10), cobalt-chrome	• Examination of tissue sections showed metallic particulate debris both within histiocytes and sometimes extracellularly. • With TEM, metallic particles from CoCr were identified in intracellular and extracellular spaces • Ti debris differed from other metallic debris with angular or shard-shaped particles	• Mean size of metallic particles with the isolation method (short, long dimensions mean ± SD in um) ○ Ti 0.88±1.01, 1.64±1.95 ○ CoCr 0.86±1.05, 1.57±1.82 ○ SS 1.06 ±1.30, 1.79±2.07 • Mean size of metallic particles with non-isolation method (short, long dimensions mean ± SD in um) ○ Ti 0.30±0.13, 0.67±0.27 ○ CoCr 0.40±0.15,	NA

		alloy (10), or stainless steel (10).			0.69±0.28 ○ SS 0.36 ±0.12, 0.64±0.26 • Particle sizes (three different metals) were similar for each technique	
The Journal of Arthroplasty La Budde et al. 1994 TKA [51]	Particulate Titanium and Cobalt-chrome Metallic Debris in Failed Total Knee Arthroplasty	• Six cobalt-chrome alloy knees (1 woman, 5 men) • six titanium alloy knees (3 women, 3 men) • 4-8mm thick sections were taken from medial gutter and femoral epicondyle • 5um thick sections were stained with H and E	• Cobalt-chrome alloy particulate debris in the tissues appeared as small black spheres l-4 um in diameter • titanium alloy debris appeared as both black spheres l-4 um in diameter and flakes 10-20 um in length		• Mean size CoCr 101.9 um • Mean size Ti 925 um	Failures with metal-on-metal wear and well-fixed components were felt to represent a worst-case scenario of extreme metallosis
The Journal of Bone and Joint Surgery Case et al. 1994 THA [97]	Widespread Dissemination of Metal Debris from Implants	• 13 post-mortem subjects with a hip orthopedic device and 7 control subjects. • Compared subjects with metal implants with and without visible wear with an age-matched control group to determine the extent and effects of dissemination of wear debris. • Collected tissues: synovium, pelvic lymph	• The amount of metal in the lymph nodes, liver and spleen was greatest in cases in which the implant was loose and in which there was discoloration of adjacent tissues. • The highest concentrations of intracellular particles were found within the iliac lymph nodes, decreasing in number to the spleen and liver. • Lymph node particles were both intracellular and extracellular.		• Iliac lymph node particles containing chromium, cobalt and iron were needle-shaped and 10 to 70 nm in diameter. • Hydroxyapatite particles were present as crystalline aggregates with well-defined edges and 0. 1 to 5 μm in diameter. • Particles size allowed for phagocytosis: ○ Particles were seen in the vesicles of macrophage cytoplasm.	Five patients had dynamic hip screws, four had hip implants without obvious wear or tissue staining and four had obvious staining of local tissues by metal wear debris.

		nodes, para-aortic lymph nodes, liver, spleen, lung and hilar nodes, kidney, frontal cortex and bone marrow adjacent to the implant. • Light microscopy, TEM, SEM was used to investigate tissues. • ICP-MS was used to describe Al, Ti, Cr, Fe, Ni, Co, Ga, Zr, and Mo concentrations.		○ Titanium and nickel were detected within the vesicles. • In the liver and spleen, particles were seen within phagocytic cells and variable amounts in elongated, intracellular vesicles.	
Journal of Biomedical Materials Research: Doorn et al. 1998 THA [98]	Metal wear particle characterization from metal on metal total hip replacements: Transmission electron microscopy study of periprosthetic tissues and isolated particles	• 100-150 mg of periprosthetic tissue was collected from 13 patients undergoing revision MOM THA • Tissues were analyzed and particles were isolated and analyzed • Tissue was defatted, lyophilized, boiled in buffered solution (MOPS), digested in papain proteinase k digestion • Shape and size characterization with TEM	• Majority of CoCr MO wear particles were smaller than 50 nm (range 6–834 nm) and round to oval in shape with irregular boundaries. Smaller than reported PE particles size. • Less severe local tissue reaction to metal particles may result from corrosion, dissolution, and dissemination of metal particles.	• Particles were seen individually, as well as agglomerated, in both tissue sections and isolated preparations. • On the average, $6.7*10^{12}$, $4.9*10^{13}$, and $2.5*10^{14}$ particles were produced per year in three of the metal on metal prostheses that failed by aseptic loosening.	NA
The Journal of Arthroplasty	Accumulation in liver and spleen of metal	• light and electron microscopy	• Sub micrometer metal particles were identified	• 0.1 up to 8 micrometers	NA

Urban et al. 2004 THA [62]	particles generated at nonbearing surfaces in hip arthroplasty		with x-ray microanalysis • Particles were generated at nonbearing surfaces (Fretting at ancillary fixation devices, loose components, and modular connections).	in 11/15 patients with a revised arthroplasty and in 2/15 patients with primary hip arthroplasty • The macrophages formed focal aggregates in the organs without apparent toxicity.		
Journal of Biomedical Materials Research Part B: Applied Biomaterials Catelas et al. 2004 THA [101]	Comparison of in vitro with in vivo characteristics of wear particles from metal-metal hip implants		• Tissues from 7 patients with M-O-M hips were harvested at revision (1-43 months). • Wear particles were collected from 0 to 0.25 million cycles (run-in wear period) and 1.75 to 2 million cycles (steady-state wear period). • Particles were centrifuged and embedded in epoxy resin. Particle characterization occurred with TEM, and EDXA.	• NA	• simulator particles were round to oval, but a substantial number of needle-shaped particles were also found, especially from 0 to 0.25 Mc. • Particles generated from 0 to 0.25 Mc had an average length of 53 nm, whereas those generated from 1.75 to 2 Mc had an average length of 43 nm. • two patients at 23 and 43 months were the most comparable in composition, average length (57 nm), and shape to particles generated in the hip simulator during the run-in wear period.	
The Knee De Baets et al. 2008	Analysis of third body particles generated during total knee arthroplasty: is		• Seven patients primary cemented TKA	• The presence of metal debris is limited, and contributes only 1.5% to the total amount	• Average debris consisted of 75.8 mg of bone particles (range 41.2–109.3 mg), 57.2 mg (range	NA

TKA [71]	metal debris an issue?	• Debris quantity was measured at the end of the operation immediately before closure. The debris was retrieved using pulsed irrigation with 1 l of normal saline.			31.2–83.9 mg) of cement particles, and 1.96 mg (range 0–7.2 mg) of metal particles. • On average the total amount metal debris was 1.5%	
Journal of Biomedical Materials Research Part A: An official Journal of the Society of Biomaterials MiloŠey et al. 2009 THA [102]	In vivo production of nanosized metal wear debris from tribochemical reaction as confirmed by high resolution TEM and XPS Analysis	• Periprosthetic tissue was collected during revision surgery • Particles were isolated from frozen tissues using enzymatic protocol • Particles were characterized with TEM, SEM and EDS	• NA		• Needle-shaped particles ranged from 40 to 120 nm and contained both Co and Cr. • Globular particles ranged up to 90 nm and contained high levels of Cr and no Co. • Ti- and Ca-based particles were also identified.	NA
Nanomedicine: Nanotechnology, Biology and Medicine Xia et al. THA 2011 [96]	Characterization of metal-wear nanoparticles in pseudotumor following metal-on-metal hip resurfacing	• Samples were collected at biopsy for a typical case of pseudotumor following metal-on-metal hip resurfacing • light and transmission electron microscopy, backscatter scanning electron microscopy and energy dispersive x-ray spectrometry (EDS).	• Metal nanoparticles (NPs) were observed exclusively within phagosomes of living macrophages and fragments of dead macrophages. • Although dead fibroblasts were found to be juxtaposed with dead and disintegrated macrophages, the NPs were not seen within either live or dead fibroblasts. • Chromium (Cr) but not cobalt	• Nano particle sized	Heavy macrophage infiltration was observed in black pigmented specimens

	(Co) was the predominant component of the remaining wear NPs in tissue.	

Despite this knowledge of periprosthetic metal concentrations and related adverse reactions for THA, similar understanding for total knee arthroplasty (TKA) is limited. With over 700,000 primary and revision TKA procedures occurring annually in the United States [6], understanding the effects of metal release in TKA is critical. TKA failure, often requiring a revision procedure, is a multifactorial issue which may be influenced by surgeon technique, implant characteristics, and patient factors [7]. Failures attributed to metal reactions include hypersensitivity to ionic metals, foreign body reactions to wear debris particles, and responses to metal corrosion products [8], which can exhibit as hypersensitivity or dermatitis [9]. Similar to THA, inflammatory response in total knee arthroplasty is thought to be related to particulate load and material [103]. Clinically, metal sensitivity can present itself in two ways, dermatitis and/or synovitis of the knee [79, 80], which in many cases has been reported to resolve after removal of the sensitizing metal component. Additionally, there is evidence of blood metal levels increasing post TKA procedure [5, 82, 83]. One study analyzed six patients with a CoCr TKA device and six patients with a Ti alloy TKA [51]. They observed particles shaped like black spheres (1 to 4 μm) for both alloys and flakes of Ti alloy (10-20 μm in length). Few previous studies have analyzed particle shapes of metallic debris collected from in vivo TKA, and differences

between tissue sampling locations have, to the author's knowledge, never been reported.

During the first cohort study, we investigated the relationship between measured periprosthetic tissue metal ion concentration and sample location, inflammatory cytokines, and implant damage in TKA. We hypothesized that metallic debris would preferentially collect in the medial and lateral gutter tissue samples and that the metallic debris would be correlated with inflammatory cytokines shown to adversely affect bone homeostasis. We asked: (1) Is there an association between sampling region and metal concentration; (2) How much metallic debris collects in the medial gutter, lateral gutter, inferior patella, superior patella, and tibia after TKA; and (3) Is there an association between tissue metallosis and tissue metal concentration? Finally, we asked (4) Is there a correlation between tissue metal concentration, implant damage, and inflammatory cytokines?

During the second cohort study, we sought to confirm whether a validated isolation method, previously used in fetal calf serum [104] and adapted for application to animal tissue [46], would also allow successful isolation of metal wear particles from human peri-prosthetic tissues. These methods were chosen due to their ability to recover metallic wear particles (densities greater than 1.6 g/cm3) free from contamination and with high recovery of particles in low wear rate situations [46, 104]. We investigated the association between periprosthetic tissue metal debris, sampling location, and metallosis, and determined whether the debris size and shape would have the potential to elicit an immune response. We hypothesized that the

metallic debris shape and sizes would be statistically different between locations. We asked the following questions: (1) Does the weight of isolated debris captured on 1 μm nucleopore polycarbonate filters correlate with visible tissue metallosis; (2) Is there an association between sampling region and the diameter or estimated shape of isolated periprosthetic tissue metal debris; (3) Is there an association between the metallic alloys present in the TKA device and the diameter or estimated shape of isolated periprosthetic tissue metal debris.

3.3 Experimental Design

3.3.1 First Cohort (n=20) Patient Demographics and Implant Characterization

Twenty-seven necropsy TKA devices were collected as part of an IRB-approved orthopaedic implant retrieval program. Because this study evaluated metal ion concentrations, the cohort was limited to patients with CoCr femoral components with a tibial tray and tibial insert. The resulting cohort consisted of 20 patients. The following companies manufactured these devices: Cintor (n=1), Smith and Nephew (n=3), Stryker (n=4), Depuy Synthes (n=5), and Zimmer Biomet (n=10). Additionally, 35% (n = 7/20) of the tibial trays were composed of CoCr, and 20% (n = 4/20) were a mobile bearing design (Table 3.3.1). Although there was limited patient data, the following information was available: estimated implantation time (n=12), cause of death (n=20), gender (n=20), age at death (n=20), and surgical site (n=20) (Table 3.3.1). The mean estimated implantation time was 20 years (interquartile range=6; range: 6 to 45 years). The main causes of death were cancer-related (n=12), heart disease-related (n=2), COPD (n=1), stroke (n=2), and other

(n=3). Patients had a median age at death of 77 years (IQR=62; range: 62 to 93 years). Seventy percent (n = 14/20) of the cohort was female, and 65% (n=13/20) of the study cohort was implanted on the right side.

Table 3.3.1: Description of device design, device features, and patient factors included within the necropsy cohort. Within this table F-75 and Ti6-4 refer to implant materials, specifically cobalt chromium alloy and titanium alloy respectively.

IMPLANT REFERENCE NUMBER	MANUFACTURER	DESIGN	INSERT STYLE	TRAY MATERIAL	CONDYLE MATERIAL	AGE (YEARS)	SURGICAL SITE	SEX	CAUSE OF DEATH	ESTIMATED IMPLANTATION TIME (YEARS)
1	Biomet	Vanguard	Fixed	F-75	F-75	77	R	F	Other	NA
2	Depuy	Sigma Mobile Bearing	Mobile	F-75	F-75	78	L	M	Cancer	NA
3	Depuy	Sigma Mobile Bearing	Mobile	F-75	F-75	78	R	M	Cancer	NA
4	Depuy	LCS Mobile Bearing	Mobile	F-75	F-75	66	L	F	Heart Failure	NA
5	Depuy	AMK	Fixed	Ti6-4	F-75	62	L	M	Cancer	45
6	Depuy	LCS Mobile Bearing	Mobile	F-75	F-75	66	R	F	Heart Failure	NA

7	Smith and Nephew	Genesis	Fixed	Ti6-4	F-75	79	L	F	Cancer	NA
8	Smith and Nephew	Unknown	Fixed	Ti6-4	F-75	63	L	F	other	31
9	Smith and Nephew	Genesis	Fixed	Ti6-4	F-75	79	R	F	Cancer	NA
10	Stryker	Scorpio	Fixed	F-75	F-75	71	R	F	Lung	11
11	Stryker	Scorpio	Fixed	Ti6-4	F-75	83	R	F	Cancer	22
12	Stryker	Triathlon CR	Fixed	F-75	F-75	93	R	M	Stroke	NA
13	Zimmer	Nexgen LPS Flex	Fixed	Ti6-4	F-75	80	R	F	Cancer	11
14	Zimmer	Nexgen LPS	Fixed	Ti6-4	F-75	65	R	M	Cancer	15
15	Zimmer	Natural Knee	Fixed	Ti6-4	F-75	89	L	F	Other	10
16	Zimmer	Nexgen LPS Flex	Fixed	Ti6-4	F-75	62	R	F	Cancer	7
17	Zimmer	Nexgen LPS Flex	Fixed	Ti6-4	F-75	76	R	F	Stroke	10
18	Zimmer	Nexgen LPS Flex	Fixed	Ti6-4	F-75	62	L	F	Cancer	6
19	Zimmer	IB II	Fixed	Ti6-4	F-75	68	R	F	Cancer	45
20	Zimmer	Nexgen LPS	Fixed	Ti6-4	F-75	79	R	M	Cancer	21

3.3.2 ICP-MS Analysis of Peri-prosthetic Tissue

Each patient had five tissue samples collected from around the joint capsule. One sample each was taken from the medial and lateral gutter located on the medial and lateral sides of the femoral component bearing region. One sample each was taken from the inferior and superior patella regions, situated above and below the patellar tracking region along the femoral component. Finally, one sample was taken from the tibia region, located anterior to the tibial tray. Tissues were initially stored in Umfix tissue fixative (Sakura Finetek, Netherlands) before analysis. Samples were washed with ethanol (100 v/v) twice before being stored in ethanol (100 v/v) at refrigerated temperatures (~4˚C). Tissues were visually inspected for metallic debris, and samples with noticeable blackened staining or grey regions were considered indicative of metallosis. The degree of tissue discoloration was documented as either having or not having metallosis.

Prior to handling specimens and performing digestions, equipment and supplies that came into direct contact with the samples were soaked overnight in an acid solution (10% trace metal nitric acid in ultrapure water) to remove trace amounts of metallic debris. Portions of tissue from each anatomical location were then cut with a ceramic knife to achieve a mass of approximately 0.25 grams per tissue sample. Samples were first washed in ultrapure water to remove ethanol, followed by acid digestion using a modified method from Kerger et al. [105].

Digestion was performed in a water bath set to 95°C for 4 hours in an acid solvent that was composed of 2 ml 70% w/w trace metal grade nitric acid (Fisher

Scientific, cat. A509P212), 1 ml 30% w/w hydrogen peroxide (Ricca Chemical Company, cat. 3821.7), and 3 ml 37% w/w trace metal grade hydrochloric acid (Fisher Scientific, cat. A508P212). Three blank acid samples were also processed in parallel to determine baseline levels of metals in the solvent. One ml digest was aspirated and transferred to 1 ml ultrapure water. The 2 ml sample was then evaluated by inductively coupled plasma mass spectrometry (ICP-MS) analysis (Brooks Applied Labs; Seattle, WA) to determine concentrations of cobalt, chromium, and titanium. Averaged metal ion concentrations collected from the blank samples were subtracted from the samples to account for background ion levels. The digestion method was validated using a solid biological matrix certified reference material (Luts-1, National Research Council of Canada; certified for cobalt and chromium concentrations). Concentrations were reported in μg/L.

3.3.3 Synovial Fluid Cytokine Analysis

Before retrieval of the orthopaedic devices, synovial fluid was aspirated from the joint around the device for 19 out of the 20 patients. One patient did not have enough synovial fluid for analysis and was not included in this part of the study. Synovial fluid samples were centrifuged for 30 seconds at a relative centrifugal force (RCF) of 1000, solution was then aspirated and transferred to another vial, and the vial was stored in a freezer at -40 ˚C. Sample cytokine concentrations were analyzed using a Magnetic Luminex Screening Assay (R&D Systems, Minnesota USA) for TNFα, IL-1β, IL-2, IL-6, IL-8, MCP-1, M-CSF and MIP-3α.

3.3.4 Damage Scoring of Femoral and Tibial Components

Polyethylene (PE) insert damage was scored using the Hood method [106]. For this method, 7 damage modes are analyzed and given a score of 0 to 3 based on the area of damage present, with a score of 0 for minimal, 1 for mild, 2 for moderate, and 3 for severe damage. The damage modes analyzed include burnishing, pitting, delamination, abrasion, embedded debris, scratching, and surface deformation. The results were summed to provide an overall damage score with maximum total scores of 61 for the condyle, 66 for the backside, and 22 for the post (Table 3.4.1).

Femoral component third-body damage score was assessed as described previously [107]. Each region was assigned a representative score for the observed damage, with a score of 0 for minimal, 1 for mild, 2 for moderate, and 3 for severe damage. Results were presented as a component sum representing all four regions analyzed with a maximum score of 12 (Table 3.4.1). Tissue metallosis was also observed and documented for the tissues surrounding the TKA. This observation was recorded as yes (any visible appearance of metallosis) or no.

3.3.5 Statistical Methods

Continuous variables within this study were tested for normality using Shapiro-Wilk test and determined to be non-normal. To describe the relationship between tissue collection site and metal ion concentration, a Friedman non-parametric statistical test was used (SPSS, Endicott, New York). A Spearman rank correlation test was performed to determine associations between metal ion concentration, synovial fluid cytokines, femoral component metallic damage score, and polyethylene damage score. All statistical tests were performed with an alpha value of 0.05.

3.3.6 Second cohort (N=3) Patient Demographics and Implant Characterization

Three TKA systems were collected at necropsy. One of the devices was a Zimmer Nexgen LPS (tibial tray: Ti alloy, femoral condyle: CoCr, insert: gamma inert). It was implanted on the right side of a male patient. This patient had an estimated implantation time of 21 years and passed away at the age of 79 from mesothelioma. The second device was a Depuy LCS Mobile Bearings (tibial tray: CoCr, femoral condyle: CoCr, insert: gamma inert). It was implanted on the left side of a female patient. This patient had an unknown estimated implantation time and passed away at the age of 66 from congestive heart failure. The final device was a Zimmer Miller-Galante II (tibial tray: Ti alloy, femoral condyle: Ti alloy, insert: gamma air). It was implanted on the left side of a male patient. The estimated implantation time was 45 years, and the patient passed away at the age of 65 from cardiac arrest.

3.3.7 Tissue Metallosis Analysis

Five tissue samples were collected from each patient, one each from the medial gutter (MG), lateral gutter (LG), the infra patella (IP), supra patella (SP), and the tibia (T). These samples were collected utilizing relevant operating tools and procedures[108]. Fluoroscopy images were taken for each patient before extracting the tissue samples and the device to rule out the presence of osteolysis. The initial tissue samples were stored in Umfix tissue fixative and washed with ethanol (100%) for two consecutive times before being stored in ethanol (100%) at refrigerated

temperatures (~4˚C). A daughter sample weighing approximately 150 mg was taken from each of the five regions and reserved for particle isolation.

Tissues were visually inspected for signs of metallosis, often described as blackened staining or grey discolored regions [91]. Tissues were given a score from 1 to 5 (Figure 3.3.1). A score of 1 indicated no visible presence of metal, and a score of 2 indicated light grey coloring in small locations equivalent to < 30% of the tissue volume. A score of 3 referred to large grey regions of tissue taking up between 30% and 50% of tissue, while a score of 4 described large grey and black stained regions covering between 50% and 75% of tissue. Finally, a score of 5 described black staining covering more than 75% of tissue.

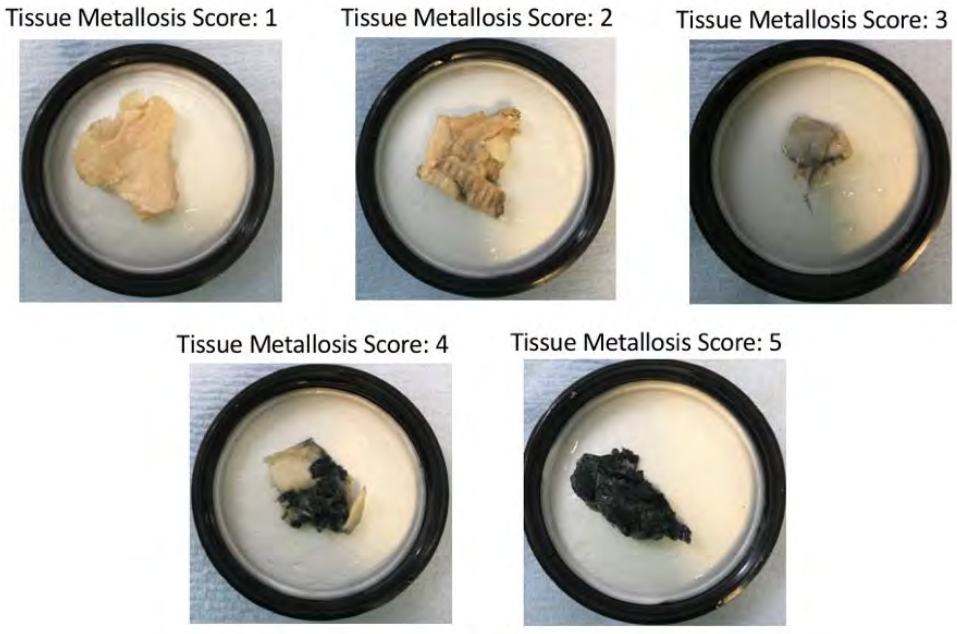

Figure 3.3.1: Pictorial description of tissue metal scoring system used to visually evaluate the degree of metallosis in periprosthetic tissue.

3.3.8 Particle Isolation

The tissues were digested following an enzymatic protocol by Patel et al. [46] using papain and proteinase K. The tissues were finely minced, placed within a 15 ml centrifuge tube, and sonicated in an ice-cold water bath for 20 minutes. Samples were digested in an environment at 50^{o}C with gentle agitation for 6 hours and had a final volume in each tube of 3ml. The final chemical concentrations within the 3ml volume were 0.1M HEPES buffer, 0.33M glycine and 1.56 mg.ml^{-1} papain. A proteinase K stock solution was created using sterile water (~5 ml), proteinase K (20 mg.ml^{-1}), $CaCl_2$ (0.33 mg.ml^{-1}), and HEPES buffer (23.83 mg.ml^{-1}). The proteinase K stock solution was aliquoted into 1ml volumes and stored at -20^{o}C. After the 6-hour incubation period at 50^{o}C, 10% (v/v) sodium dodecyl sulfate was added to each sample creating a final concentration of 0.5% (v/v). Proteinase K stock solution (150 µl) was added to each sample creating a final concentration of 1 mg.ml^{-1}. The samples were returned to the environment at 50^{o}C with gentle agitation. Proteinase K replenishment was repeated every 6 hours, with the entire digestion concluding after 48 hours.

Particles were retrieved from digested tissue samples by density gradient ultracentrifugation with sodium polytungstate [46, 104], (Figure 3.3.2). Particles were isolated by density gradient ultracentrifugation, which was used to separate the

digest fluid, potential polyethylene debris, and particles of interest (i.e. CoCr or Ti Alloy particles). Three polytungstate solutions were created with concentrations of 2 $g.ml^{-1}$, 1.6 $g.ml^{-1}$, 1.2 $g.ml^{-1}$. The polytungstate solutions were layered in 2 ml volumes within the centrifuge tubes beginning with the 2 $g.ml^{-1}$ concentration, followed with 1.6 $g.ml^{-1}$ concentration, and finally 1.2 $g.ml^{-1}$. The digested tissue sample was added to the centrifuge tube, with additional sterile water being added to each tube to balance the centrifuge. Initial particle separation was performed at an average RCF of 202,048g for 4 hours. This was followed by supernatant removal, leaving remaining particles pelleted within the tube. Washing phases were performed with filtered water at an average RCF of 154,693g for 1 hour, repeated three times. Isolated particles were sealed with parafilm and stored at $-20^{o}C$.

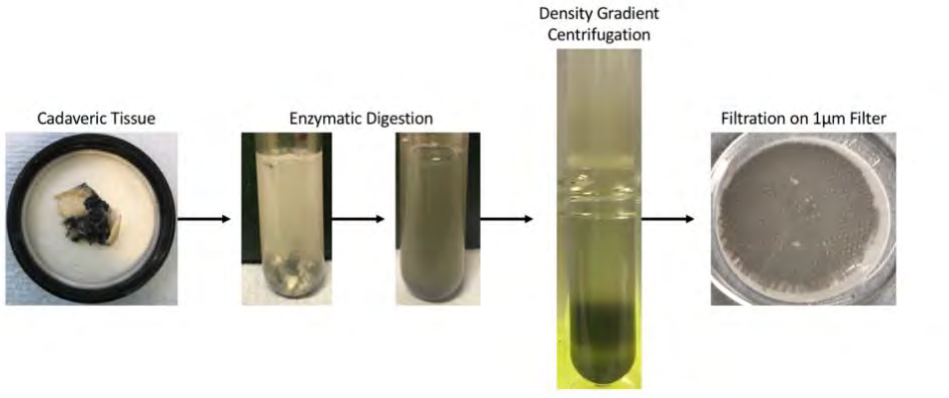

Figure 3.3.2: Description of protocol used to digest and isolate metallic debris from periprosthetic tissue in TKA.

3.3.9 Particle Characterization

Samples were filtered onto polycarbonate membranes of 1 μm pore sizes. The 1 μm filters were rinsed with ethanol and weighed before and after filtration to determine the mass of particles 1 μm and larger.

The larger particle debris was analyzed for the medial gutter, lateral gutter and infra patellar tissues for all three patients. All five locations were analyzed for the LCS mobile bearing device. Scanning electron microscopy (SEM) images were taken of the 1μm pore filter with 33 random images taken at 10 kV and 1,000x magnification. This was performed to further characterize particle size and shape. Backscatter detection was used to confirm metallic debris on the filter taken at 10kV and 1,000x magnification. Energy dispersive X-Ray spectroscopy (EDS) was used to confirm the composition of metallic debris. EDS was performed on three images per sample with seven points of interest per image at 10 kV and 1,000x magnification.

Image processing software (ImageJ, U. S. National Institutes of Health, Bethesda, Maryland, USA) was used to measure and calculate two particle dimensions in adherence with ASTM F1877 [49], and to calculate particle count. These measurements were only performed for the particles captured on the 1μm polycarbonate filters. These dimensional measurements included the equivalent circle diameter, which is defined as the diameter of a circle with an area equivalent to the area of the particle, calculated as $ECD = (\frac{4*A}{\pi})^{\frac{1}{2}}$ with units of length, where A indicates area. The aspect ratio (AR) is defined as a ratio of the major diameter (d_{max})

to the minor diameter (d_{min}), calculated as $AR = \frac{d_{max}}{d_{min}}$. Aspect ratio was used to estimate particle shape where $1 \leq AR < 1.5$ is round, $1.5 \leq AR < 2.5$ is oval, and $AR \geq 2.5$ is needle-shaped [50].

A 1 ml aliquot of the filtrate filtered through the 1 μm pore size polycarbonate membranes and was analyzed using nanoparticle tracking analysis (NTA; Nano Sight, Salisbury, United Kingdom) to analyze the distribution of sub-micron particles. Each sample was observed six different times for 10 seconds each. A blank sample was also observed six times for 10 seconds to simulate the background noise. The background noise was removed from all fifteen samples. The average diameter size for nanoparticles were reported, as well as the number of particles in each diameter size.

3.3.10 Statistical Methods

Continuous variables within this study were tested for normality using the Shapiro-Wilk test and determined to be non-normal. A spearman rank correlation test was performed to determine associations between tissue metallosis score, 1 μm filter particle weight, and particle diameter. Kruskal-Wallis test was performed to determine associations between particle dimensional measurements, patient, and tissue sampling location.

3.4 Results

3.4.1 First Cohort (N=20) Results

Contrary to our hypothesis, metal concentration levels were similar between the 5 distinct sampling regions for Co (p=0.98), Cr (p=0.71) and Ti (p=0.84), as shown in table 3.4.2. Two patients (patient 4 and patient 20) demonstrated significantly higher metal ion concentrations (samples were noted to have severe metallosis). Samples from patient 4 were noted to have elevated Co and Cr concentrations (Figure 3.4.1 and 3.4.2), while samples from patient 20 were noted to have elevated Ti concentrations when compared to the other samples in the cohort (Figure 3.4.3). To ensure that the results were not skewed by the inclusion of the two outliers (samples from patient 4 and patient 20 from Table 3.4.2), the statistical tests were repeated without the data from those two patients. Again, there was no significant difference between metal concentration and tissue collection site for Co (p=0.96), Cr (p=0.62), and Ti (p=0.86). Following this observation, metal concentrations were averaged across all 5 sampling locations for each patient. The median metal concentrations were measured to be 17 µg/L for cobalt (range: 1.3 to 28,705 µg/L; IQR: 47, Figure 3.4.1), 51 µg/L for chromium (range: 5 to 66,532 µg/L; IQR: 107, Figure 3.4.2), and 10 µg/L for titanium (range: 0.5 to 1,136 µg/L; IQR: 43, Figure 3.4.3).

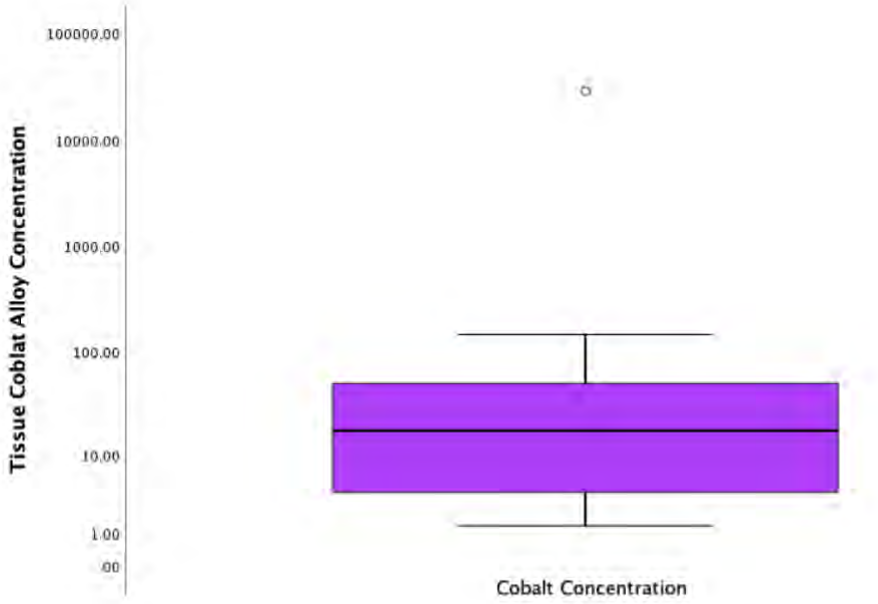

Figure 3.4.1: Logarithmic-scaled boxplot showing the tissue metal concentrations for cobalt, as determined by ICP-MS. The graph summarizes the data from Table 3.4.2 and shows the 5-number summary for tissue cobalt concentrations. The open circle indicates the outlier datum (28,705 μg/L, patient 4).

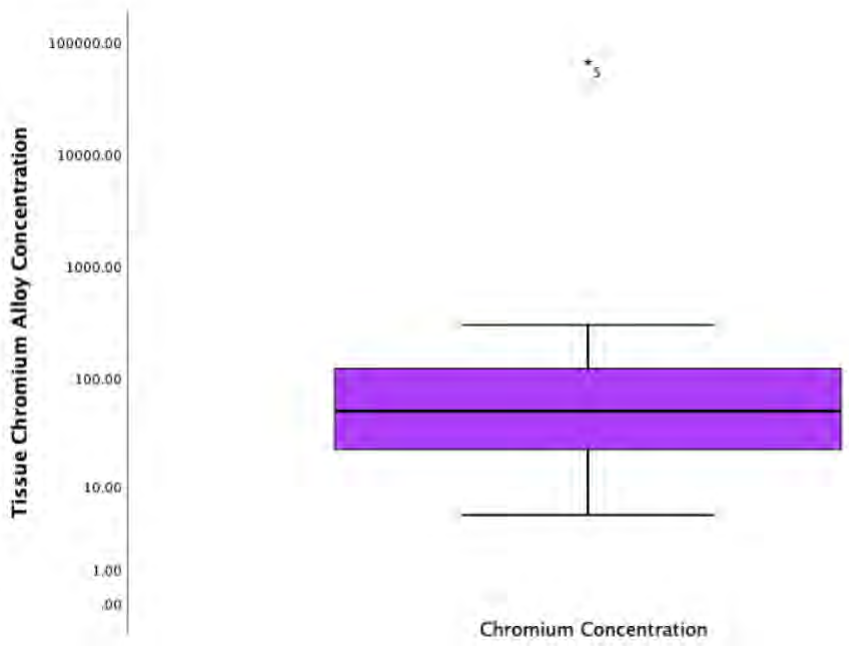

Figure 3.4.2: Logarithmic-scaled boxplot showing the tissue metal concentrations for chromium, as determined by ICP-MS. The graph summarizes the data from Table 3.4.2 and shows the 5-number summary for tissue chromium concentrations. The open circle indicates the outlier datum (66,532 µg/L, patient 4).

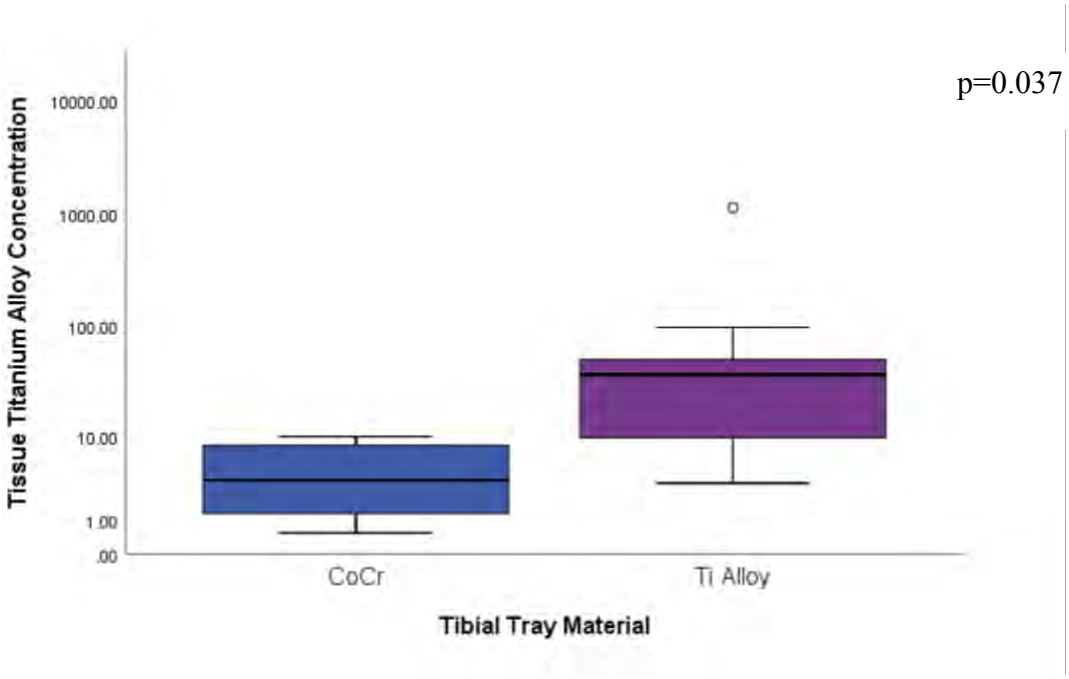

Figure 3.4.3: Logarithmic-scaled boxplot showing the tissue metal concentrations for titanium, as determined by ICP-MS. Results were summarized for patients with CoCr tibial trays (left) and titanium tibial trays (right). The graph summarizes the data from Table 3.4.2 and shows the 5-number summary for tissue titanium concentrations. The open circle indicates the outlier datum (1,136 µg/L, patient 20).

Table 3.4.2: Description of expressed inflammatory cytokines measured from patient synovial fluid and tissue metal concentration for Co, Cr, and, Ti measured for each patient described using nonparametric summary statistics.

	TNF-α (µg/ml)	IL-6 (µg/ml)	IL-8 (µg/ml)	MCP-1 (µg/ml)	IL- 1β (µg/ml)	MIP-3α (µg/ml)	IL-2 (µg/ml)	M-CSF (µg/ml)	Cobalt Tissue Concentration (µg/L)	Chromium Tissue Concentration (µg/L)	Titanium Tissue Concentration (µg/L)
100.0% (Maximum)	25.7	2532.4	44358.7	7940.0	372.4	2545.7	75.6	56552.3	28705.3	66532.2	1136.3
90.0%	18.8	1180.0	28668.3	7940.0	310.4	777.8	60.3	48829.2	139.3	290.3	94.0
75.0% (Q3)	13.8	278.7	12978.9	7940.0	151.3	361.3	39.8	37681.5	50.7	128.9	46.2
50.0% (Median)	9.3	135.3	5671.2	1660.0	50.3	115.7	21.1	27263.4	17.4	50.9	9.7
25.0% (Q1)	6.1	62.9	1140.0	598.1	21.1	48.6	7.6	16622.9	3.7	21.8	3.6
10.0%	3.3	37.3	1060.0	235.4	8.0	26.1	3.5	8361.5	1.7	7.8	0.8
0.0% (Minimum)	2.5	28.7	622.6	213.3	4.6	18.8	0	5565.7	1.3	5.1	0.5

Sixty percent (n = 12/20) of the patients had at least one tissue sample that demonstrated metallosis, Table 3.4.1. There was no statistical correlation between observed tissue metallosis and cobalt concentration ($p>0.05$), chromium concentration ($p>0.05$), or titanium concentration ($p>0.05$). After removing the two previously mentioned outliers (sample 4 and sample 20), there was still no statistical

correlation between observed tissue metallosis and cobalt concentration ($p>0.05$), chromium concentration ($p>0.05$), or titanium concentration ($p>0.05$).

Increased Cr concentration was associated with decreased TNFα ($\rho= -0.51$, $p= 0.03$), MIP-3α ($\rho= -0.47$, $p= 0.04$), PE backside damage ($\rho= -0.46$, $p= 0.05$), and increased cobalt ions ($\rho= 0.64$, $p= 0.002$), Table 3.4.2. Increased Co was associated with decreased TNFα ($\rho= -0.51$, $p= 0.03$) and increased chromium ions ($\rho= 0.64$, $p= 0.002$), Table 3.4.2. Increased Ti concentration was not correlated with inflammatory cytokines or implant damage. However, Ti concentration correlated with tibial tray material (median difference: 33 μg/L; $p=0.037$), Table 3.4.2. When removing the two outliers (sample 4 and sample 20 from the analysis), similar trends are observed. Chromium concentration was associated with cobalt concentration ($\rho= 0.60$, $p= 0.009$), PE backside damage ($\rho= -0.59$, $p= 0.014$), and PE post damage ($\rho= -0.75$, $p= 0.005$), but not cytokines. Cobalt concentration was associated with decreased TNFα ($\rho= -0.56$, $p= 0.02$), chromium concentration ($\rho= 0.60$, $p= 0.009$), PE backside damage ($\rho= -0.49$, $p= 0.047$), and PE post damage ($\rho= -0.78$, $p= 0.003$). Titanium concentration still did not correlate with inflammatory cytokines or implant damage.

3.4.2 Second Cohort (N=3) Results

All fifteen of the tissue samples were successfully digested. The presence of metallic debris was confirmed visually by observing grey staining on the filters, and via SEM imaging with backscatter imaging. EDS confirmed that metal particles were composed of Ti alloy and CoCr for the Nexgen LPS, Ti alloy for the Miller-Galante II device, and CoCr for the LCS mobile bearing device, Figure 3.4.4.

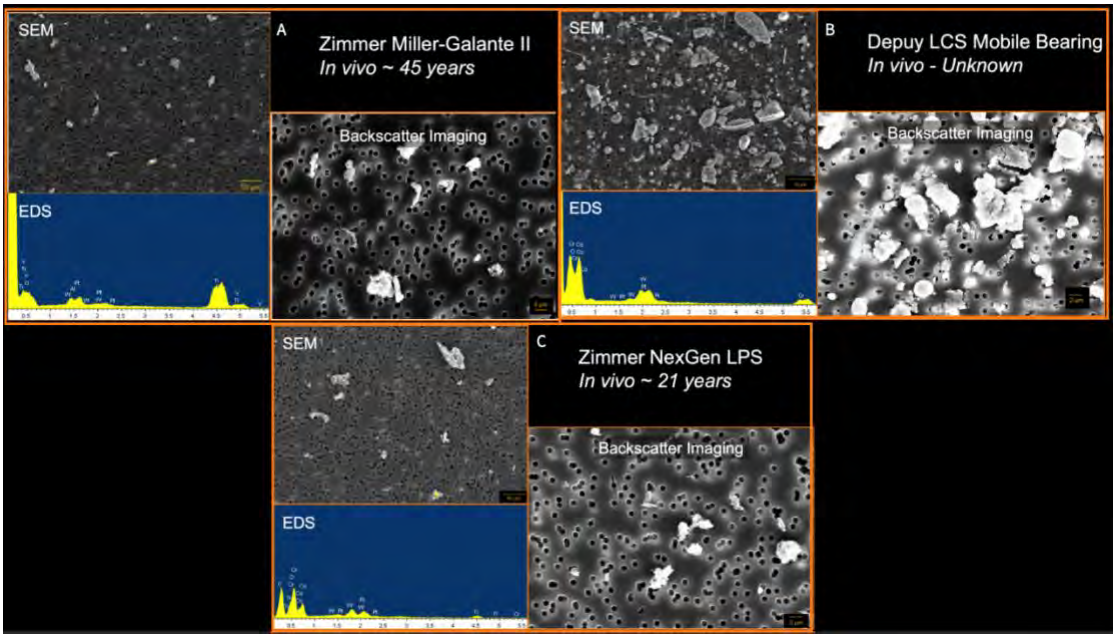

Figure 3.4.4: Exemplar SEM image, Backscatter image, and EDS analysis for each patient, A) Ti alloy for the Miller-Galante II device, B) CoCr for the LCS mobile bearing device and, C) Metal particles were composed of Ti alloy and CoCr for the Nexgen LPS.

The median weight ± SD of debris captured on 1 μm filters was 0.5 ± 0.6 mg (range: 0-1.9 mg). The weight of debris captured on the 1 μm filters correlated with the metallosis score ($\rho = 0.82$, $p=0.002$).

The median particle diameter measured by nanoparticle tracking analysis was 162.5 nm (range: 62.5 - 999.5 nm). The median particle diameter was not significantly different across the five tested locations, and three different material

pairings. A cumulative frequency distribution curve was generated for all samples to account for data dispersion, Figure 3.4.5. Within the plot, notable differences occurred within the Nexgen LPS in the IP and SP locations.

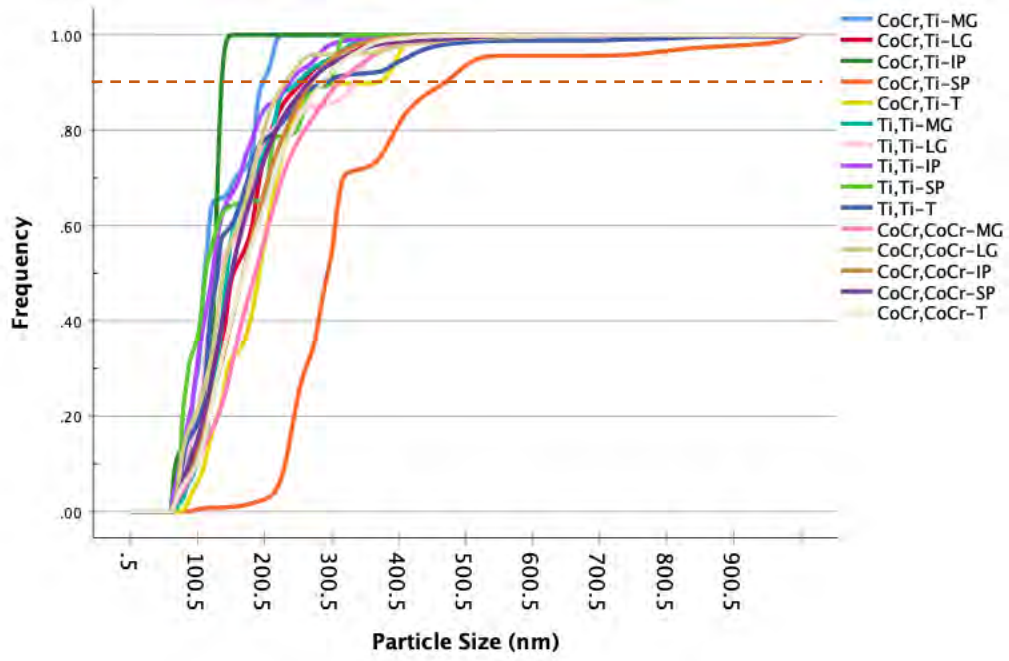

Figure 3.4.5: Cumulative frequency plot illustrating the frequency of particles within a specific nanoparticle diameter size range. The dotted line indicates the 90th percentile.

The median microparticle equivalent circular diameter and weight of debris from 1µm filter for all components was 1.3 µm (range: 0.4 - 32.6 µm) and 0.5 mg (range: 0.1 - 1.9 µm), respectively. The equivalent circular diameter was statistically

different across the five tested locations ($p>0.001$), and three different material pairings ($p>0.001$), table 3.4.3.

From the 1 μm filters, the particle shape was not statistically different across categories of patient ($p=0.368$), and location ($p=0.406$). For particles observed from the patient with the Miller-Galante II device, 6.7% of the particles were needle-shaped, 38.5% of the particles were oval shaped, and 54.8% of the particles were round shaped. For particles observed from the patient with the LCS mobile bearing device, 5.5% of the particles were needle-shaped, 32.8% of the particles were oval shaped, and 61.7% of the particles were round shaped. For particles observed from the patient with the Nexgen LPS device, 3.5% of the particles were needle-shaped, 39.7% of the particles were oval shaped, and 56.7% of the particles were round shaped.

For particles observed from the patient with the LCS mobile bearing device infra patella, 3.3% were needle-shaped, 41.5% were oval shaped, and 55.2% were round shaped. For particles observed from the patient with the LCS mobile bearing device lateral gutter, 2.6% were needle-shaped, 33.2% were oval shaped, and 64.2% were round shaped. For particles observed from the patient with the LCS mobile bearing device medial gutter, 4.2% were needle-shaped, 40.3% were oval shaped, and 55.4% were round shaped. For particles observed from the patient with the LCS mobile bearing device supra patellar, 4.3% were needle-shaped, 40.5% were oval shaped, and 55.2% were round shaped. Finally, for particles observed from the

patient with the LCS mobile bearing device medial gutter, 4.7% were needle-shaped, 35.8% were oval shaped, and 59.5% were round shaped.

Four tissues had no visible metallosis (score of 1), and one tissue had light grey coloring or a score of 2. Five tissues had a score of 3 for metallosis, and four tissues had a score of 4 for metallosis. One tissue had a score of 5 with severe metallosis (Table 3.4.3). The weight of debris captured on the 1 μm filters correlated with the tissue-metal score, ($\rho = 0.822$, $p=0.002$).

Table 3.4.3: Summary of micron-sized particle characteristics in accordance with ASTM F1877

Device Design	Insert Material	Tibial Component Material	Femoral Component Material	Tissue Location	Median Estimated Circular Diameter (μm)	Total Micron Particles	% Micron Particles Needle-Shaped	% Micron Particles Oval Shaped	% Micron Particles Round Shaped
Miller-Galante II	Gamma Air	Ti Alloy	Ti Alloy	Medial Gutter	0.97	1195	7.95%	41.84%	50.21%
				Lateral Gutter	1.15	1957	7.31%	39.70%	52.99%
				Infer Patella	1.22	2942	5.81%	36.40%	57.78%
LCS Mobile Bearing	Gamma Inert	CoCr	CoCr	Medial Gutter	1.4	1617	4.27%	40.32%	55.41%
				Lateral Gutter	1.32	765	2.61%	33.20%	64.18%
				Infer Patella	1.48	2315	3.33%	41.51%	55.16%
				Super Patella	1.42	1689	4.32%	40.50%	55.18%
				Tibia	1.5	1140	4.74%	35.79%	59.47%

Nexgen LPS	Gamma Inert	Ti Alloy	CoCr	Medial Gutter	1.09	1640	3.96%	30.37%	65.67%
				Lateral Gutter	1.26	1157	7.26%	35.78%	56.96%
				Infer Patella	1.17	1468	5.93%	33.04%	61.04%

3.5 Discussion:

Within these two studies, we attempted to describe debris characteristics observed for total knee arthroplasty retrieved at necropsy. The purpose of the initial cohort (n=20) was to analyze the concentration of metal in periprosthetic tissue associated with total knee arthroplasty retrieved at autopsy; a secondary goal was to determine if there were correlations between the metal ion concentrations and other variables such as sampling region, visible metallosis, device damage, and levels of inflammatory cytokines. No difference was found in the metal concentrations between the five distinct periprosthetic tissue sampling regions. Our findings also did not support the hypothesis that tissue metal concentration would correlate with inflammatory cytokines, perhaps due to limitations associated with postmortem synovial fluid or increased cytotoxicity associated with large volumes of metal debris. Additionally, this lack of correlation could be a symptom of biomarker degradation from time of death to sample acquisition. Large volumes of debris also could potentially explain the statistical similarity between tissue sampling regions, essentially allowing debris to distribute equally around the capsule. Our findings in regard to visual appearance of tissue show that visual darkening is not necessarily

predictive of levels of metal content in the tissues, a theory that is already supported in the literature for THA [109].

In the second necropsy study (n=3), we showed that the nano-sized particle diameter and volume were independent of the five sampling locations and the three different material combinations. We showed that contrary to a previous investigation where a binary approach was used to describe metallosis [110], micron-sized particle statistically correlated with a semi-quantitative tissue metallosis scoring method. We also showed that the estimated shape, equivalent circular diameter, and total particles amount for micron-sized particles varied across the five sampling locations of the LCS mobile bearing device and the three different material combinations. Within all patients, we observed particles sizes within range for phagocytosis (150nm-10 μm) by a range of cell types such as osteoblasts, fibroblasts, and endothelial cells [43]. Additionally, submicron particles (less than 150 nm) which were observed for all patients, can be ingested by endocytosis or pinocytosis [43].

Within both of these studies there were limitations. First, because of the donation process associated with the postmortem collection, only partial patient information was available. This, in turn, limited the ability to conduct an analysis of patient-specific factors. However, analysis was performed for the patient information available (such as cause of death). Secondly, within the initial cohort (n=20), the device damage was characterized using visual damage scores for both the polymer and metallic components. Although these methods are unable to quantify volumetric wear, there is precedence in the literature of using such damage scores to assess the

extent of in vivo damage in retrieved components [65, 106, 111]. The cytokine analysis within initial cohort (n=20) was performed post-autopsy. Although there was a potential for this to compromise the cytokines present, the observed trends indicate a potential severe metallic reaction in response to the large volumes of metal present. Another limitation is the variability of device materials in this study. Although not all of the implantation times were disclosed for the 20 patients within this cohort, the range was very broad (6 to 45 years). Because the formulation of polymers and techniques used to implant TKA have changed and improved over the years, there are limitations to drawing correlations related to the length of implantation. Furthermore, this study excluded any analysis of polyethylene debris that may have been present, which may have also contributed to cellular response and increased cytokine levels. The method used within the initial cohort (n=20) to measure the metal concentration known as ICP-MS ionizes all metallic debris present. The measured concentration is, therefore, a description of all metal debris present in the periprosthetic tissues. However, because ICP-MS ionizes all metal, it does not allow more discretized analysis of the particulate matter metal (i.e., differentiation between oxides, ions, metal debris) to be determined. For the second cohort, we were limited by a small sample size of n = 3. However, the study still provided valuable insight into differences associated with sampling regions, tissue discoloration, and in vivo debris size, shape, and volume. Additionally, the strength of the findings were bolstered by using multiple tissues from each patient. The particle size measurements may have been compromised, in part, by agglomeration and/or aggregation. This was

minimized by agitation techniques such as sonication, vortexing, and aspiration, however, agglomeration could not be completely eliminated. These techniques have been used by previous investigators who analyzed particles within tissues and compared with those isolated. Indicting that these techniques help disperse agglomeration and do not alter particle characteristics [46]. It was further countered by SEM imaging and image J analysis techniques to differentiate between individual particles agglomerated into a larger particle. Additionally, the NTA (Nano Sight) measurements were repeated six times to increase the accuracy of the measurement with a blank measurement removed from the sample measurements.

Within the initial cohort (n=20), the lack of an association between tissue sampling location and metal concentration may be helpful to simplify future clinical study designs. The sampling locations in the present study were chosen because they are located around potential metal release regions of the TKA components. Specifically, the medial and lateral gutters are located on the corresponding regions of the femoral component bearing zones, the supra- and infra- patellar locations are located along the tracking of the patella over the femoral component, and the tibia sampling location was chosen for its position directly anterior to the tibial tray. This location is similar to the "fat pad" that is evaluated in particle injection animal models, which is generally chosen due to the proximity to the injection site [112] and the potential for more collection of metal debris [113]. However, injected particles have been noted to be distributed throughout the joint capsule [112]. We had hypothesized that the gutter regions would demonstrate the highest CoCr levels due to

their proximity to the bearing surface, a region often studied for metal release [10, 111]. The lack of association between tissue sample location and concentration could be indicative of the metal debris being dispersed and embedding around the joint capsule. Alternatively, this finding could suggest that non-articulating device components, such as the tibial tray, were also releasing metal debris and dispersing this debris throughout the joint capsule. Metal concentrations within these retrieved periprosthetic tissues were generally lower compared with previous studies of THA periprosthetic tissues. For example, in this study, the median concentrations for cobalt, chromium, and titanium were 17 μg/L, 51 μg/L, and 10 μg/L, respectively, compared with literature reports of samples with 19.5 mg/L of cobalt in MOM THA [40]. This is not particularly surprising since MOM THA involves two articulating metal surfaces, while TKA includes one metal and one polyethylene articulating surface. The two outliers, samples 4 and 20 (which demonstrated a high level of cobalt/chromium and titanium alloy, respectively) also had the highest femoral condyle damage and polyethylene damage scores, respectively. Although there is limited clinical data, it is possible that such high damage scores could be representative of third-body damage or complete wear through of the tibial tray, both of which could have resulted in significant generation of wear debris.

It should also be noted that local periprosthetic tissue has been shown to have greater metal concentrations (22 to 6,000 mg/L) compared to systemic samples such as blood (0.006 mg/L), urine (0.024 mg/L), and organs (liver 3 mg/L, brain 1 mg/L, and kidney 1 mg/L) in THA [39]. These findings were supported in a separate study

that found urinary cobalt concentrations that ranged from 20 – 40 μg/L across four patients and organ metal concentrations that range from 1 mg/L to 27 mg/L [40]. Within our cohort, the measured metal concentrations in periprosthetic tissue were significantly less (measured in parts per billion instead of parts per million). It was hypothesized that periprosthetic metal debris would be detected and measurable, and while the concentrations of metals were significantly lower than in THA, there was still a significant amount of metal in the joint space. The levels detected were not initially anticipated due to the lack of direct metal-on-metal articulation within the designed device. Without the direct metal-on-metal articulation, it is possible that the metal ion concentrations observed may be due, at least in part, to the generally long implantation times of the devices analyzed in this study (average of 20 years, range of 6-45 years).

Furthermore, the formulations of the polyethylene inserts from historical TKA systems evaluated in this study were different from more recent formulations. Therefore, it is anticipated that some of the devices with long implantation times likely had polyethylene that did not resist wear as well as modern implants [114]. Therefore, because of the significant damage of the polyethylene inserts in the older TKAs, there would be an increased likelihood of damage and failure allowing for metal-on-metal articulation and therefore metal debris generation. Unfortunately, information about the activity level and patient comfort with the device were unavailable due to data limitations associated with the use of cadavers.

Within the initial cohort (n=20), the term metallosis was used to describe visible blackening of the synovial tissue in an attempt to simulate surgeon visual evaluation upon revision. It was noted that 16 of the samples had visible metallosis. The absence of a correlation between visual metallosis and metal concentration indicates that similar to THA, the appearance of collected TKA periprosthetic tissue is not indicative of metal concentration or bioreactivity. However, it has also been noted that beyond potential visual misidentification, specific tissue reactions can exhibit themselves in different visible ways [109]. Essentially, it is thought that visual appearance is not sufficient to determine the quantity of metallic debris and whether further testing is necessary to diagnosis the concentration of metal within patients. Within the literature, there are different methods such as the Mirra classification [115] or the ALVAL score [109] that are used to analyze stained tissue sections and determine the biological reactions present. These methods were not employed within this study as the collected cadaver tissues may have deteriorated over time, making the histology unreliable.

We hypothesized that for the initial cohort of 20 TKA patients, the metal concentration in the tissues would be correlated with inflammatory cytokines in the serum. However, our findings did not support this hypothesis, perhaps due to limitations associated with postmortem synovial fluid analysis or increased cytotoxicity associated with large volumes of metal debris [116]. Both cobalt and chromium had negative correlations with measured cytokines, while titanium alloy had no statistical correlation with any measured cytokines. It is possible that there

was an observed negative correlation with Co and Cr due to larger wear debris, which is thought to be less toxic due to the lack of ability for cells to phagocytose the debris [44]. However, this theory does not take into account the presence and contribution of polyethylene particles to inflammatory responses, nor does it account for the active device surface area which could release metal ions and the lack of a correlation with titanium alloy metal debris. It is unclear whether the particles obtained a stable oxide layer or were small or large within this study. The resulting lack of a positive correlation with cytokines and metal concentration is possibly indicative of increased toxicity within the system [44, 116].

Overall, this study supports the continued observation of metal sensitivity for TKA patients and confirms the presence of metallic debris within TKA. Due to the nature of retrospective cadaver studies, it is difficult to draw correlations between patient factors and device performance, and future prospective studies should evaluate TKA with respect to device wear, including both polymeric and metal wear debris generation.

Within the second cohort (n=3), the volume of microparticles correlated with a tissue metallosis score that focused on blackened staining or grey staining. The second tissue metallosis score used was more descriptive compared to the binary nature of the first scoring method. It was hypothesized that the metal concentration would correlate with the tissue coloring because cobalt and chromium corrosion by-products can be black or grey in color [34]. In contrast, titanium corrosion products can be violet or black deposits with the addition of white deposits [34]. The tissue

scoring criteria and noted color variations may explain why the volume of titanium debris negatively correlated with tissue metallosis score. These results indicate that due to colored corrosion products, a relative estimation for the volume of larger micron-sized particles may be possible. However, further research is recommended for use of this technique within the operating room, as the results conflict with previous findings.

In a previous study, using a binary approach (having or not having metallosis) to simulate the operating room, we reported that you could not accurately predict debris volumes based on visual assessment of tissues [110]. We were mainly commenting on the significance of the reported visual appearance of the joint capsule or tissue section.

The median nanoparticle diameter and micro particle shape was not associated with the sampling locations, consistent with previous findings in which metal concentrations (Co, Cr, and Ti) were statistically similar between sample locations (i.e. the infra patella, supra patella, medial gutter, lateral gutter, and tibia) [110]. Previous studies attempting to determine the appropriate tissue harvesting locations have mentioned the scenario in which particles would distribute evenly throughout the joint capsule [112], preferentially collecting in particular regions. The microparticle diameters, however, were statistically different across different locations of the single patient, though this could be specific to that patient.

Notably, tissue metallosis scores correlated with the mass of micron-sized particles. These findings suggest that for a specific study, tissues should be collected

from the same location to avoid any unintentional variations in larger particle diameter.

Differing equivalent circular diameters for micron-sized particles was observed with the three different materials, which may be explained by differing elastic modulus and hardness values, with CoCr being the harder material. Metallic debris from implants is thought to be from corrosion, fretting or sliding [117], and when modeling wear mechanics, the hardness of the material is an important characteristic that can impact the size, shape and quantity of debris [118]. We speculate that the physical and chemical differences between the metals affected the micron-sized debris, creating different micron-sized particle diameters.

The particles within the second cohort (n=3) had a size range from 62.5 nm to 32.6 μm, which falls within the hypothesized size range for particles phagocytosis, between 150 nm-10 μm, for a range of peri-implant cell types such as osteoblasts, fibroblasts, and endothelial cells [43]. Additionally, submicron particles less than 150 nm can be ingested by endocytosis or pinocytosis [43]. It has been suggested that the size of metal particles may not be as critical as the reactive surface area of the particle [44]. However, it is also noted that micron-sized particles persist within the joint capsule [44], while nanoparticles are thought to be up taken by macrophages and transported with intracellular phagosomes [45]. *In vitro* experiments have shown that particles within the size range of 0.5 - 50 μm can elicit TNFα production by human synoviocytes, and that particles between (10-15 μm) can elicit TNFα production from J774 macrophages[99]. Cobalt ions and cobalt nanoparticles may be cytotoxic,

inducing apoptosis, with high concentrations leading to necrosis [119]. Additionally, soluble metal ions can transport through protein-metal complexes into the blood and surrounding organs [43]. The particles measured in the current study are within range for macrophage phagocytosis. In previous in vivo THA studies, observations of particles within living macrophages and fragmented dead macrophages surrounding them have been observed [96, 97]. These findings would indicate that the metal fragments were phagocytosed by macrophages which subsequently died, or that the presence of metallic debris could have caused cell death. Particles within the size range from 10-70 nm, observed within the synovium of the present patients, have the potential to migrate to the lymph nodes, indicating that the measured diameters of metal particles in the present study have the potential to move throughout the body or elicit proinflammatory reactions.

In summary, we reported the metal concentrations for periprosthetic tissues collected around synovial joint capsules for an initial cohort of 20 postmortem TKA and found that there was no association with the tissue collection site and the metal concentration for cobalt, chromium, and titanium. These findings indicate that similar metal concentrations can be measured from these five locations around the joint capsule. Additionally, we reported a lack of association with apparent metallosis and the measured tissue metal content. This potentially indicates a lack of specificity associated with this term and the need for quantitative analysis upon revision beyond the naked eye. The concentrations of metals found in the joint space were generally measured in μg/L, and the concentrations of metals were inversely

correlated with cytokine measurements for cobalt and chromium. It is possible that the negative correlation was caused by metal toxicity, however, it may also be attributed to limitations associated with postmortem synovial fluid analysis. Within the second study (n=3), the digestion and particle isolation method used in animal or simulator wear fluid models was also determined to be successful with human peri-prosthetic tissues. We showed that a semi-quantitative visual scoring method for tissue metallosis was correlated with larger debris volume, however more supporting research is advised before this approach is used in the operating room. We confirmed that the microparticle shapes, and nano particle diameters were not associated with sampling location around the knee or with the material combinations. However, the equivalent circular diameter of the micron-sized particles was associated with sampling regions and material combinations. This suggests that researchers should collect samples from a singular tissue site for an appropriate statistical comparison, potentially the medial or lateral gutter regions. Additionally the tissue collection site should be noted within studies to allow for inter institutional comparisons. Finally, we assessed the proinflammatory nature of the debris and determined that the size of debris is within range for cell phagocytosis and for potential movement throughout the body. Ultimately, these findings represent the first in-depth characterization of metallic debris for TKA and may be useful for future study design and clinical practice.

Chapter 4

4.1 Abstract:

The local and systemic effects of cobalt have been a concern for total joint arthroplasty. This project's goal was to update a biokinetic model previously used to discuss the oral ingestion of cobalt. Instead, the updated model will discuss the mobility of cobalt debris and ions resulting from a total knee arthroplasty femoral component. The initial model was proposed by Leggett et al. [4] and discussed systemic cobalt movement with transfer coefficients of concentration per day determined from previous studies. In this work, modeled compartments and accompanying transfer coefficients for the new exposure point, TKA, were determined by analyzing previously completed research studies. These studies explained the initial dosing of metallic debris from TKA, the tissue cobalt concentrations for periprosthetic tissue, and tissue blood cobalt concentrations. The model was calibrated using seven patients with measured tissue and blood cobalt levels and reported implantation times. This model represents the average TKA patient and shows the potential for cobalt to collect within the joint capsule and peripheral organs. For this study, it was hypothesized that using a preexisting first-order kinetic model and adding transfer coefficients with connected compartments could describe the relationship of peri-prosthetic tissues connecting to the blood. The blood value must be connected to the remainder of the system due to its dynamic concentration value, as the blood circulates cobalt to the organs, bones, and remaining body tissues. The model was not able to fit linearly to the provided biological cobalt

concentrations for seven patients. However, a dose dependent version of this model, where doses were adjusted from patient to patient, was a more accurate description of the cobalt concentrations in both tissue and blood. It was anticipated that the amount of debris would be greater within the joint capsule compared to the peripheral organs, and thus be a greater local burden instead of a systemic burden. However, it was also hypothesized that by altering the dosing of the model to simulate a fall or other exaggerated wear scenarios, the model could show tissue and blood cobalt concentrations consistent with MOM adverse reactions. The organ connections to the model were not calibrated using TKA patient bone, kidney, and liver samples. Therefore the observations made about the systemic collection of cobalt within these organs were based on the preexisting systemic biokinetic model of cobalt movement. However, this model was tracking the same ionic form of cobalt (Co(II)), and it was shown that a larger amount of debris collected within the joint capsule tissue compared to organ compartments. Additionally, a symptomatic blood metal concentration was achievable using a large dose multiple, either 1,000 or 3,000, depending on the concentrations and times described. These high values indicate that although it is theoretically possible, it is less likely that a symptomatic blood cobalt concentration would be reached within a TKA patient.

4.2 Introduction:

Cobalt, a component of cyanocobalamin (B12), is a biologically important element required for red blood cell production and the prevention of pernicious anemia with doses as high as 300 mg/day [31, 120, 121]. Cobalt has historically been

used to treat anemia. However, adverse side effects have been observed, specifically thyroid impairment in children and reversible hearing and vision impairment in adults [31, 122-126]. In the 1960's cobalt was utilized as a foam stabilizing agent in beer, resulting in adverse side effects, specifically, cardiomyopathy [31, 127]. The symptoms appeared to be related to patient health or beer intake as symptomatic patients and non-symptomatic patients had identical theoretical cobalt doses of 0.09mg Co/kg-day [31]. These observations agree with literature reports indicating that certain disease states or conditions, such as sickle cell anemia, may render patients more suspectable to cobalt toxicity[31]. Modern cobalt exposure exists in the form of dietary supplements containing cobalt, cobalt supplements used as a doping agent by athletes, and total hip arthroplasties containing cobalt alloys [28, 29, 31, 128-131]. Within the body of a healthy individual, around 90-95% of cobalt in the blood is bound to serum albumin [31, 132]. However, free ionic Co (II) is thought to cause toxic effects through its interactions with biological receptors and proteins [31], indicating that increased levels of free Co (II), potentially caused by shifts in homeostasis, could cause susceptibility to adverse effects[31]. The form of cobalt thought to predominantly be produced by implants is Co (II) [133, 134], the same form found in dietary supplements [31].

Leggett et al. created a model of systemic cobalt movement through the body using studies focusing on both human subjects and a variety of different laboratory animals exposed to radioactive or stable cobalt under controlled conditions [4]. Within Leggett's model, first-order kinetics was assumed, and controlled human

studies were chosen whenever possible. The modeled prediction of total body retention and blood parameter values were derived from human subjects injected with $^{60}CoCl_2$ and $^{58}CoCl_2$ [4]. These studies also considered fecal excretion rates and uptake and retention by the liver. This data was supplemented with time-dependent observations of liver, kidney, skeleton, and other tissues of animals that received inorganic cobalt by inhalation, ingestion, or injection [4]. The original Leggett model was created using autoradiography and summarized using percentages of cobalt transfer from different tissues, organs, and bones [2, 4].

The Leggett model's layout was composed of different compartments representing areas of element retention or collection and transport coefficients describing how the element moves between compartments in a time-dependent manner. Within the drawn model, the compartments are represented by drawn boxes, and the transfer coefficients are represented by arrows connecting boxes. These translate to differential equations where the compartment concentration is multiplied by the transfer coefficients. A positive value represents the inflow, and a negative value represents the outflow.

This model was later updated by Unice et al., which used available literature to add and edit preexisting compartments [55]. Unice et al. also observed 10 human volunteers who ingested around 1mg Co/day for up to 3 months, in order to calibrate the model [55]. It has also been proposed that a similar first-order kinetic model could be used to describe cobalt movement resulting from a total hip arthroplasty [56]. Within this theoretical total hip arthroplasty model framework, a potential

direct connection to the blood plasma, and an indirect pathway through the periprosthetic tissue were proposed [56].

A summarized version of the Leggett model [4] and the ICRP model of systemic cobalt movement was described by Czarnek et al. [2] describing cobalt circulation between blood and four major tissue compartments (liver, kidney, bone and other organs) [2]. This was utilized as the systemic aspect of the model to predict an accurate simulation of blood cobalt concentration. This portion of the model described the movement of cobalt once it was in the bloodstream and how it moved to the other compartments of the model representing the systemic organs. The Czarnek model described 6% of cobalt bound and 94% of cobalt circulating in the blood and organs per day [2]. The 94% of the cobalt fed into the organs, mainly the liver, kidney, skeleton, and other tissues per day. This reservoir fed 35% of the cobalt per day into the liver. The liver returned 40% of the cobalt per day to the circulating blood supply [2]. Twenty percent of the cobalt within the liver moved to the intestines, and 5% of cobalt ions remained in the liver [2]. The cobalt in the intestines moved all material into the fecal excretion and out of the body [2]. From the organ reservoir, 16% of the cobalt per day was transported to other tissues, 30% of cobalt per day moved to the urinary bladder, 4.5% of cobalt per day moved to the kidney, and 6% of the cobalt per day moved to the skeleton [2]. The urinary bladder cobalt ions fed into the urinary excretion, while 0.5% of cobalt ions per day remained within the kidneys, eventually moving into urinary excretion [2]. The skeleton cobalt ions

moved to the trabecular bone surface and cortical bone surface. These ions finally move to bone volume [2]. Fifteen percent of cobalt ions remained in the skeleton [2].

During this study, we sought to alter the exposure point of the systemic biokinetic model of cobalt movement from oral intake to the knee joint capsule, and to use the model to predict local and systemic cobalt concentrations resulting from TKA. For this study, we asked: (1) can we create a model that predicts blood and joint capsule tissue cobalt concentrations at specific time iterations observed for 7 different TKA patients by altering the exposure point of cobalt from oral intake to the joint capsule; (2) should the dose of cobalt introduced from the TKA device be patient specific in order to better predict blood and joint capsule tissue cobalt measurements at specific time iterations observed for 7 different TKA patients; and (3) by altering the dose of cobalt introduced from the TKA device, can this model simulate blood cobalt concentrations consistent with adverse patient symptoms?

4.3 Experimental Design:

4.3.1 Model Compartment Layout

It was initially thought that the connection of cobalt from TKA devices could be directly linked to the joint capsule and then to the blood using experimentally derived transfer coefficients, similar to the ailment track model used to connect oral cobalt ingestion to the remainder of the body [4]. Essentially, cobalt material would be produced through the use of the joint replacement, then wear debris would move from the synovial fluid into the tissue and subsequently into the blood. However, upon implementation of the model, it was determined that a connection or

compartments were missing. Instead, the current model contains all of the previously described connected compartments and a direct connection between the generated particles and the bloodstream, Figure 4.3.1. This concept has been present in other models, where there is a hypothesized faster or more direct movement for nanometer-sized particles and free floating ions, compared with other larger particles [56].

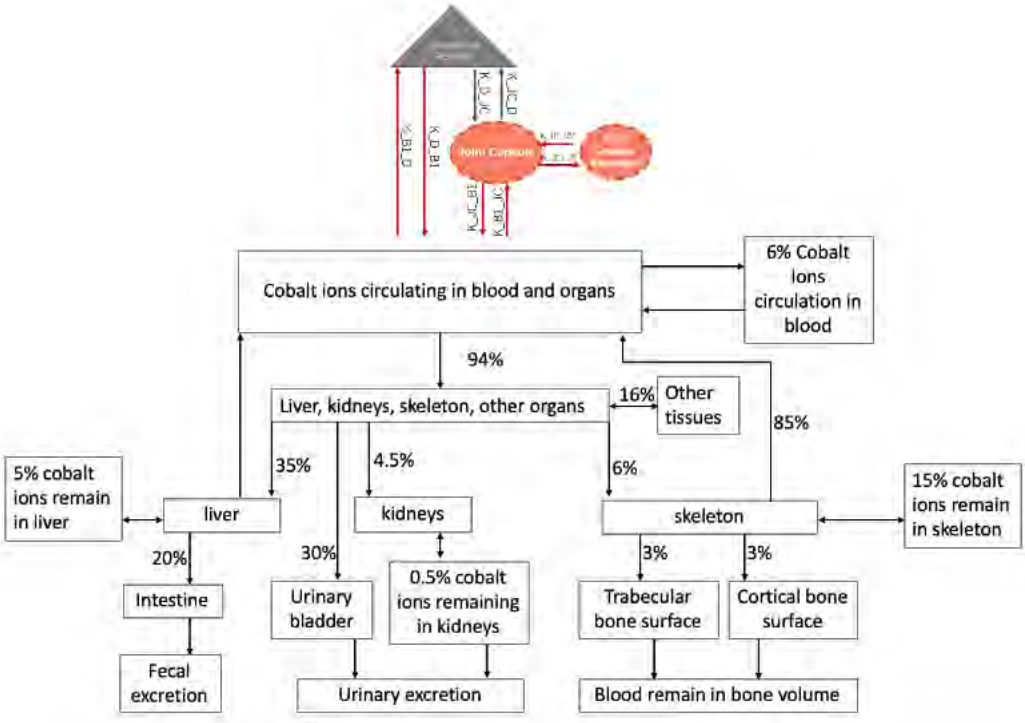

Figure 4.3.1: Proposed model attached to blood systemic cobalt model proposed by Czarnek et al. [2].

The remaining compartments of the model were chosen from Czarnek et al.[2] and Leggett et al. [4]. The Leggett model describes cobalt ions circulating in the blood and depositing in the liver, kidney, skeleton, and other organs [2]. The connection of dynamic compartments was critical to model success as the main attachment point blood concentration, is a dynamic value.

This model was coded in Berkeley Madonna 10.0.1 software. The model utilized first-order kinetics and auto integration method within the software, as shown in Section 1: Model Control of Appendix A. The start and stop time of the model were dictated in days, along with start and stop days for dosing of patients used in the simulation of symptomatic patients.

4.3.2 Model Dose

The initial dosing parameter for the TKA model was based on a study by Kretzer et al. [86]. Within this study, the authors avoided contamination from the fixture used for the simulation by composing the simulation chamber of polyurethane and polycarbonate or coating metallic components with per-fluoride ethylene-propylene [86]. To distinguish between surface corrosion and articulation-induced debris, the authors compared the serum samples of the soak control with the serum collected from the simulation [86]. The idea was that metal ions measured from the control were due to corrosion of the implant surface, whereas the remaining debris was due to articulation [86]. From this experiment, it was determined that corrosion damage represented 0.06 mg/10_6 cycles (~7% of metal wear, $K_{corrosion}$) and that

articulating surface metal debris represented 0.8 mg/10_6 cycles (~93% of metal wear, $K_{BearingSurface}$), as shown in Section 2: Scaling and Knee Joint Dosing Parameters of Appendix A [86]. Through ICP-MS analysis, they determined that there was 1.63 mg of cobalt per 5 x10_6 cycles [86]. With the understanding that 2 x10_6 cycles represent a year of implant use [135], the initial dose for the TKA model originating from implant use was determined to be 0.893 μg/day (Dose1), as shown in Section 2: Scaling and Knee Joint Dosing Parameters of Appendix A. During the TKA model implementation, the initial dose was multiplied by 7% for the direct connection between the corrosion debris and blood and by 93% for the articulating derived debris and the joint capsule tissue.

4.3.3 Initial Model Parameters

Within the TKA model, there are sixteen model compartments. The compartments manipulated within this research consist of the joint capsule (jc), joint capsule reservoir (jc1), the blood (B1), and the blood reservoir (CB1). The Leggett [4] and Czarnek [2] systemic model included the organs (ORG), the skeleton (SK), the liver (liv), the other tissues (OT), the kidney (K), the kidney reservoir (K1), the urinary bladder (UB), the trabecular bone (TB), the cortical bone (CB), the skeletal reservoir (SK1), the liver reservoir (Liv 1), and the intestine (Intest). The initial compartment cobalt concentrations for both blood (B1) and the joint capsule (jc) were determined from Hallab et al. and were 0.002 μg Co and 0.085 μg Co respectively [43]. The remaining initial compartment cobalt concentrations were left at 0 μg Co, as shown in Section 3: Initial Model Parameters of Appendix A.

4.3.4 Model Transfer Coefficients

The transfer coefficient used within the TKA model describing direct movement of corrosion debris from the device into the blood stream was chosen from the Leggett et al. model [4]. Within this model there are three different tissue groups described with transfer coefficients for two directions of cobalt transfer, ST0, ST1, and ST2 [4]. All three of the coefficients were tested, and ST0 was determined to be the most accurate simulation. Within the TKA model the transfer of material from the device to the blood was 0.099021 $\frac{\mu g\ Co}{day}$ ($K_{sf,b}$), and the transfer of material from the blood to the device was 18$\frac{\mu g\ Co}{day}$ ($K_{b,sf}$), as shown in Section 4: Knee Joint Transfer Coefficients of Appendix A [4]. In the functional TKA model these terms were scaled during model calibration.

The transfer coefficient used in the TKA model for the movement of articulating derived cobalt debris was determined by observing patients previously described in Aim 2 [110]. Within the first cohort of 20 patients the estimated implantation times (n=12 patients), were used to create a relationship of cobalt transferred from the device into the joint capsule tissues per day, as shown in figure 4.3.2. The determined transfer coefficient for articulating debris transfer to the joint capsule tissue was 0.0007 $\frac{\mu g\ Co}{day}$ ($K_{sf,jc}$), as shown in Section 4: Knee Joint Transfer Coefficients of Appendix A. To determine the reverse transfer coefficient, an estimated linear relationship between the three tissue types within the Leggett model was observed, as shown in figure 4.3.3 [4]. The transfer of cobalt from the joint

capsule to the device was 6.07 $\frac{\mu g\ Co}{day}$ ($K_{jc,sf}$) , as shown in Section 4: Knee Joint Transfer Coefficients of Appendix A. In the functional model these terms were scaled during model calibration.

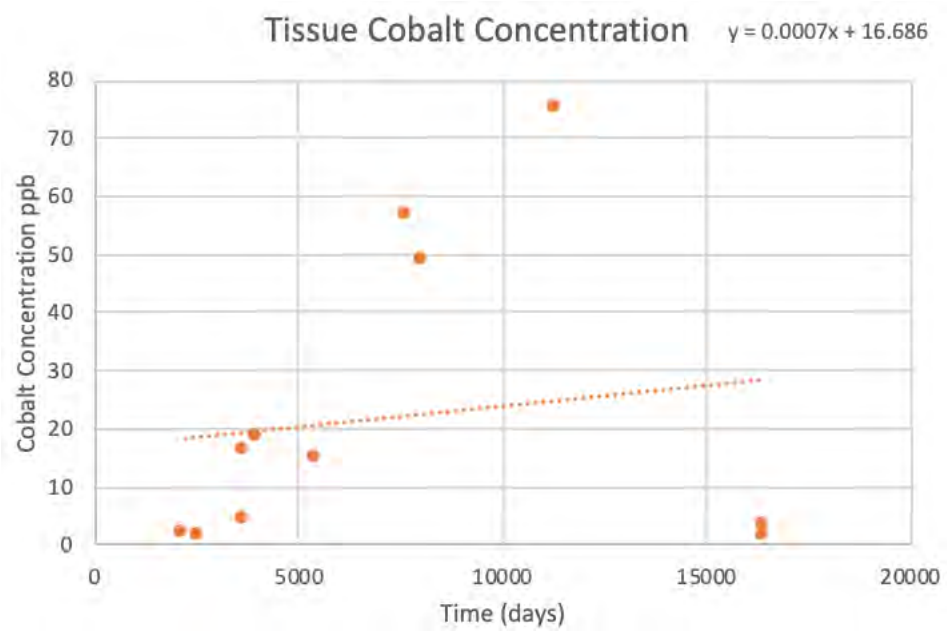

Figure 4.3.2: Linear relationship describing cobalt transferred from the device into the joint capsule tissues per day.

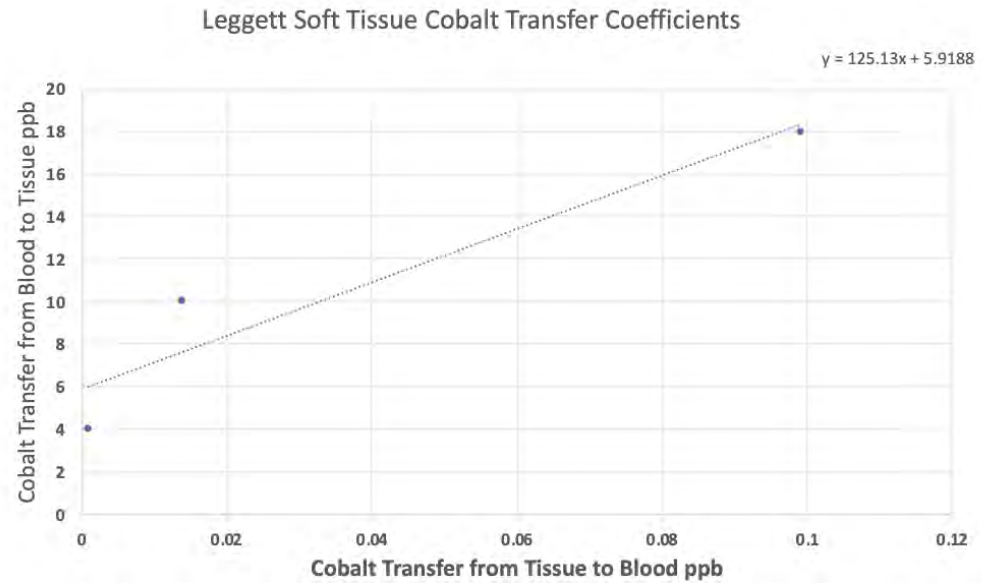

Figure 4.3.3: The estimated linear relationship between the three soft tissue types within the Leggett model [4].

To determine the transfer coefficient used in the TKA model connecting the joint capsule to blood for articulating derived cobalt debris, a study by Lons et al. was chosen [5]. This study observed blood metal measurements for patients with either a posterior stabilized prosthesis, uni compartmental prosthesis, or stem prosthesis, and determined the resulting metal ion levels. These measurements were conducted at three time points, 0 days, 180 days, and 365 days [5]. A trend line was created to determine the rate of cobalt movement into the blood stream using the combined measurements from all observed patients (posterior stabilized prosthesis, uni compartmental prosthesis, and stem prosthesis), as shown in figure 4.3.4. The value

was determined to be 0.0023 $\frac{\mu g\ Co}{day}$ ($K_{jc,b}$), as shown in Section 4: Knee Joint Transfer Coefficients of Appendix A. The transfer coefficient connecting the blood back to the joint capsule was determined using an estimated linear relationship between the three tissue types within the Leggett model, as shown in figure 4.3.3 [4]. The transfer of cobalt from the joint capsule to the device was 6.26 $\frac{\mu g\ Co}{day}$ ($K_{b,jc}$), as shown in Section 4: Knee Joint Transfer Coefficients of Appendix A. In the functional model these terms were scaled during model calibration.

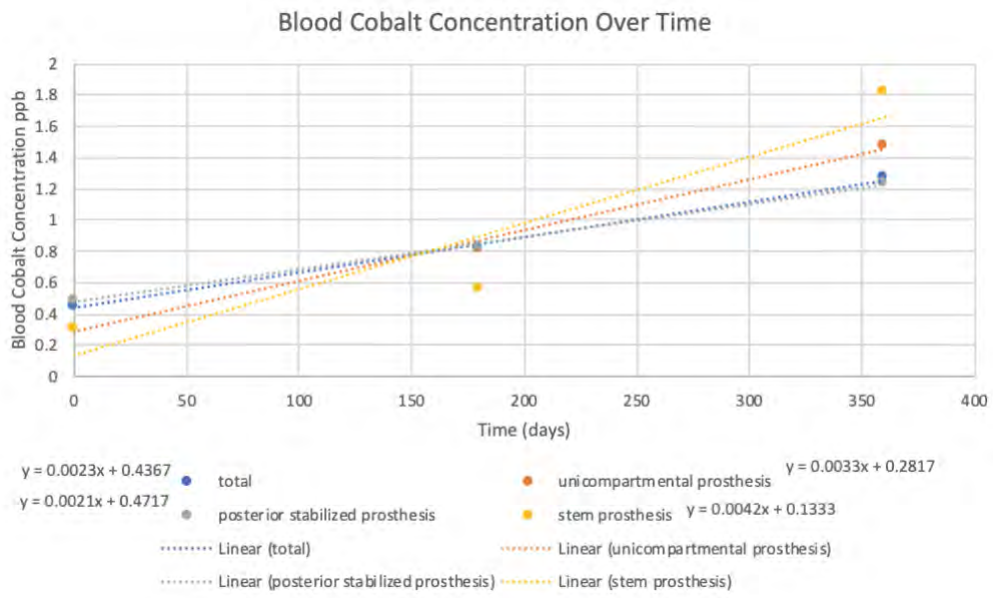

Figure 4.3.4: The rate of cobalt movement into the blood stream described by an estimated linear relationship created using the combined measurements from

posterior stabilized prosthesis, uni compartmental prosthesis, stem prosthesis, and all observed patients.

4.3.5 Consistent Dose and Dose Dependent Simulations

Terms were scaled in a similar fashion to previous models of this type [55]. The initial TKA model ran for a total of 12 years (in units of days: 4380), with consistent dosing of 7 times 0.893 $\frac{\mu g\ Co}{day}$ for the entirety of the 12 years. The finalized scaled transfer coefficients for the model are in Table 4.3.1. The finalized drawn model is shown in Figure 4.3.1. A secondary approach was taken with the TKA model to optimize the dose of debris to achieve a more accurate modeled blood and joint capsule tissue value for each individual patient. The only optimization of the model for this simulation occurred through multiplying the dosing value by different values. Each modeled approach was summarized by comparing the joint capsule tissue and blood cobalt concentrations (matched by implantation time in days) to a single patient measured joint capsule tissue and blood cobalt concentrations (represented by a single implantation time in days). Percent error was calculated and reported.

Throughout this research the main update to the model was altering the exposure point from an oral intake model utilizing ICRP's ailment track model, to the knee joint capsule. The main equations altered to achieve this were equation 1

describing the joint capsule intake and outputs. This compartment connected to equation 2 and 3 which describe a retention compartment for cobalt in the joint capsule tissue (jc1) and blood (B1). Equation 4 describes the bound blood reservoir (CB1). The remaining equations for the systemic model of cobalt movement that correspond with Figure 4.3.1 are reported in Appendix A with the Berkeley Madonna code used to simulate cobalt movement from a TKA device.

$$d/dt(jc) = Dose1 * K_{BearingSurface} * K_{sf,jc} - K_{jc,sf} * B1 - K_{jc,B1} * jc + K_{B1,jc} * B1 - K_{jc,JC1} * jc + K_{JC1,jc} * jc1;$$

Equation 1: Equation for cobalt moving in and out of the joint capsule tissues (jc).

$$d/dt(jc1) = K_{jc,JC1} * jc - K_{JC1,jc} * jc1;$$

Equation 2: Equation for cobalt moving in and out of the joint capsule reservoir (jc1).

$$d/dt(B1) = K_{jc,B1} * jc - K_{B1,jc} * B1 + K_{Corrosion} * Dose1 * K_{sf.B1} B1 * K_{B1,sf} + liv * K_{liv,B1} + Sk * K_{Sk,B1} + CB1 * K_{CB1,B1} - B1 * K_{B1,CB1} - B1 * K_{B1,OR};$$

Equation 3: Equation for cobalt moving in and out of the blood stream (B1).

$$d/dt(CB1) = B1*K_{B1,CB1} - CB1*K_{CB1,B1} ;$$

Equation 4: Equation for cobalt moving in and out of the blood reservoir (CB1).

Table 4.3.1: Finalized Transfer Coefficients used for the Modeling of Cobalt Movement with units of $\frac{\mu g\ Co}{day}$.

$K_{sf,jc}$	0.0007	$K_{liv,b}$	0.05872559	$K_{sk,tb}$	0.03
$K_{jc,sf}$	0.002428	$K_{b1,b}$	0.03915039	$K_{sk,cb}$	0.03
$K_{b,jc}$	0.002504	$K_{jc,jc1}$	0.99714286	$K_{sk,sk1}$	0.15
$K_{jc,b}$	0.00092	$K_{jc1,jc}$	0.996216	$K_{sk1,sk}$	0.15
$K_{sf,b}$	0.3465735	$K_{or,ot}$	0.16	$K_{k,k1}$	0.005
$K_{b,sf}$	0.063	$K_{or,sk}$	0.06	$K_{k1,k}$	0.005
$K_{b,or}$	0.87842624	$K_{or,k}$	0.045	$K_{liv,Int}$	0.2
$K_{b,b1}$	0.05606976	$K_{or,liv}$	0.35	$K_{liv,Liv1}$	0.05
$K_{sk,b}$	0.55463053	$K_{or.ub}$	0.3	$K_{Liv1,liv}$	0.05

Periprosthetic joint capsule tissue and peripheral blood cobalt concentrations were measured from 7 patients using methods previously described in Aim 2 [110].

The 7 implantation times, the measured cobalt concentrations for blood and joint capsule tissue, and device designs are summarized in Table 4.3.2 and Table 4.3.3. The clinical patient and expanded device information for the 7 patients used for model calibration can be found in table 4.3.4 and 4.3.5 respectively.

Table 4.3.2: Cobalt concentrations measured and simulated with a consistent dose for joint capsule tissue and blood. The dose used for this simulation was 7 times the dose value for all patients.

Implantation Time (days)	Femoral Component Design	Tibial Component Design	Measured Blood Cobalt Concentration (μg/L)	Initial Modeled Blood Cobalt Concentration (μg/L)	Initial Model Blood Cobalt Percent Error	Measured Joint Capsule Tissue Cobalt Concentration (μg/L)	Initial Modeled Joint Capsule Tissue Cobalt Concentration (μg/L)	Initial Model Joint Capsule Cobalt Percent Error
822	Posterior Stabilized	Fixed bearing	0.271	0.190	-29.89	0.80	1.42	77.50
912	Cruciate Retaining	Fixed Bearing	0.31	0.190	-38.71	2.30	1.55	-32.61
1004	Posterior Stabilized	Fixed Bearing	0.341	0.190	-44.28	0.97	1.67	71.81
1369	Cruciate Retaining	Fixed Bearing	0.247	0.191	-22.67	1.03	2.09	102.91
2283	Cruciate Retaining	Mobile Bearing	0.421	0.191	-54.63	4.19	2.9	-30.79
3195	Posterior Stabilized	Fixed Bearing	0.241	0.192	-20.33	2.01	3.43	70.65
4291	Cruciate Retaining	Fixed Bearing	0.538	0.192	-64.31	3.04	3.83	25.99

Table 4.3.3: Cobalt concentrations measured and simulated with a patient specific dose for joint capsule tissue and blood.

Implantation Time (days)	Femoral Component Design	Tibial Component Design	Measured Blood Cobalt Concentration (μg/L)	Dose Dependent Modeled Blood Cobalt Concentration (μg/L)	Dose Dependent Model Blood Cobalt Percent Error	Measured Joint Capsule Tissue Cobalt Concentration (μg/L)	Dose Dependent Modeled Joint Capsule Tissue Cobalt Concentration (μg/L)	Dose Dependent Model Joint Capsule Cobalt Percent Error	Dose Multiple Chosen for Dose Dependent Model
822	Posterior Stabilized	Fixed bearing	0.271	0.163	-39.85	1.23	1.19	53.75	6 Times
912	Cruciate Retaining	Fixed Bearing	0.31	0.272	-12.26	2.2	2.31	-4.35	10 Times
1004	Posterior Stabilized	Fixed Bearing	0.341	0.163	-52.20	1.43	1.39	47.12	6 Times
1369	Cruciate Retaining	Fixed Bearing	0.247	0.164	-33.60	1.8	1.75	74.76	6 Times
2283	Cruciate Retaining	Mobile Bearing	0.421	0.274	-34.92	4.13	4.34	-1.43	10 Times
3195	Posterior Stabilized	Fixed Bearing	0.241	0.165	-31.54	2.94	2.85	46.27	6 Times
4291	Cruciate Retaining	Fixed Bearing	0.538	0.165	-69.33	3.28	3.19	7.89	6 Times

Table 4.3.4: Clinical information for 7 patients used for model calibration.

Implantation Time (Days)	Revision Reason	Patient BMI	Patient Gender	Patient Age at Insertion
822	Instability	35.01	M	60
912	Instability	27.26	M	57
1004	Instability	26.50	F	58
1369	Femoral Loosening	26.43	F	71

2283	Femoral Loosening	27.53	F	75
3195	Other	41.62	F	62
4291	Stiffness	35.88	M	59

Table 4.3.5: Device information for 7 patients used for model calibration.

Implantation Time (Days)	Manufacturer	Design	Polyethylene Component Material	Tibial Component Material	Tibial Component Type	Femoral Component Type
822	Biomet	Maxim	Unknown	CoCr	Fixed	posterior stabilized
912	Stryker	Triathlon CR	X3	Ti Alloy	Fixed	cruciate retaining
1004	Stryker	Triathlon PS	X3	CoCr	Fixed	posterior stabilized
1369	Zimmer	Persona CR Left	Gamma Inert	Ti Alloy	Fixed	cruciate retaining
2283	Depuy	Sigma Mobile Bearing	Unknown	CoCr	Mobile Bearing	cruciate retaining
3195	Stryker	Triathlon PS	X3	CoCr	Fixed	posterior stabilized
4291	Zimmer	Nexgen CR Flex	Unknown	Ti Alloy	Fixed	cruciate retaining

4.3.6 Simulating Symptomatic Blood Cobalt Concentrations

A secondary simulation was conducted to determine the likelihood of adverse symptoms due to cobalt circulating within the body. A previous study by Tower et al.

observed two patients with metal-on-metal total hip devices who had elevated cobalt blood metal concentrations that correlated with adverse symptoms such as anxiety, headaches, irritability, fatigue, tinnitus, and hearing loss [29]. For the two case studies, systemic blood cobalt measurements correlated with implantation time of cobalt chromium devices.

The first patient had a blood metal measurement of 83 μg/L at 1290 days [29]. The device was removed, and symptoms subsided at 1620 days. To model this scenario, a multiple of the dosing parameter was applied for 1290 days, and the simulation ran for the remaining time until 1620 days was reached.

The second patient had a blood metal measurement of 23 μg/L at 365 days [29]. The device was removed, and symptoms subsided at 575 days. To model this scenario, a multiple of the dosing parameter was applied for 365 days, and the simulation ran for the remaining time until 575 days was reached.

4.4 Results:

The median measured blood cobalt concentration was 0.31 $\boldsymbol{\mu}$g/L ± 0.11 (range: 0.24 to 0.54 µg/L, Figure 4.4.1), and the median measured joint capsule tissue cobalt concentration was 2.01 $\boldsymbol{\mu}$g/L ± 1.25 (range: 0.8 to 4.19 µg/L, Figure 4.4.2), as provided in Table 4.3.2 and Table 4.3.3.

The median initial modeled blood cobalt concentration was 0.19 μg/L ± 0.0008 (range: 0.190 to 0.192 µg/L, Figure 4.4.1), and the median initial modeled joint capsule tissue cobalt concentration was 2.09 μg/L ± 0.97 (range: 1.42 to 3.83 µg/L, Figure 4.4.2), as provided in Table 4.3.2.

Finally, the median dose dependent blood modeled concentration was 0.17 μg/L ± 0.053 (range: 0.16 to 0.27 µg/L, Figure 4.4.1), and the median dose dependent modeled joint capsule tissue cobalt concentration was 2.20 $\boldsymbol{\mu}$g/L ± 1.06 (range: 1.23 to 4.13 µg/L, Figure 4.4.2), as provided in Table 4.3.3.

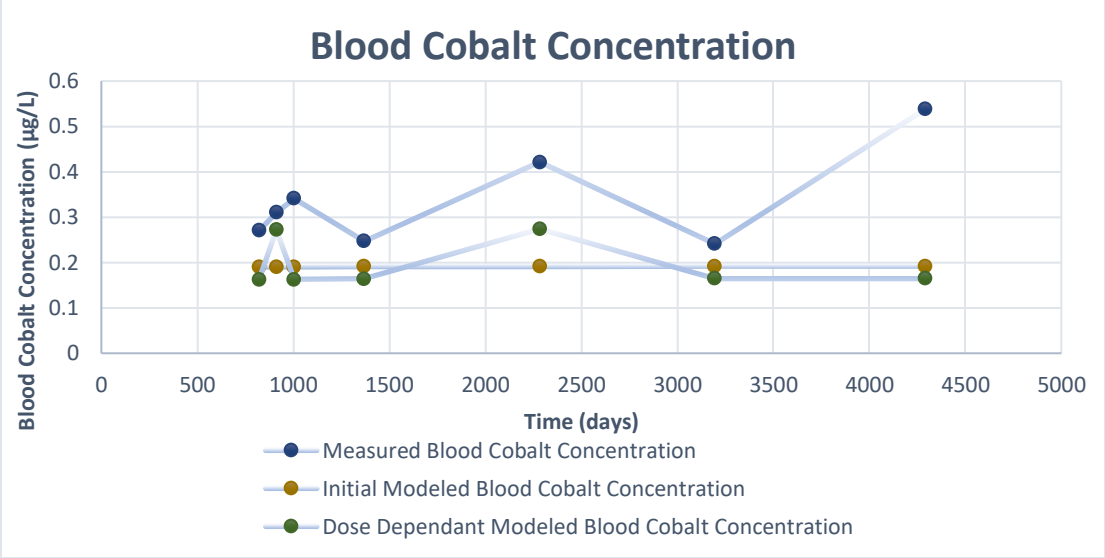

Figure 4.4.1: Comparison of measured blood cobalt concentration and simulated blood cobalt concentrations.

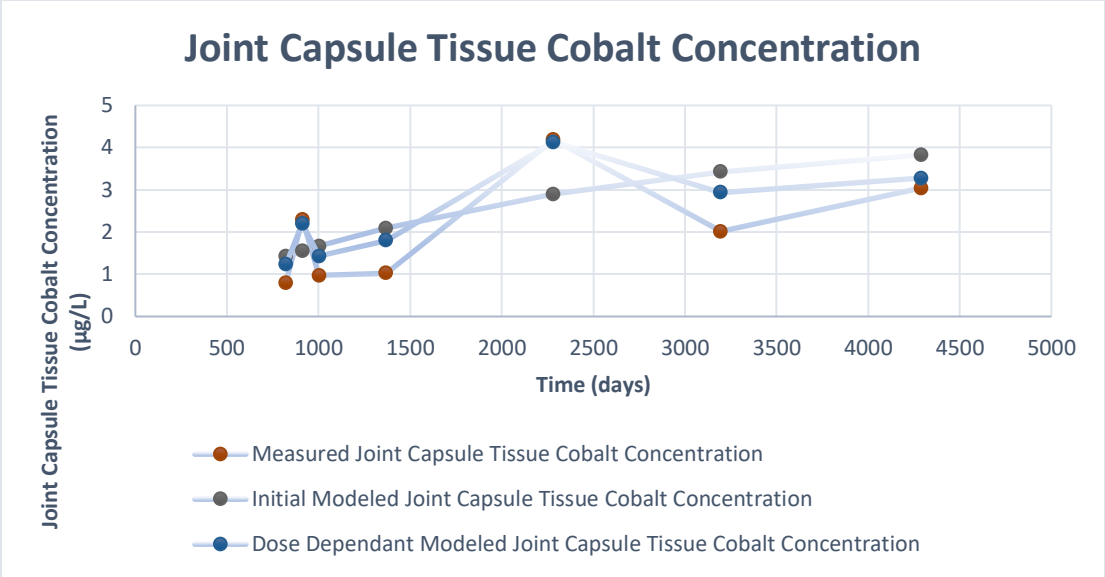

Figure 4.4.2: Comparison of measured joint capsule tissue cobalt concentration and simulated joint capsule tissue cobalt concentrations.

The median percent error between measured and consistent dose TKA modeled blood cobalt concentration was -38% (range: -64.31 to -20.33%), as provided in Table 4.3.2. The median percent error between measured and consistent dose TKA modeled joint capsule tissue cobalt concentration was 70.65% (range: -32.61 to 102.91 %), as provided in Table 4.3.2.

The median percent error between measured and dose dependent TKA modeled blood cobalt concentration was -34.92% (range: -69.33 to -12.26 %), as provided in Table 4.3.3. The median percent error between measured and dose dependent TKA modeled joint capsule tissue cobalt concentration was 46.27% (range: -4.35 to 74.76 %), as provided in Table 4.3.3.

When looking at the dose multiples used in the second modeling approach, there is consistency between 5 patients who have a multiple of 6 (at 822 days, 1004 days, 1369 days, 3195 days, and 4291 days). These 5 patients include 3 posterior stabilized devices and 2 cruciate retaining devices. All 5 patients had a fixed bearing tibial component. The two patients at 912 days and 2283 days had a larger dose multiple of 10 times compared with the other patients. Both of these patients have cruciate retaining devices and the patient at 2283 days had a mobile bearing tibial component.

The current model was used to predict metal ion concentrations for the case studies reported by Tower et al. [29]. In the first case report, the patient had blood cobalt concentration 83 μg/L after 1290 days [29]. The device was removed, and symptoms withdrew after a total of 1620 days. Within the model, a dose of 3,000 times for a duration of 1290 days yielded a blood cobalt concentration of 82 μg/L. The joint capsule measurement was estimated to be 852 μg/L. The model ran for the remainder of the simulation without additional cobalt, and blood cobalt measurement decreased to 0.84 μg/L at 1620 days. The joint capsule measurement decreased to 731 μg/L.

In the second case report, the patient had blood cobalt concentration of 23 μg/L at 365 [29]. The device was removed, and the symptoms withdrew after a total of 575 days. In the model, a dose of 1,000 times for a duration of 365 days yielded a blood cobalt concentration of 27 μg/L. The joint capsule cobalt concentration was estimated to be 98 μg/L. The model ran for the remainder of the

simulation without additional cobalt, and the blood cobalt measurement decreased to 0.10 μg/L at 575 days. The joint capsule cobalt concentration decreased to 89 μg/L.

4.5 Conclusions:

In this study, we attempted to describe the transfer of cobalt within the body of an average total knee arthroplasty patient. The model adapted for our use was initially used for oral ingestion, which most commonly has Co (II) free ions similar to those produced from joint arthroplasty. All of the transfer coefficients were derived from total knee arthroplasty in vivo studies, while the dosing was determined using a total knee arthroplasty simulator study. We explored two approaches, consistent dosing throughout the model and dose dependent modeling, and found that the second approach was more successful. Through the observation of the dose dependent model we observed dose multiple consistencies with consistent device designs, specifically fixed tibial component and posterior stabilized TKA. Additionally, using existing case studies of metal ion concentration, we were able to show that a dose multiple thousands of times larger than the initial dose could potentially produce the blood cobalt concentration consistent with symptomatic patients.

Within this study, there were limitations. The transfer of cobalt from the joint capsule tissue to the bloodstream was derived from a study in which both values were measured for patients. The blood cobalt concentration was assumed to be directly related to the tissue cobalt concentration, however, in the current model, we also assume direct transfer from the device to the blood. This limitation was addressed through model calibration and scaling of transfer coefficients. However, this could

contribute to some of the discrepancies in the model predictions. For this model, the different cobalt concentrations used to derive joint capsule transfer coefficients were measured using ICP-MS. This style of concentration measurement ionizes all cobalt present regardless of the shape or size of the particles. This could alter the transfer rate of cobalt, as smaller debris is thought to move faster through different systems compared to larger particles. This limitation was also addressed through model calibration and the scaling of transfer coefficients. Within this model, calibration was performed with seven patients who had noncontrolled device designs. It is important to note that patients with a posterior stabilized device had a consistent dose dependent multiple of 6, and that the only mobile bearing tibial tray design had one of the largest dose multiples of 10. Additionally, the number of patients was consistent with similar studies used to calibrate models [55]. The model has mild discrepancies between modeled and simulated blood and joint capsule tissue cobalt concentrations. Due to literature limitations, the transfer coefficients were derived from different styles of devices including posterior stabilized and cruciate retaining femoral components. Future work could be used to calibrate the model further by controlling for the device.

When comparing the constant dose model and measured values for cobalt concentration of blood and joint capsule tissue, the constant dose was less accurate compared to the dose dependent approach. This may be because our model was created using transfer coefficients that represent different total knee arthroplasty device designs. The initial dose was based on a simulator study that observed fixed

bearing without a posterior stabilized polyethylene [86], while the transfer coefficients that described the movement of cobalt from the joint capsule to the blood were based on a study including posterior stabilized knee arthroplasty, uni compartmental knee arthroplasties, and stemmed knee arthroplasties [5]. Different device designs have different metal quantities used in the device, which could lead to increased ionized corrosion damage [34, 86]. Additionally, different geometries have different articulating surfaces and areas of stress concentration [136]. We attempted to address these discrepancies through model calibration. However, the components used for model calibration also contained posterior stabilized, cruciate retaining, and one mobile bearing device.

When comparing the dose dependent model and measured cobalt concentrations for the joint capsule tissue and the blood were more accurate compared with the consistent dose approach. When looking more in depth, the patient with the implantation time of 2283 days had a larger multiple of 10, as seen in Table 4.3.3. This represented the only mobile bearing tibial design in the cohort. The mobile bearing tibial device design introduced more metallic wear compared to the fixed design. Mobile bearing tibial insert designs have been shown to improve polyethylene performance on the bearing surface while introducing the possibility of wear on the lower surface [137]. The posterior stabilized designs appear to perform more consistently compared to the cruciate retaining devices, as within Table 4.3.3, these designs all had a consistent dose multiple of 6. The patient represented by 912 days also had a larger multiple of 10 and had a cruciate retaining device. When

analyzing cruciate retaining and posterior stabilized devices, it has been shown that the posterior stabilizing designs can replicate kinematics having consistent and more natural function [138]. Decreased patellofemoral pressure and superior patellofemoral kinematics with posterior stabilized devices are also thought to relate to greater and more consistent posterior femoral rollback and less anterior sliding [139, 140].

It was shown that in order for this model to simulate blood cobalt concentrations consistent with those reported for symptomatic patients [29], a significantly higher dose multiple would be required. These findings suggest that within a functional knee patient, the cobalt burden would be local within the joint instead of systemic, although this dose could be achieved by complete polyethylene wear-through leading to metal on metal articulation, implant malpositioning, or polyethylene fracture. These findings are consistent with TKA patient symptoms, which generally consists of skin allergies and device loosening [80, 81, 92].

In conclusion, we were able to accurately simulate joint capsule and blood cobalt concentrations using a preexisting biokinetic model of inorganic cobalt. The most accurate simulation occurred when the doses were varied from patient to patient. However, 5 of the 7 patients had the same multiple of 6. The dose multiples appeared to describe design features of the TKA devices. The consistent multiple of 6 represented both posterior stabilized device designs and cruciate retaining designs agreeing with literature reports of consistent device performance for posterior stabilized devices. This was compared to cruciate retaining designs which had dose

multiples of either 6 or 10 indicating that the device could have variable performances. The largest dose multiple of 10 was required to simulate the mobile bearing tibial device agreed with literature reports describing increased wear due to two potential sources. We were also able to simulate blood cobalt concentrations consistent with symptomatic concentrations previously reported. However, the required doses indicate that for most patients, similar adverse outcomes would be unlikely. These findings also agree with literature reports of local reactions for TKA metal sensitivity compared with systemic reactions observed in specific metal on metal total hip arthroplasty patients. In conclusion, we highlighted the importance of device design and its relationship to the initial dose released and described a scenario where a TKA patient could have systemic symptoms. It appears that with the current observed patients and TKA device designs that cobalt toxicity symptoms in TKA patients is less likely to occur. However, continued observation of new designs is important as this could change the dose and more importantly the patient outcome.

Chapter 5

5.1 Conclusions and Future Work

This body of work sought to describe metallic debris release from TKA and described the potential dangers this could pose to patient outcomes after arthroplasty. The beginning of this work sought to outline mechanisms that could release metallic debris from a total knee femoral component and describe each mechanism's prevalence. This investigation determined that the most abundant damage mechanism was third-body damage on the bearing surface. This information was used when forming a hypothesis for the preferred location of debris collection. For this, it was initially hypothesized that the medial and lateral gutter regions, located on either side of the bearing surface, would be the preferred location. However, within the second aim, it was determined that the different periprosthetic tissues were statistically similar in terms of concentration of metallic debris, the size of isolated debris (except for ECD of the micron-sized debris), and the shape of debris. Due to these findings, it was less critical where the tissue was collected, as any of the retrieved tissues were thought to not be statistically different between sampling locations. The final aspect of this dissertation was a discussion of cobalt mobility throughout the body as it is an element of the CoCr alloy used to create most femoral components. Additionally, cobalt is a trace element within the human body, which can have toxic effects and adverse patient symptoms in large concentrations. The simulation was validated using a cohort of 7 patients, highlighting the relationship between design and dose of metallic debris.

It was also shown through simulations that a dose of 3,000 and 1,000 times the initial dose of a total knee patient would be required to achieve literature reported symptomatic blood cobalt concentrations. Although these conclusions infer that it is unlikely for a total knee patient to reach a high enough blood cobalt concentration, it is still possible. Different patients have shown different susceptibilities to cobalt toxicity and systemic symptoms based on preexisting conditions and patient genetics [30]. Additionally, although systemic impairment may be less likely, local reactions to cobalt and other metallic debris have elicited negative patient symptoms.

Evidence was presented throughout this body of work, showing the potential for metal release from total knee arthroplasty. In the first aim of this research, we investigated different damage modes observed in the long term implanted femoral components (>15 years in vivo). Due to the prevalence, third-body damage received further investigation. In a second study, observing 256 femoral knee components in situ between 1 and 15 years, the cumulative femoral damage score was correlated with increased surface roughness measurement [141]. The surface roughness measurements were performed using white light interferometry (Zygo, NewView 6000, Middlefield, CT) [141]. The medial and lateral sides of each component were evaluated in 3 locations in a straight line across the apex of the bearing surface [141]. The Ra (arithmetic average height parameter) and the Rq (standard deviation of the distribution of surface heights) were reported [141, 142]. Both the Ra ($r=0.196$; $P=0.002$) and Rq ($r=0.157$; $P=0.012$) measurements increased with increased damage score [141]. Other important findings from this investigation included observations

of similar damage mechanisms compared to long-term TKA [141]. Additionally, associations between loosening, patient weight, and anterior-posterior device conformity were associated with increased surface damage [141].

The joint capsule debris was characterized by describing concentration, shape, size, and inferring the material's bioreactivity. A smaller cohort of three patients with different materials was used to describe the shape and size of debris. In order to confirm the findings reported, we would recommend repeating these studies. Additionally, due to the findings in aim 3 regarding device design, it would be useful to control the device design. Specifically, differentiating between posterior stabilized femoral device design and cruciate-retaining device design. Differentiating between the mobile-bearing and fixed tibial device design would also be useful. It would be recommended to have a minimum of 3 patients with the same style of the device. In order to maintain complete control of the study outcomes, it is also recommended that the metals used for the devices be the same. An example would be a posterior stabilized cobalt-chrome femoral device with a fixed bearing titanium tibial device. These findings could help to increase knowledge of debris dosing for the model used in aim three, while also providing debris characteristics for specific devices that could infer the potential for a biological reaction.

Within the second aim we also described the biological reactivity of the debris by analyzing cytokines within the collected synovial fluid. Contrary to our hypothesis, the cytokines were inversely correlated with cobalt and chromium concentration. We hypothesized that this could have occurred for a number of

reasons. One was the large concentration of each metal debris may have caused necrosis in the region. A separate theory was that instead of the macrophage recruitment pathway that the cytokines we analyzed were a part of, that a different pathway such as a pathway involving adaptive and innate immunity. Finally, it could be due to the synovial fluid being collected at autopsy and the cytokines were already denatured. In order to determine the correct answer, we recommend repeating the study to confirm the same or similar findings. This could address the first theory of necrosis due to concentration. Additionally, the study could be repeated with a different cytokine analysis observing cytokines recruited for this different pathway. Finally, if deemed appropriate synovial fluid can be aspirated from a living patient and analyzed. The shortcoming of this approach is that aspirating synovial fluid is invasive as the synovial fluid is the joint lubricant and needed for joint success.

A separate approach that could imply the biological reactions to debris within the system could be reactive oxygen and nitrogen species within the blood or synovial fluid [143]. These species are naturally occurring within the body occurring mainly at the site of electron transport within cell mitochondria [143]. Oxidative stress can also be produced in response to bodily trauma such as surgery [143]. Essentially under normal conditions the formation of reactive species is balanced with enzymatic and nonenzymatic antioxidant systems [143]. However, under adverse conditions the formation of these species exceeds this control mechanism [143]. Oxidative stress can be induced by inflammation and hypoxia derived from phagocytic cells in the synovium such as macrophages, monocytes, and neutrophils [143]. These cells are

thought to be recruited in response to metallic and other debris released from in vivo use of arthroplasty devices. Essentially observed oxidative stress would provide commentary of the biological reaction occurring.

Finally, cobalt movement throughout the human body of an average patient was modeled by changing the exposure point of a preexisting biokinetic model describing Co (II). This model was used to provide commentary of systemic cobalt movement. Specifically, the topic of cobalt related toxicity in the context of a total knee patient was described.

Throughout model simulations, the relationship between device design and the dose of cobalt was highlighted. In response to this, future work should control for device design. Specifically, the model transfer coefficients and initial dose could be altered to increase the model accuracy. The initial dose was derived from a simulator study where they observed cruciate retaining femoral components and a fixed tibial component. For the posterior stabilized model, this simulation could be repeated to determine the dose of a posterior stabilized device. Similarly, the transfer coefficient used to describe cobalt movement from the tissues into the bloodstream was derived from a study where they observed a posterior stabilized femoral component and a fixed tibial component. For the cruciate-retaining model, this study could be repeated to determine a new transfer coefficient that is cruciate-retaining specific. A matched cohort controlling for the device design could be created controlling for patient weight, implantation time, and the revision reason, specifically loosening or infection, as these were shown to be associated with increased third-body damage [141]. The

recommended device design groups to observe differences in femoral components would be a posterior stabilized femoral component paired with a fixed tibial tray and a cruciate-retaining femoral component paired with a fixed tibial tray. The recommended device design groups to observe differences in tibial components would be the posterior stabilized femoral component with a fixed tibial tray and posterior stabilized femoral component with a mobile-bearing tibial tray.

Future work with the model could also include further model calibration, and sensitivity analysis. One aspect of model calibration could occur through observations of a post-mortem total knee patient observing joint capsule tissue cobalt concentrations and organ sample cobalt concentrations of the same patient harvested on the same day with reported implantation times. The recommended organs would be those observed within the model, specifically the kidney, the liver, and bone. By collecting all three samples and the joint capsule tissue sample from the same patient with the same implantation time, it would allow for an understanding of material traveling from the larger organ reservoir into the specific organ compartments. The joint capsule tissue cobalt concentration would maintain the connection to the total knee joint. Model sensitivity analysis would be achievable with a larger cohort size for comparing actual measured blood and tissue cobalt concentrations with those predicted by the model. A statistical model observing the associations between patient and device factors and increased percent error between measured and predicted cobalt concentrations would help determine factors that the model was sensitive to. Specific patient factors could include the patients gender, weight,

incidence of kidney or liver related disease, and revision related to device loosening. Specific device factors could include the femoral device design (cruciate retaining vs. posterior stabilized), the tibial device design (mobile bearing vs. fixed bearing), and the device conformity ratio (describing how well the femoral bearing surface fits into the tibial insert. Beyond this, manipulation of the transfer coefficients and reported changes to the predicted blood or tissue cobalt concentrations would be valuable. Modifying different transfers of material and describing its effect on the models predictions would describe the sensitivity and specificity of the model.

Overall this body of work discussed potential patient reactions to released metallic debris, specifically cobalt debris from the femoral component. Beyond the above-discussed examinations that could further describe the potential for patient reactions to this metallic debris, there is an alternative solution. The metal, a known sensitizing material [43], could be removed and replaced with alternative materials. This approach is similar to the adverse reaction to metal debris simulation, where the solution to the patient's affliction due to cobalt was to remove the source of cobalt, the medical device [29]. Ceramic components have existed within arthroplasty for many years, specifically in total hip arthroplasty. Ceramic components are used to replace cobalt-chromium femoral heads and liners. Similarly, in total knee arthroplasty, surgeons could replace the cobalt-chromium femoral component with a ceramic femoral component to solve metal sensitivity [144]. Studies of implantation of femoral components composed of modern ceramic material, zirconia toughened alumina, have been conducted [145]. Additionally, a fully metal-free system has

been proposed to replace the tibial component with a ceramic component [146]. However, within these different studies, there is a discussion of radiolucent lines indicating device loosening [145, 146]. Interest in implant loosening is partly related to stress shielding, which can occur with metallic components and ceramic components due to increased material strength leading to a lack of bone stress. Long term effects of this could result in a loss of bone stock and implant loosening.

In contrast to this material, there is another material being investigated for total knee replacement, polyetheretherketone (PEEK). This material has been shown to be able to perform similarly to cobalt chrome in pre-clinical studies [147]. Simulator studies showed a statistically significant increase in surface roughness of the PEEK; however, they claimed that this did not affect the wear rate of the materials [148]. Additionally, finite element analysis has shown that due to PEEK material properties, it can reduce stress shielding and protect the bone stock preventing loosening of the device [147]. Either approach would remove the source of cobalt, alleviating patient symptoms for individuals with metal sensitivity.

In conclusion, this body of work outlined different metallic release mechanisms, highlighting the most abundant mechanism as third-body damage. Secondly, it was described that different tissue collection sites were statistically similar, allowing for the selection of tissues independent of location. Isolated debris was observed in a size range that could be phagocytosed by a range of peri-implant cells such as osteoblasts and fibroblasts. However, cytokines thought to be involved with adverse bone homeostasis were negatively correlated with metallic debris.

Finally, a biokinetic model was updated to describe the cobalt movement throughout the body of an average TKA patient. This model was used to try to simulate blood cobalt concentrations associated with symptomatic patients. It was shown that this was less likely due to the required dose multiple in the thousands. However, changes to implant design could alter the potential for larger quantities of debris to be released. For patients with metal sensitivity, it is recommended to remove the source of the metal debris and replace it with an alternate material such as PEEK or zirconia toughened alumina.

Vita

Christina M. Arnholt

Education

(in progress) **Drexel University, Philadelphia, Pennsylvania**
School of Biomedical Engineering, Science, and Health Systems
PhD in Biomedical Engineering
Cumulative GPA: 3.89

June 2015 **Drexel University, Philadelphia, Pennsylvania**
School of Biomedical Engineering, Science, and Health Systems
MS in Biomedical Engineering
BS in Biomedical Engineering
Cumulative GPA: 3.62

Professional Experience

Drexel University, Implant Research Core, Philadelphia, PA
Current PhD, September 2015 to Present

Dissertation Topic: Total Knee Replacement: *Evaluating the Local and Systemic Collection, and Biological Impact of Cobalt and other Metallic Debris*

- Analyzed long term, and moderate term TKA devices for severity of surface damage and used statistical analysis to determine patient or implant factors that may be associated with damage
    - Created a semi-quantitative scoring mechanism to determine bearing surface damage of TKA devices
- Analyzed peri-prosthetic tissues, blood, and organs from revised and postmortem TKA devices for metallic content
    - Developed a protocol for acid reflux of synovial tissues for ICP-MS analysis of ion content
- Performed particle isolation at the University of Leeds.
    - Particles were analyzed for particle shape and size in accordance with ASTM standard F1877-5 Standard Practice for Characterization of Particles

- Updated a biokinetic model to discuss cobalt mobility within total knee arthroplasty

Master's Degree, June 2015

Dissertation Topic: Micro-grooved Surface Topography Does Not Influence Fretting Corrosion of Tapers in THA: Classification and Retrieval Analysis

- Created a classification system for surface morphology of a THA taper and utilized for the generation of two cohorts: smooth and micro-grooved surface topographies.
- Preformed a step forward Anova analysis for the determination of variables associated with mechanically assisted crevice corrosion (MACC)
- Created a cohort matched for previously determined parameters that were associated with MACC taper damage, to analyze the effect of surface morphology

Engineering Assistant, September 2011 to 2014

- Provided maintenance of information and organization of Arthroplasty retrievals (total hip arthroplasty, total knee arthroplasty, total shoulder arthroplasty)
- Coauthor on review article on ceramic composites in orthopedics
- Co-researcher on a polymer composite study, including research of different standards and comparable materials
- Completed destructive testing of materials (metals, ceramic, polyethylene and porous metals) discovering properties of degradation

Publications

Kurtz, S. M., Kocagöz, S., Arnholt, C., Huet, R., Ueno, M., & Walter, W. L. (2014). Advances in zirconia toughened alumina biomaterials for total joint replacement. *Journal of the mechanical behavior of biomedical materials*, *31*, 107-116.

Arnholt, C. M., MacDonald, D. W., Tohfafarosh, M., Gilbert, J. L., Rimnac, C. M., Kurtz, S. M., ... & Lee, G. C. (2014). Mechanically assisted taper corrosion in modular TKA. *The Journal of arthroplasty*, *29*(9), 205-208.

Gilbert, J. L., Sivan, S., Liu, Y., Kocagöz, S. B., Arnholt, C. M., & Kurtz, S. M. (2015). Direct in vivo inflammatory cell-induced corrosion of CoCrMo alloy orthopedic implant surfaces. *Journal of Biomedical Materials Research Part A*, *103*(1), 211-223.

Arnholt C, Underwood R, MacDonald D, Higgs G, Chen A, Klein G, Hamlin B, Lee GC, Mont M, Cates H, Malkani A. (2015) Microgrooved surface topography does not influence fretting corrosion of tapers in total hip arthroplasty: classification and retrieval analysis. In Modularity and tapers in total joint replacement devices 2015 Dec. ASTM International. (Masters dissertation, Drexel University).

Arnholt, C. M., MacDonald, D. W., Malkani, A. L., Klein, G. R., Rimnac, C. M., Kurtz, S. M., ... & Implant Research Center Writing Committee. (2016). Corrosion Damage and Wear Mechanisms in Long-Term Retrieved CoCr Femoral Components for Total Knee Arthroplasty. *The Journal of Arthroplasty*, *31*(12), 2900-2906.

Arnholt, C. M., MacDonald, D. W., Underwood, R., Guyer, E. P., Rimnac, C. M., Kurtz, S. M., ... & Hamlin, B. (2016). Do Stem Taper Microgrooves Influence Taper Corrosion in Total Hip Arthroplasty? A Matched Cohort Retrieval Study. *The Journal of Arthroplasty*.

Day, J., MacDonald, D., Arnholt, C., Williams, G., Getz, C., Kraay, M., ... & Kurtz, S. (2016). TAPER CORROSION IN RETRIEVED TOTAL SHOULDER REPLACEMENT. *Bone Joint J*, *98*(SUPP 1), 108-108.

Arnholt, C.M., MacDonald, D. W., Gregg, K. R., Cates, H. E., Rimnac, C. M. Kurtz S.M. (2018) What is the Incidence of CoCr Damage Modes on the Bearing Surface of Contemporary Femoral Component Designs for Total Knee Replacements? *The Journal of arthroplasty* 33.10 (2018): 3313-3319.

Arnholt, C., Lowell, J., Perkins, M., Kurtz, S., & Mihalko, W. (2018). Analysis Techniques for Polyethylene Implants in Total Knee Arthroplasty. In *Beyond the Implant: Retrieval Analysis Methods for Implant Surveillance*. ASTM International.

Perkins, M., Lowell, J., Arnholt, C., MacDonald, D., Kerkhof, A. L., Kurtz, S. M., Mihalko, W. M. (2018). Is Soft Tissue Laxity Associated with Tissue Metal

Concentrations after Total Knee Arthroplasty?. *Journal of long-term effects of medical implants*, *28*(2).

Heise G, Arnholt C, Sorrels JH, Morrow B, Kurtz S, Mihalko WM. (2019). Comparison of Inflammatory Cell-Induced Corrosion and Electrocautery-Induced Damage of Total Knee Implants. Journal of Long-Term Effects of Medical Implants, 29 (3).

Arnholt CM, White JB, Lowell JA, Perkins MR, Mihalko WM, Kurtz SM. (2020). Postmortem retrieval analysis of metallosis and periprosthetic tissue metal concentrations in total knee arthroplasty. *The Journal of Arthroplasty* 35 (2).

Perkins M, Arnholt C, MacDonald D, Kurtz SM, Mihalko WM. (2020). Retrieval Analysis of Cruciate-Retaining and Posterior-Stabilized Total Knee Arthroplasty and Correlations to Laxity and Wear. *The Journal of Arthroplasty*.

Presentations

Arnholt CM, Patel J, Lal S, White JB, Perkins MR, Mihalko WM, Tipper J, Kurtz SM. **Metallic Wear Debris Isolation and Characterization: A Cadaver TKA Study.** Paper 5904, International Society for Technology in Arthoplasty, London, UK, October 10-13, 2018.

Arnholt CM, White JB, Macdonald DW, Lowell JA, Perkins MR, Mihalko WM, Kurtz SM. **Metallosis and Tissue Metal Concentrations from Autopsy Retrieved TKA.** Paper 5905, International Society for Technology in Arthoplasty, London, UK, October 10-13, 2018.

Arnholt CM, White JB, Higgs GB, MacDonald DW, Lowell JA, Perkins MR, Mihalko WM, Kurtz
SM. **Associations Between Metallosis andTissue Metal Concentration in Autopsy Retrieved TKA.** Paper 207, Transactions of the Orthopaedic Research Society, New Orleans, LA, March 10-13, 2018.

Arnholt CM, MacDonald DW, Lowell J, Mihalko W, Kurtz SM, **Metal Release and Damage Mechanisms in Autopsy Total Knee Arthroplasty Femoral**

Components. Symposium on Beyond the Implant: Retrieval Analysis Methods for Implant Surveillance, May 9, 2017, Toronto, ON, Canada

Arnholt CM, MacDonald DW, Kocagoz S, Chen AF, Cates H, Klein GR, Rimnac CM, Kurtz SM. **Bearing Surface Corrosion and Damage Mechanisms in Retrieved Total Knee Arthroplasty Femoral Components.** Paper 468. 82nd Annual Meeting of the American Academy of Orthopaedic Surgeons. Orlando, FL, March 1 - 5, 2016.

Arnholt CM, MacDonald DW, Kocagoz S, Chen AF, Cates H, Klein GR, Rimnac CM, Kurtz SM. **Does a Micro-grooved Surface Topography Influence Fretting Corrosion of Tapers in THA?** 28th Annual Congress of the International Society for Technology in Arthroplasty. Vienna, Austria October 1st – 3rd, 2015.

Arnholt CM, Underwood RJ, MacDonald DW, Higgs GB, Chen A, Klein GR, Kraay M, Rimnac CM, Kurtz SM. **Micro-Grooved Surface Topography Does Not Influence Fretting Corrosion of Tapers in THA: Classification and Analysis.** 16th EFORT Congress. Prague, Czech Republic, May 27th – 29th 2015.

Arnholt CM, Underwood RJ, MacDonald DW, Higgs GB, Chen A, Klein GR, Hamlin B, Lee GC, Mont MA, Cates H, Malkani A, Rimnac CM, Kurtz SM. **Micro-grooved Surface Topography Does Not Influence Fretting Corrosion of Tapers in THA: Classification and Retrieval Analysis.** Symposium on Modularity and Tapers in Total Joint Replacement Devices. ASTM International, New Orleans, LA, November 10th, 2014.

Arnholt C, MacDonald DW, Tohfafarosh M, Gilbert JL, Klein GR, Mont MA, Parvizi J, Rimnac CM, Kurtz SM. **Mechanically Assisted Taper Corrosion in Modular TKA.** Paper No 318, 81st Annual Meeting of the American Academy of Orthopaedic Surgeons, New Orleans, LA, March 11–15, 2014.

Arnholt CM, Kocagoz SB, MacDonald DW, Gilbert JL, Parvizi J, Malkani A, Klein GR, Rimnac CM, Kurtz SM. **Corrosion and Damage Mechanisms in Retrieved Long-Term TKA Femoral Components.** 1st Annual Pan Pacific Orthopaedic Congress, International Congress for Joint Reconstruction, Kona, Hawaii, USA, July 16 - 19, 2014.

Arnholt CM, Kocagoz SB, MacDonald DW, Gilbert JL, Parvizi J, Malkani AL, Klein GR, Kraay MJ, Rimnac CM, Kurtz SM. **Corrosion and Damage Mechanisms in Retrieved Long-Term TKA Femoral Components.** 27th Annual Congress of the International Society for Technology in Arthroplasty, Kyoto, Japan, Sept 24 - 27, 2014.

Arnholt C, MacDonald DW, Tohfafarosh M, Gilbert JL, Rimnac CM, and Kurtz SM. **Mechanically Assisted Taper Corrosion in TKA.** Paper No. 34. 23rd Annual Meeting of the American Association of Hip and Knee Surgeons, Dallas, TX, November 8-10, 2013.

References

1. Protection, I.C.o.R., *Human alimentary tract model for radiological protection.* ICRP Publication 100. Ann. ICRP, 2006. **36**(1–2).
2. Czarnek, K., S. Terpiłowska, and A.K. Siwicki, *Selected aspects of the action of cobalt ions in the human body.* Central-European journal of immunology, 2015. **40**(2): p. 236.
3. Gilbert, J.L., et al., *Direct in vivo inflammatory cell-induced corrosion of CoCrMo alloy orthopedic implant surfaces.* Journal of Biomedical Materials Research Part A, 2014.
4. Leggett, R.W., *The biokinetics of inorganic cobalt in the human body.* Science of the total environment, 2008. **389**(2-3): p. 259-269.
5. Lons, A., et al., *Metallic ion release after knee prosthesis implantation: a prospective study.* International orthopaedics, 2017. **41**(12): p. 2503-2508.
6. Inacio, M., et al., *Projected increase in total knee arthroplasty in the United States–an alternative projection model.* Osteoarthritis and cartilage, 2017. **25**(11): p. 1797-1803.
7. Pitta, M., et al., *Failure after modern total knee arthroplasty: a prospective study of 18,065 knees.* The Journal of arthroplasty, 2018. **33**(2): p. 407-414.
8. Niki, Y., et al., *Screening for symptomatic metal sensitivity: a prospective study of 92 patients undergoing total knee arthroplasty.* Biomaterials, 2005. **26**(9): p. 1019-1026.
9. Basko-Plluska, J.L., J.P. Thyssen, and P.C. Schalock, *Cutaneous and systemic hypersensitivity reactions to metallic implants.* Dermatitis, 2011. **22**(2): p. 65-79.
10. Arnholt, C., et al., *Bearing Surface Corrosion and Damage Mechanisms in Retrieved Total Knee Arthroplasty Femoral Components.* ISTA Conference. Vienna, Austria 2016. **Podium Presentation**.
11. Hosip-Flor, S. and D.K. Lester, *Human postmortem retrieval of total hip arthroplasty.* The Journal of arthroplasty, 1997. **12**(5): p. 562-567.
12. Jacobs, J.J., et al., *Postmortem retrieval of total joint replacement components.* Journal of Biomedical Materials Research: An Official Journal of The Society for Biomaterials, The Japanese Society for Biomaterials, and The Australian Society for Biomaterials, 1999. **48**(3): p. 385-391.
13. Hirakawa, K., et al., *Mechanisms of failure of total hip replacements: lessons learned from retrieval studies.* Clinical Orthopaedics and Related Research®, 2004. **420**: p. 10-17.
14. Knowlton, C.B., P. Bhutani, and M.A. Wimmer, *Relationship of surface damage appearance and volumetric wear in retrieved TKR polyethylene liners.* Journal of Biomedical Materials Research Part B: Applied Biomaterials, 2017. **105**(7): p. 2053-2059.

15. Pourzal, R., et al., *How does wear rate compare in well-functioning total hip and knee replacements? A postmortem polyethylene liner study.* Clinical Orthopaedics and Related Research®, 2016. **474**(8): p. 1867-1875.
16. Skurla, C.P. and S.P. James, *Assessing the dog as a model for human total hip replacement: Analysis of 38 postmortem-retrieved canine cemented acetabular components.* Journal of Biomedical Materials Research Part B: Applied Biomaterials: An Official Journal of The Society for Biomaterials, The Japanese Society for Biomaterials, and The Australian Society for Biomaterials and the Korean Society for Biomaterials, 2005. **73**(2): p. 260-270.
17. de Uhlenbrock, A.G., et al., *Influence of time in-situ and implant type on fixation strength of cemented tibial trays—a post mortem retrieval analysis.* Clinical Biomechanics, 2012. **27**(9): p. 929-935.
18. Miller, M.A., et al., *Loss of cement-bone interlock in retrieved tibial components from total knee arthroplasties.* Clinical Orthopaedics and Related Research®, 2014. **472**(1): p. 304-313.
19. Miller, M.A., et al., *Increased initial cement–bone interlock correlates with reduced total knee arthroplasty micro-motion following in vivo service.* Journal of biomechanics, 2014. **47**(10): p. 2460-2466.
20. Böhm, G., et al., *Morphometric examination of straight, tapered titanium stems: a retrieval study.* Clinical Orthopaedics and Related Research®, 2001. **393**: p. 13-24.
21. Campbell, P., et al., *Autopsy analysis thirty years after metal-on-metal total hip replacement: a case report.* JBJS, 2003. **85**(11): p. 2218-2222.
22. Zywiel, M., et al., *Fatal cardiomyopathy after revision total hip replacement for fracture of a ceramic liner.* The bone & joint journal, 2013. **95**(1): p. 31-37.
23. Robertsson, O., et al., *Patient satisfaction after knee arthroplasty: a report on 27,372 knees operated on between 1981 and 1995 in Sweden.* Acta Orthopaedica Scandinavica, 2000. **71**(3): p. 262-267.
24. Heck, D.A., et al., *Patient outcomes after knee replacement.* Clinical Orthopaedics and Related Research®, 1998. **356**: p. 93-110.
25. Wylde, V., et al., *Patient-reported outcomes after fixed-versus mobile-bearing total knee replacement: a multi-centre randomised controlled trial using the Kinemax total knee replacement.* The Journal of bone and joint surgery. British volume, 2008. **90**(9): p. 1172-1179.
26. Hawker, G., et al., *Health-related quality of life after knee replacement. Results of the knee replacement patient outcomes research team study.* Jbjs, 1998. **80**(2): p. 163-73.
27. Bourne, R.B., et al., *Patient satisfaction after total knee arthroplasty: who is satisfied and who is not?* Clinical Orthopaedics and Related Research®, 2010. **468**(1): p. 57-63.

28. Gessner, B.D., et al., *A systematic review of systemic cobaltism after wear or corrosion of chrome-cobalt hip implants.* Journal of patient safety, 2019. **15**(2): p. 97-104.
29. Tower, S.S., *Arthroprosthetic cobaltism: neurological and cardiac manifestations in two patients with metal-on-metal arthroplasty: a case report.* JBJS, 2010. **92**(17): p. 2847-2851.
30. Leyssens, L., et al., *Cobalt toxicity in humans—A review of the potential sources and systemic health effects.* Toxicology, 2017. **387**: p. 43-56.
31. Paustenbach, D.J., et al., *A review of the health hazards posed by cobalt.* Critical reviews in toxicology, 2013. **43**(4): p. 316-362.
32. Scharf, B., et al., *Molecular analysis of chromium and cobalt-related toxicity.* Scientific reports, 2014. **4**: p. 5729.
33. Narayan, R.J., *13. Biologic Aspects of Implant Wear*, in *ASM Handbook, Volume 23 - Materials for Medical Devices*. ASM International.
34. Jacobs, J.J., J.L. Gilbert, and R.M. Urban, *Current Concepts Review-Corrosion of Metal Orthopaedic Implants*.* The Journal of Bone & Joint Surgery, 1998. **80**(2): p. 268-82.
35. Willert, H.G. and M. Semlitsch, *Reactions of the articular capsule to wear products of artificial joint prostheses.* Journal of biomedical materials research, 1977. **11**(2): p. 157-164.
36. Chang, J.-D., et al., *Revision total hip arthroplasty in hip joints with metallosis: a single-center experience with 31 cases.* The Journal of arthroplasty, 2005. **20**(5): p. 568-573.
37. Lohmann, C., et al., *Periprosthetic tissue metal content but not serum metal content predicts the type of tissue response in failed small-diameter metal-on-metal total hip arthroplasties.* JBJS, 2013. **95**(17): p. 1561-1568.
38. Matusiewicz, H., *Potential release of in vivo trace metals from metallic medical implants in the human body: from ions to nanoparticles–a systematic analytical review.* Acta biomaterialia, 2014. **10**(6): p. 2379-2403.
39. Dobbs, H. and M. Minski, *Metal ion release after total hip replacement.* Biomaterials, 1980. **1**(4): p. 193-198.
40. Jones, D.A., et al., *Cobalt toxicity after McKee hip arthroplasty.* The Journal of bone and joint surgery. British volume, 1975. **57**(3): p. 289-296.
41. Kerger, B.D., et al., *Total cobalt determination in human blood and synovial fluid using inductively coupled plasma-mass spectrometry: method validation and evaluation of performance variables affecting metal hip implant patient samples.* Toxicological & Environmental Chemistry, 2015. **97**(9): p. 1145-1163.
42. Batista, B.L., et al., *Determination of trace elements in biological samples by inductively coupled plasma mass spectrometry with tetramethylammonium*

hydroxide solubilization at room temperature. Analytica chimica acta, 2009. **646**(1-2): p. 23-29.
43. Hallab, N.J. and J.J. Jacobs, *Biologic effects of implant debris.* Bulletin of the NYU hospital for joint diseases, 2009. **67**(2): p. 182.
44. Madl, A.K., et al., *Toxicology of wear particles of cobalt-chromium alloy metal-on-metal hip implants Part II: Importance of physicochemical properties and dose in animal and in vitro studies as a basis for risk assessment.* Nanomedicine: Nanotechnology, Biology and Medicine, 2015. **11**(5): p. 1285-1298.
45. Madl, A.K., et al., *Toxicology of wear particles of cobalt-chromium alloy metal-on-metal hip implants Part I: Physicochemical properties in patient and simulator studies.* Nanomedicine: nanotechnology, biology and medicine, 2015. **11**(5): p. 1201-1215.
46. Patel, J., et al., *Recovery of low volumes of wear debris from rat stifle joint tissues using a novel particle isolation method.* Acta biomaterialia, 2018. **71**: p. 339-350.
47. Nine, M., et al., *Wear debris characterization and corresponding biological response: artificial hip and knee joints.* Materials, 2014. **7**(2): p. 980-1016.
48. Catelas, I., et al., *Effects of digestion protocols on the isolation and characterization of metal–metal wear particles. II. Analysis of ion release and particle composition.* Journal of Biomedical Materials Research: An Official Journal of The Society for Biomaterials, The Japanese Society for Biomaterials, and The Australian Society for Biomaterials and the Korean Society for Biomaterials, 2001. **55**(3): p. 330-337.
49. International, A., *Standard Practice for Characterization of Particles*. 2010: ASTM International.
50. Catelas, I., et al., *Effects of digestion protocols on the isolation and characterization of metal–metal wear particles. I. Analysis of particle size and shape.* Journal of Biomedical Materials Research: An Official Journal of The Society for Biomaterials, The Japanese Society for Biomaterials, and The Australian Society for Biomaterials and the Korean Society for Biomaterials, 2001. **55**(3): p. 320-329.
51. La Budde, J.K., et al., *Particulate titanium and cobalt-chrome metallic debris in failed total knee arthroplasty: a quantitative histologic analysis.* The Journal of arthroplasty, 1994. **9**(3): p. 291-304.
52. Estey, M.P., et al., *Cobalt and chromium measurement in patients with metal hip prostheses.* Clinical chemistry, 2013. **59**(6): p. 880-886.
53. Rabinowitz, M., *Historical perspective on lead biokinetic models.* Environmental health perspectives, 1998. **106**(suppl 6): p. 1461-1465.
54. *Center for Radiation Protectioin Knowledge*. [cited 2020 8/5/2020]; Available from: https://www.ornl.gov/crpk/program-history.

55. Unice, K.M., et al., *Refined biokinetic model for humans exposed to cobalt dietary supplements and other sources of systemic cobalt exposure.* Chemico-biological interactions, 2014. **216**: p. 53-74.
56. Keegan, G.M., I.D. Learmonth, and C. Case, *A systematic comparison of the actual, potential, and theoretical health effects of cobalt and chromium exposures from industry and surgical implants.* Critical reviews in toxicology, 2008. **38**(8): p. 645-674.
57. Heekin, R.D., C.A. Engh, and T. Vinh, *Morselized allograft in acetabular reconstruction. A postmortem retrieval analysis.* Clinical orthopaedics and related research, 1995(319): p. 184-190.
58. Lester, D.K., *Cross-section radiographic analysis of 10 retrieved titanium alloy press-fit femoral endoprostheses.* The Journal of arthroplasty, 1997. **12**(8): p. 930-937.
59. Urban, R.M., et al., *Dissemination of wear particles to the liver, spleen, and abdominal lymph nodes of patients with hip or knee replacement.* JBJS, 2000. **82**(4): p. 457.
60. Harman, M.K., S.A. Banks, and W.A. Hodge, *Polyethylene damage and knee kinematics after total knee arthroplasty.* Clinical Orthopaedics and Related Research®, 2001. **392**: p. 383-393.
61. Tonino, A., et al., *Hydroxyapatite-coated acetabular components: histological and histomorphometric analysis of six cups retrieved at autopsy between three and seven years after successful implantation.* JBJS, 2001. **83**(6): p. 817-825.
62. Urban, R.M., et al., *Accumulation in liver and spleen of metal particles generated at nonbearing surfaces in hip arthroplasty.* The Journal of arthroplasty, 2004. **19**(8): p. 94-101.
63. Mann, K.A., et al., *Peri-implant bone strains and micro-motion following in vivo service: A postmortem retrieval study of 22 tibial components from total knee replacements.* Journal of Orthopaedic Research, 2014. **32**(3): p. 355-361.
64. Bryant, M., et al., *Characterisation of the surface topography, tomography and chemistry of fretting corrosion product found on retrieved polished femoral stems.* Journal of the mechanical behavior of biomedical materials, 2014. **32**: p. 321-334.
65. Goldberg, J.R., et al., *A multicenter retrieval study of the taper interfaces of modular hip prostheses.* Clinical orthopaedics and related research, 2002. **401**: p. 149-161.
66. Black, J., *Requirements for successful total knee replacement. Material considerations.* The Orthopedic clinics of North America, 1989. **20**(1): p. 1-13.
67. Arnholt, C.M., et al., *Mechanically assisted taper corrosion in modular TKA.* The Journal of arthroplasty, 2014. **29**(9): p. 205-208.

68. Gilbert, J.L., et al., *Direct in vivo inflammatory cell-induced corrosion of CoCrMo alloy orthopedic implant surfaces.* Journal of Biomedical Materials Research Part A, 2015. **103**(1): p. 211-223.
69. Wasielewski, R.C., et al., *Wear patterns on retrieved polyethylene tibial inserts and their relationship to technical considerations during total knee arthroplasty.* Clinical orthopaedics and related research, 1994(299): p. 31-43.
70. Hirakawa, K., et al., *Relationship between wear debris particles and polyethylene surface damage in primary total knee arthroplasty.* The Journal of arthroplasty, 1999. **14**(2): p. 165-171.
71. De Baets, T., W. Waelput, and J. Bellemans, *Analysis of third body particles generated during total knee arthroplasty: is metal debris an issue?* The Knee, 2008. **15**(2): p. 95-97.
72. Malikian, R., et al., *In vivo roughening of retrieved total knee arthroplasty femoral components.* The Knee, 2014. **21**(1): p. 278-282.
73. Que, L. and L.T. Topoleski, *Third-body wear of cobalt-chromium-molybdenum implant alloys initiated by bone and poly (methyl methacrylate) particles.* Journal of Biomedical Materials Research: An Official Journal of The Society for Biomaterials, The Japanese Society for Biomaterials, and The Australian Society for Biomaterials and the Korean Society for Biomaterials, 2000. **50**(3): p. 322-330.
74. Campbell, P., et al. *Re-examining the concept of inflammatory cell-induced corrosion*. in *Orthopaedic Proceedings*. 2017. The British Editorial Society of Bone & Joint Surgery.
75. Heise, G., et al., *Comparison of Inflammatory Cell-Induced Corrosion and Electrocautery-Induced Damage of Total Knee Implants.* Journal of Long-Term Effects of Medical Implants, 2019. **29**(3).
76. Hood, R.W., T.M. Wright, and A.H. Burstein, *Retrieval analysis of total knee prostheses: a method and its application to 48 total condylar prostheses.* Journal of biomedical materials research, 1983. **17**(5): p. 829-842.
77. Grochowsky, J., et al., *Digital photogrammetry for quantitative wear analysis of retrieved TKA components.* Journal of Biomedical Materials Research Part B: Applied Biomaterials: An Official Journal of The Society for Biomaterials, The Japanese Society for Biomaterials, and The Australian Society for Biomaterials and the Korean Society for Biomaterials, 2006. **79**(2): p. 263-267.
78. Higgs, G.B., et al., *Is increased modularity associated with increased fretting and corrosion damage in metal-on-metal total hip arthroplasty devices?: a retrieval study.* The Journal of arthroplasty, 2013. **28**(8): p. 2-6.
79. Lachiewicz, P.F., T.S. Watters, and J.J. Jacobs, *Metal Hypersensitivity and Total Knee Arthroplasty.* Journal of the American Academy of Orthopaedic Surgeons, 2016. **24**(2): p. 106-112.

80. Post, Z.D., F.R. Orozco, and A.C. Ong, *Metal sensitivity after TKA presenting with systemic dermatitis and hair loss.* Orthopedics, 2013. **36**(4): p. e525-e528.
81. Gao, X., et al., *Dermatitis associated with chromium following total knee arthroplasty.* The Journal of arthroplasty, 2011. **26**(4): p. 665. e13-665. e16.
82. Luetzner, J., et al., *Serum metal ion exposure after total knee arthroplasty.* Clinical Orthopaedics and Related Research®, 2007. **461**: p. 136-142.
83. Liu, T.-K., et al., *Concentration of metal elements in the blood and urine in the patients with cementless total knee arthroplasty.* The Tohoku journal of experimental medicine, 1998. **185**(4): p. 253-262.
84. Heyse, T.J., et al., *Matched-pair total knee arthroplasty retrieval analysis: oxidized zirconium vs. CoCrMo.* The Knee, 2011. **18**(6): p. 448-452.
85. Muratoglu, O.K., et al., *Knee simulator wear of polyethylene tibias articulating against explanted rough femoral components.* Clinical Orthopaedics and Related Research (1976-2007), 2004. **428**: p. 108-113.
86. Kretzer, J.P., et al., *Wear in total knee arthroplasty—just a question of polyethylene?* International orthopaedics, 2014. **38**(2): p. 335-340.
87. Medel, F., et al., *Clinical, surface damage and oxidative performance of poly II tibial inserts after long-term implantation.* Journal of long-term effects of medical implants, 2008. **18**(2).
88. Kurtz, S.M., et al., *2006 Otto Aufranc Award Paper: significance of in vivo degradation for polyethylene in total hip arthroplasty.* Clinical Orthopaedics and Related Research®, 2006. **453**: p. 47-57.
89. Kurtz, S.M., et al., *In vivo degradation of polyethylene liners after gamma sterilization in air.* JBJS, 2005. **87**(4): p. 815-823.
90. Underwood, R.J., et al., *Edge loading in metal-on-metal hips: low clearance is a new risk factor.* Proceedings of the Institution of Mechanical Engineers, Part H: Journal of Engineering in Medicine, 2012. **226**(3): p. 217-226.
91. Matsuda, Y., et al., *Severe metallosis due to abnormal abrasion of the femoral head in a dual bearing hip prosthesis: A case report.* The Journal of arthroplasty, 1992. **7**: p. 439-445.
92. Hallab, N., *Biologic aspects of implant wear.* ASM handbook Vol. 23 Materials for Medical Devices, 2012: p. 157-168.
93. Lehtovirta, L., et al., *Association between periprosthetic tissue metal content, whole blood and synovial fluid metal ion levels and histopathological findings in patients with failed metal-on-metal hip replacement.* PloS one, 2018. **13**(5).
94. *Medicines and Healthcare products Regulatory Agency (MHRA).* . Medical Device Alert: all metal-on-metal (MOM) hip replacements:updated advice for follow up of patients 2017 29 June 2017 [cited 2020 April 23]; MDA/2017/018:[Available from:

https://assets.publishing.service.gov.uk/media/5954ca1ded915d0baa00009b/MDA-2017-018_Final.pdf.

95. Hart, A., et al., *Sensitivity and specificity of blood cobalt and chromium metal ions for predicting failure of metal-on-metal hip replacement.* The Journal of bone and joint surgery. British volume, 2011. **93**(10): p. 1308-1313.
96. Xia, Z., et al., *Characterization of metal-wear nanoparticles in pseudotumor following metal-on-metal hip resurfacing.* Nanomedicine: Nanotechnology, Biology and Medicine, 2011. **7**(6): p. 674-681.
97. Case, C., et al., *Widespread dissemination of metal debris from implants.* The Journal of bone and joint surgery. British volume, 1994. **76**(5): p. 701-712.
98. Doorn, P.F., et al., *Metal wear particle characterization from metal on metal total hip replacements: transmission electron microscopy study of periprosthetic tissues and isolated particles.* Journal of Biomedical Materials Research: An Official Journal of The Society for Biomaterials, The Japanese Society for Biomaterials, and the Australian Society for Biomaterials, 1998. **42**(1): p. 103-111.
99. Ingham, E. and J. Fisher, *Biological reactions to wear debris in total joint replacement.* Proc Inst Mech Eng H, 2000. **214**(1): p. 21-37.
100. Lee, J.-M., et al., *Size of metallic and polyethylene debris particles in failed cemented total hip replacements.* The Journal of bone and joint surgery. British volume, 1992. **74**(3): p. 380-384.
101. Catelas, I., et al., *Comparison of in vitro with in vivo characteristics of wear particles from metal–metal hip implants.* Journal of Biomedical Materials Research Part B: Applied Biomaterials: An Official Journal of The Society for Biomaterials, The Japanese Society for Biomaterials, and The Australian Society for Biomaterials and the Korean Society for Biomaterials, 2004. **70**(2): p. 167-178.
102. Milošev, I. and M. Remškar, *In vivo production of nanosized metal wear debris formed by tribochemical reaction as confirmed by high-resolution TEM and XPS analyses.* Journal of Biomedical Materials Research Part A: An Official Journal of The Society for Biomaterials, The Japanese Society for Biomaterials, and The Australian Society for Biomaterials and the Korean Society for Biomaterials, 2009. **91**(4): p. 1100-1110.
103. Middleton, S. and A. Toms, *Allergy in total knee arthroplasty: a review of the facts.* The bone & joint journal, 2016. **98**(4): p. 437-441.
104. Lal, S., R. Hall, and J. Tipper, *A novel method for isolation and recovery of ceramic nanoparticles and metal wear debris from serum lubricants at ultra-low wear rates.* Acta biomaterialia, 2016. **42**: p. 420-428.
105. Kerger, B.D., et al., *Cobalt speciation assay for human serum, Part I. Method for measuring large and small molecular cobalt and protein-binding capacity using size exclusion chromatography with inductively coupled plasma-mass*

spectroscopy detection. Toxicological & Environmental Chemistry, 2013. **95**(4): p. 687-708.

106. Hood, R.W., T.M. Wright, and A.H. Burstein, *Retrieval analysis of total knee prostheses: a method and its application to 48 total condylar prostheses.* J Biomed Mater Res, 1983. **17**(5): p. 829-42.
107. Arnholt, C.M., et al., *What Is the Incidence of Cobalt-Chromium Damage Modes on the Bearing Surface of Contemporary Femoral Component Designs for Total Knee Arthroplasty?* The Journal of arthroplasty, 2018.
108. Michael B. Cross, M. *Revision Total Knee Replacement*. 2015 [cited 2020; Available from: https://orthoinfo.aaos.org/en/treatment/revision-total-knee-replacement/.
109. Ebramzadeh, E., et al., *Can wear explain the histological variation around metal-on-metal total hips?* Clinical Orthopaedics and Related Research®, 2015. **473**(2): p. 487-494.
110. Arnholt, C.M., et al., *Postmortem Retrieval Analysis of Metallosis and Periprosthetic Tissue Metal Concentrations in Total Knee Arthroplasty.* The Journal of Arthroplasty, 2020. **35**(2): p. 569-578.
111. Arnholt, C.M., et al., *Corrosion Damage and Wear Mechanisms in Long-Term Retrieved CoCr Femoral Components for Total Knee Arthroplasty.* The Journal of Arthroplasty, 2016.
112. Rae, T., *The biological response to titanium and titanium-aluminium-vanadium alloy particles: II. Long-term animal studies.* Biomaterials, 1986. **7**(1): p. 37-40.
113. Rushton, N. and T. Rae, *The intra-articular response to particulate carbon fibre reinforced high density polyethylene and its constituents: an experimental study in mice.* Biomaterials, 1984. **5**(6): p. 352-356.
114. Thiele, K., et al., *Current failure mechanisms after knee arthroplasty have changed: polyethylene wear is less common in revision surgery.* JBJS, 2015. **97**(9): p. 715-720.
115. Korovessis, P., et al., *Metallosis after contemporary metal-on-metal total hip arthroplasty: five to nine-year follow-up.* JBJS, 2006. **88**(6): p. 1183-1191.
116. Bitar, D. and J. Parvizi, *Biological response to prosthetic debris.* World journal of orthopedics, 2015. **6**(2): p. 172.
117. Catelas, I., M.A. Wimmer, and S. Utzschneider. *Polyethylene and metal wear particles: characteristics and biological effects*. in *Seminars in immunopathology*. 2011. Springer.
118. Williams, J.A., *Wear and wear particles—some fundamentals.* Tribology International, 2005. **38**(10): p. 863-870.
119. Simonsen, L.O., H. Harbak, and P. Bennekou, *Cobalt metabolism and toxicology—a brief update.* Science of the Total Environment, 2012. **432**: p. 210-215.

120. Barceloux, D.G. and D. Barceloux, *Cobalt.* Journal of Toxicology: Clinical Toxicology, 1999. **37**(2): p. 201-216.
121. Catalani, S., et al., *Neurotoxicity of cobalt.* Human & experimental toxicology, 2012. **31**(5): p. 421-437.
122. Bowie, E. and P. Hurley, *Cobalt chloride in the treatment of refractory anaemia in patients undergoing long-term haemodialysis.* Australian and New Zealand Journal of Medicine, 1975. **5**(4): p. 306-313.
123. Duckham, J. and H. Lee, *The treatment of refractory anaemia of chronic renal failure with cobalt chloride.* QJM: An International Journal of Medicine, 1976. **45**(2): p. 277-294.
124. Gross, R.T., J.P. Kriss, and T.H. Spaet, *The hematopoietic and goitrogenic effects of cobaltous chloride in patients with sickle cell anemia.* Pediatrics, 1955. **15**(3): p. 284-371.
125. Kriss, J.P., W.H. Carnes, and R.T. Gross, *Hypothyroidism and thyroid hyperplasia in patients treated with cobalt.* Journal of the American Medical Association, 1955. **157**(2): p. 117-121.
126. Sederholm, T., K. Kouvalainen, and B.A. Lamberg, *COBALT-INDUCED HYPOTHYROIDISM AND POLYCYTHEMIA IN LIPOID NEPHROSIS.* Acta Medica Scandinavica, 1968. **184**(1-6): p. 301-306.
127. Kesteloot, H., et al., *An enquiry into the role of cobalt in the heart disease of chronic beer drinkers.* Circulation, 1968. **37**(5): p. 854-864.
128. Jelkmann, W. and C. Lundby, *Blood doping and its detection.* Blood, 2011. **118**(9): p. 2395-2404.
129. Lippi, G., M. Franchini, and G.C. Guidi, *Blood doping by cobalt. Should we measure cobalt in athletes?* Journal of Occupational Medicine and Toxicology, 2006. **1**(1): p. 18.
130. Ebreo, D., et al., *Metal ion levels decrease after revision for metallosis arising from large-diameter metal-on-metal hip arthroplasty.* Acta Orthopædica Belgica, 2011. **77**(6): p. 777.
131. Hasegawa, M., et al., *Cobalt and chromium ion release after large-diameter metal-on-metal total hip arthroplasty.* The Journal of arthroplasty, 2012. **27**(6): p. 990-996.
132. Jansen, H.M., et al., *Pharmacokinetics and dosimetry of cobalt-55 and cobalt-57.* 1996.
133. Goode, A.E., et al., *Chemical speciation of nanoparticles surrounding metal-on-metal hips.* Chemical Communications, 2012. **48**(67): p. 8335-8337.
134. Hart, A.J., et al., *Cobalt from metal-on-metal hip replacements may be the clinically relevant active agent responsible for periprosthetic tissue reactions.* Acta biomaterialia, 2012. **8**(10): p. 3865-3873.

135. Silva, M., et al., *Average patient walking activity approaches 2 million cycles per year: pedometers under-record walking activity.* The Journal of arthroplasty, 2002. **17**(6): p. 693-697.
136. Kuwashima, U., et al., *Contact stress analysis of the anterior tibial post in bi-cruciate stabilized and mobile-bearing posterior stabilized total knee arthroplasty designs.* Journal of the Mechanical Behavior of Biomedical Materials, 2016. **60**: p. 460-467.
137. Lu, Y.-C., et al., *Wear-pattern analysis in retrieved tibial inserts of mobile-bearing and fixed-bearing total knee prostheses.* The Journal of bone and joint surgery. British volume, 2010. **92**(4): p. 500-507.
138. Yue, B., et al., *Kinematics of medial osteoarthritic knees before and after posterior cruciate ligament retaining total knee arthroplasty.* Journal of orthopaedic research, 2011. **29**(1): p. 40-46.
139. Becher, C., et al., *Posterior stabilized TKA reduce patellofemoral contact pressure compared with cruciate retaining TKA in vitro.* Knee Surgery, Sports Traumatology, Arthroscopy, 2009. **17**(10): p. 1159-1165.
140. Hamai, S., et al., *Kinematic analysis of kneeling in cruciate-retaining and posterior-stabilized total knee arthroplasties.* Journal of orthopaedic research, 2008. **26**(4): p. 435-442.
141. Arnholt, C.M., et al., *What Is the Incidence of Cobalt-Chromium Damage Modes on the Bearing Surface of Contemporary Femoral Component Designs for Total Knee Arthroplasty?* The Journal of arthroplasty, 2018. **33**(10): p. 3313-3319.
142. Gadelmawla, E., et al., *Roughness parameters.* Journal of materials processing Technology, 2002. **123**(1): p. 133-145.
143. Hameister, R., et al., *Reactive oxygen/nitrogen species (ROS/RNS) and oxidative stress in arthroplasty.* Journal of Biomedical Materials Research Part B: Applied Biomaterials, 2020. **108**(5): p. 2073-2087.
144. Bergschmidt, P., R. Bader, and W. Mittelmeier, *Metal hypersensitivity in total knee arthroplasty: revision surgery using a ceramic femoral component—a case report.* The Knee, 2012. **19**(2): p. 144-147.
145. Bergschmidt, P., et al., *Ceramic femoral components in total knee arthroplasty-two year follow-up results of an international prospective multi-centre study.* The open orthopaedics journal, 2012. **6**: p. 172.
146. Meier, E., et al., *First clinical study of a novel complete metal-free ceramic total knee replacement system.* Journal of orthopaedic surgery and research, 2016. **11**(1): p. 1-7.
147. de Ruiter, L., et al., *A preclinical numerical assessment of a polyetheretherketone femoral component in total knee arthroplasty during gait.* Journal of experimental orthopaedics, 2017. **4**(1): p. 3.

148. Cowie, R.M., et al., *PEEK-OPTIMA™ as an alternative to cobalt chrome in the femoral component of total knee replacement: a preliminary study.* Proceedings of the Institution of Mechanical Engineers, Part H: Journal of Engineering in Medicine, 2016. **230**(11): p. 1008-1015.

Appendix A

Berkeley Madonna Model Code:

; Cobalt knee biokinetic model

; Arnholt et al. 2020

; Contents

; Section 1: Model Control

; Section 2: Scaling and Knee Joint Dosing Parameters

; Section 3: Initial Model Parameters

; Section 4: Knee Joint Transfer Coefficients

; Section 5: Balancing Old Transfer Coefficients

; Section 6: Leggett/ Czarnek Transfer Coefficients

; Section 7: Knee Joint Model Equations

: Section 8: Leggett/ Czarnek Model Equations

; ****Begin Section One: Model Control

METHOD Auto; Integration method

TOLERANCE = 0.0001; Solution tolerance

STARTTIME = 0; Model start time in days

STOPTIME= 2190; Model stop time in days

STARTDAY=0; Dose start time in days.

STOPDAY=2190; Dose stop time in days. This term was altered for the adverse patient reaction dosing thought experiment (research question 3: can this model simulate blood cobalt concentrations consistent with adverse patient symptoms).

; **** End Section One

; **** Begin Section Two: Scaling and Knee Joint Dosing Parameters

SCALE=0.001; The scale variable was utilized during model calibration.

DAILYDOSE = .893*7; 0.893 is the dosing parameter with 5 being the continues model dose multiple. Under different test conditions this multiple was altered. These alterations are reflected in table 4.3.3 under dose multiple

Dose1 = IF (TIME >= STARTDAY) AND (TIME <=STOPDAY) THEN DAILYDOSE ELSE 0

$K_{Corrosion}$=.07; This term was used to determine the quantity of cobalt dose that was hypothesized to be produced by corrosion

$K_{BearingSurface}$=.93; This term was used to determine the quantity of cobalt dose that was hypothesized to be produced by bearing surface damage

; **** End Section Two

;**** Begin Section Three: Initial Model Parameters

init jc=.085; This term was derived from Hallab et al. for the joint capsule initial value.

init B1 =.002; This term was derived from Hallab et al. for the blood initial value.

init ORG=0; This term is the organ initial value

init Sk=0; This term is the skeleton initial value

init liv=0; This term is the liver initial value

init OT=0; This term is the other tissue initial value

init K=0; This term is the kidney initial value

init K1=0; This term is the kidney reservoir initial value

init UB=0; This term is the urinary bladder initial value

init TB=0; This term is the trabecular bone initial value

init CB=0; This term is the cortical bone initial value

init SK1=0; This term is the skeletal reservoir initial value

init Liv1=0; This term is the liver reservoir initial value

init IntEST =0; This term is the intestine initial value

init CB1=0; This term is the blood reservoir initial value

init jc1=0; This term is the joint capsule reservoir initial value.

; **** End Section Three

; **** Begin Section Four: Knee Joint Transfer Coefficients

$K_{sf,jc}$=0.007; Scaled transfer coefficient for cobalt moving from the synovial fluid to the joint capsule tissue.

$K_{jc,sf}$=6.07* scale /2.5; Scaled transfer coefficient for cobalt moving from the joint capsule to the synovial fluid.

$K_{jc,B1}$=0.0023 /2.5; Scaled transfer coefficient for cobalt moving from the joint capsule to the blood.

$K_{B1,jc}$ =6.26 *SCALE /2.5; Scaled transfer coefficient for cobalt moving from the blood to the joint capsule.

$K_{sf,B1}$ =0.099021*3.5; Scaled transfer coefficient for cobalt moving from the synovial fluid to the blood.

$K_{B1,sf}$=18 * SCALE/3.5; Scaled transfer coefficient for cobalt moving from the blood to the synovial fluid.

; **** End Section Four

; **** Begin Section Five: Balancing Transfer Coefficients

$K_{B1,OR}$=0.94-(0.94*($K_{B1,sf}$+$K_{B1,jc}$)); The transfer coefficient for cobalt moving from the blood to the organs was balanced to maintain the preexisting compartment ratios from the original model while including the new transfer coefficients.

$K_{B1,CB1}$=0.06-(0.06*($K_{B1,sf}$+$K_{B1,jc}$)); The transfer coefficient for cobalt moving from the blood to the blood reservoir was balanced to maintain the preexisting compartment ratios from the original model while including the new transfer coefficients.

$K_{Sk,B1}$=.85-(0.85*($K_{sf,B1}$+$K_{jc,B1}$)); The transfer coefficient for cobalt moving from the skeleton to the blood was balanced to maintain the preexisting compartment ratios from the original model while including the new transfer coefficients.

$K_{liv,B1}$=.09-(0.09*($K_{sf,B1}$+$K_{jc,B1}$)); The transfer coefficient for cobalt moving from the liver to the blood was balanced to maintain the preexisting compartment ratios from the original model while including the new transfer coefficients.

$K_{CB1,B1}$=.06-(0.06*($K_{sf,B1}$+$K_{jc,B1}$)); The transfer coefficient for cobalt moving from the blood reservoir to the blood was balanced to maintain the preexisting compartment ratios from the original model while including the new transfer coefficients.

$K_{jc,JC1}$=1-($K_{jc,sf}$+$K_{jc,B1}$); The transfer coefficient for cobalt moving from the joint capsule to the joint capsule reservoir was balanced.

$K_{JC1,jc}$=1-($K_{B1,jc}$+$K_{sf,jc}$); The transfer coefficient for cobalt moving from the joint capsule reservoir to the joint capsule was balanced.

; **** End Section Five

; **** Begin Section Six: Leggett/ Czarnek Transfer Coefficients

$K_{OR,OT}$=.16; Transfer coefficient for cobalt movement from the organs to the other tissues.

$K_{OR,Sk}$=.06; Transfer coefficient for cobalt movement from the organs to the skeleton.

$K_{OR,K}$=.045; Transfer coefficient for cobalt movement from the organs to the kidney.

$K_{OR,liv}$=.35; Transfer coefficient for cobalt movement from the organs to the liver.

$K_{OR,UB}$=.3; Transfer coefficient for cobalt movement from the organs to the urinary bladder.

$K_{Sk,TB}$=.03; Transfer coefficient for cobalt movement from skeleton to the trabecular bone.

$K_{Sk,CB}$=.03; Transfer coefficient for cobalt movement from the skeleton to the cortical bone.

$K_{Sk,SK1}$=.15; Transfer coefficient for cobalt movement from skeleton to the skeletal reservoir.

$K_{SK1,Sk}$=.15; Transfer coefficient for cobalt movement from the skeletal reservoir to the skeleton.

$K_{K,K1}$=.005; Transfer coefficient for cobalt movement from the kidney to the kidney reservoir.

$K_{K1,K}$=.005; Transfer coefficient for cobalt movement from the kidney reservoir to the kidney.

$K_{liv,Int}$=.2; Transfer coefficient for cobalt movement from the liver to the intestines.

$K_{liv,Liv1}$=.05; Transfer coefficient for cobalt movement from the liver to the liver reservoir.

$K_{Liv1,liv}$=.05; Transfer coefficient for cobalt movement from the liver reservoir to the liver.

; **** End Section Six

; **** Begin Section Seven: Knee Joint Model Equations

d/dt(jc) =Dose1* $K_{BearingSurface}$ *$K_{sf,jc}$ -$K_{jc,sf}$ *B1- $K_{jc,B1}$*jc +$K_{B1,jc}$*B1- $K_{jc,JC1}$ * jc+ $K_{JC1,jc}$*jc1; Equation for cobalt moving in and out of the joint capsule tissues.

d/dt(jc1)= $K_{jc,JC1}$*jc-$K_{JC1,jc}$*jc1; Equation for cobalt moving in and out of the joint capsule reservoir.

d/dt(B1)=$K_{jc,B1}$*jc-$K_{B1,jc}$*B1+$K_{Corrosion}$*Dose1*$K_{sf.B1}$B1*$K_{B1,sf}$+liv*$K_{liv,B1}$+Sk*$K_{Sk,B1}$+ CB1*$K_{CB1,B1}$-B1*$K_{B1,CB1}$-B1*$K_{B1,OR}$; Equation for cobalt moving in and out of the blood stream.

d/dt(CB1)= B1*$K_{B1,CB1}$-CB1*$K_{CB1,B1}$; Equation for cobalt moving in and out of the blood reservoir.

; **** End Section Seven

; **** Begin Section Eight: Leggett/ Czarnek Model Equations

d/dt(ORG) = B1*$K_{B1,OR}$ -ORG*$K_{OR,OT}$-ORG*$K_{OR,Sk}$-ORG*$K_{OR,K}$-ORG*$K_{OR,liv}$-ORG*$K_{OR,UB}$; Equation for cobalt moving in and out of the organs.

d/dt (OT) = ORG*$K_{OR,OT}$; Equation for cobalt moving in and out of the other tissues.

d/dt (Sk) = ORG*$K_{OR,Sk}$- Sk*$K_{Sk,B1}$-Sk*$K_{Sk,SK1}$+SK1*$K_{SK1,Sk}$-Sk*$K_{Sk,CB}$-Sk*$K_{Sk,TB}$; Equation for cobalt moving in and out of the skeleton.

d/dt (SK1)= Sk*$K_{Sk,SK1}$-SK1*$K_{SK1,Sk}$; Equation for cobalt moving in and out of the skeletal reservoir.

d/dt (TB)=Sk*$K_{Sk,TB}$; Equation for cobalt moving in and out of the trabecular bone.

d/dt (CB)=Sk*$K_{Sk,CB}$; Equation for cobalt moving in and out of the cortical bone.

d/dt (K) = ORG*$K_{OR,K}$-K*$K_{K,K1}$+K1*$K_{K1,K}$; Equation for cobalt moving in and out of the kidney.

d/dt (K1) = K*$K_{K,K1}$-K1*$K_{K1,K}$; Equation for cobalt moving in and out of the kidney reservoir

d/dt (UB) = ORG*$K_{OR,UB}$; Equation for cobalt moving in and out of the urinary bladder.

d/dt (liv) = ORG*$K_{OR,liv}$-liv*$K_{liv,Int}$-liv*$K_{liv,B1}$+Liv1*$K_{Liv1,liv}$-liv*$K_{liv,Liv1}$; Equation for cobalt moving in and out of the liver.

d/dt (Liv1) = liv*$K_{liv,Liv1}$-Liv1*$K_{Liv1,liv}$; Equation for cobalt moving in and out of the liver reservoir.

d/dt (IntEST) =liv*$K_{liv,Int}$; Equation for cobalt moving in and out of the intestines.

; **** End Section Eight